الجمهورية الجزائرية الديمقراطية الشعبية
LA REPUBLIQUE ALGERIENNE DEMOCRATIQUE ET POPULAIRE
وزارة التعليم العالي والبحث العلمي
Ministère de l'Enseignement Supérieur et de la Recherche Scientifique

Université Saad Dahlab Blida 1
Institut d'Aéronautique et des Études Spatiales
Département Construction Aéronautique

Mémoire de fin d'études
En vue de l'obtention du diplôme de
Master en Aéronautique
Option :Propulsion Des Avions

THEME

Numerical and CFD study of the combustion products flow field in Dual-Bell Nozzle

Proposé et dirigé par :
Dr.Kbab Hakim
Mr.Techarek Anis

Réalisé par :
Mr. Terai Mohamed Ramzi
Mr. Boutemtam Mohamed

Promotion : 2022 / 2023

Thank you

First of all, we would like to thank ALLAH, the Almighty, who gave us the courage and willpower to carry out this modest work.

We would like to express our sincere gratitude to our promoter, Mr. H.KBAB, and our co-promoter, Mr. A.TCHERAK who proposed and directed this work, for their guidance and advice.

Our sincere thanks also go to the chairman and members of the jury for having assessed our work and honored us with their presence.

Finally, to all those who have contributed in any way to the realization of this long work; we would like to express our most sincere thanks.

MOHAMED BOUTEMTAM

MOHAMED RAMZI TERAI

DEDICATION

I dedicate this modest work to the people most dear to me, to whom I owe my gratitude and devotion, and to whom I shall always be grateful.

Devotion and to whom I shall never cease to give thanks:

My parents, my brothers and my sister.

To all the friends who have supported me throughout my university career and with whom I have shared unforgettable moments.

To all those who have helped me in any way in the preparation of this thesis.

Finally, to all of you who have taken the trouble to read this dissertation.

B.MOHAMED & T.RAMZI

Abstract:

Dual bell nozzles may represent a possible alternative to replace conventional bell nozzles in future launcher first stages. Their main feature is the peculiar shape of the divergent section, displaying two bells separated by an inflection point. Although this is a non-optimized shape, it shows two different operating modes that provide at high altitude larger expansion ratios than conventional nozzles, while avoiding sideloads at sea-level. The aim of this project is to study the combustion products flow field inside a dual-bell nozzle by using a computational fluid dynamics (CFD) code; ANSYS Fluent.

Résumé:

Résumé : Les tuyères à double galbes peuvent représenter une alternative possible pour remplacer les tuyères conventionnelles dans les futurs premiers étages du lanceur. Leur principale caractéristique est la forme particulière de la section divergente, affichant deux cloches séparées par un point d'inflexion. Bien que ce soit un forme non optimisée, il montre deux modes de fonctionnement différents qui fournissent à haute altitude des taux d'expansion plus importants que les tuyères conventionnelles, tout en évitant les charges latérales au niveau de la mer. L'objectif de ce projet est d'étudier le champ d'écoulement des produits de combustion à l'intérieur d'une tuyère à double galbes en utilisant un code de dynamique des fluides computationnelle (CFD); ANSYS Fluent.

Table of Contents

List of Figures

Nomenclature

$\omega^{\cdot}_k$	Source term of the species k due to the chemical reaction	-
A_j	Chemical symbol for species j	-
C_p	Specific heat at constant pressure	$J/kg.K$
D_k	Molecular diffusivity of the species k	-
E_i	Activation energy of a chemical reaction	J/mol
F_i	Surface strength	N
M_j	Molar mass of species j	kg/mol
P_{atm}	Reference pressure	Pa
S_{ij}	Average strain rate	s^{-1}
T_0	Reference temperature	K
T_b	Burnt gas temperature	K
T_u	Unburnt gas temperature	K
$W^{\cdot}$	Mass production rate	$kg/s.m^3$
Y_k	Mass fraction of the species	-
k_B	Boltzmann's constant	-
k_d	Forward reaction constant	-
k_e	Equilibrium reaction constant	-
k_r	Reverse reaction constant	-
u_i	Velocity in the xi-coordinate direction	m/s
γ'_{ji} , γ''_{ji}	Stoichiometric coefficients of species j in the reaction i	-
δ_{ij}	Kronecker symbol	-
μ_{eff}	Effective viscosity	$Pa\ s$
μ_l	Laminar viscosity	$Pa\ s$

μ_t	Turbulent viscosity	$Pa\ s$
ν_T	Vortex kinematic viscosity	m^2/s
r_{ij}	Viscous force tensor	m^2/s^2
r_{ij}	Reynolds stress tensor	N/m^2
h	Mass enthalpy	J/kg
λ	Thermal conductivity	$W/m.K$
Φ (EQ)	Richness	-
ω	Specific dissipation rate	s^{-1}
C	Molar concentration	mol/m^3
Da	Damköhler number	-
H	Total enthalpy	J
P	Static pressure	Pa
Pr	Prandtl number	-
R	Universal ideal gas constant	$J/mol.K$
Re	Reynolds number	-
Sc_k	Schmidt number	-
T	Temperature	K
V	Total volume	m^3
Z	Unknown function	-
c	Progress variable	-
f	Mixing fraction	-
k	Turbulent kinetic energy	m^2/s^2
m	Total mass	kg
n	Number of total moles	mol

$p(f)$	Probability density function	-
s	Total entropy	$J/kg.K$
α	Pre-exponential factor temperature exponent	-
β	Pre-exponential factor	-
ε	Turbulent kinetic energy dissipation rate	m^2/s^3
ξ	Degree of advancement	-
ρ	Volumic mass	kg/m^3
E	Total energy	J
Y^+	Non-dimensional distance	-
Q	Heat transfer	J
Cd	Discharge coefficient	-
T_c	Temperature of the colder reservoir	K
T_h	Temperature of the hotter reservoir	K
η_c	Carnot efficiency	-
ΔU	Internal energy	J
Le	Lewis number	-
Cp_m	Heat Capacity of the mixture	J/K
r	Shear stress	Pa
r_ω	The wall shear stress	Pa
σ_k	The turbulent Prandtl number k	-
σ_ω	The turbulent Prandtl number ω	-
$\tilde{G}_k$	Turbulence kinetic energy	J/kg
G_ω	Represents the generation of ω	s^{-1}
Γ_k	The effective diffusivity of k	-
Γ_ω	The effective diffusivity of ω	-
D_ω	The cross-diffusion term	s^{-1}
$\bar{U}^+$	The average velocity	m/s

f_v	The damping function	-
$R_{i,r}$	The reaction rate	-
Y_p	The mass fraction of species p in the products	-
Y_R	The mass fraction of species r in the reactants	-
$M_{w,i}$	The molar mass of species i	g/mol
k', k'', k'''	Constants	-
V_{eff}	Effective gas velocity	m/s
F	Thrust	N
g	Acceleration of gravity	m/s^2
I_{totale}	Total impulse	N.s
I_s	Specific impulse	s
A_e	Nozzle exit section	m^2
$\dot{m}$	Mass flow rate	kg/s
x	Axial coordinate	m
y	Radial coordinate	m

General Introduction:

Propulsion refers to the action of altering the motion of a body in a general sense. It involves providing a force that can move objects from a state of rest, change their velocity, or overcome retarding forces when they are propelled through a medium. One form of propulsion is jet propulsion, which utilizes the momentum of ejected matter to impart a reaction force on a device and propel it forward.

Combustion remains a crucial means of producing energy, serving as the primary source for all kinds of transport and energy generation. Despite its importance, most of this energy is generated from limited fossil fuel resources that release pollutants and contribute to local and global environmental issues such as nitrogen oxide's destruction of the ozone layer and carbon dioxide's contribution to global warming.

Air transport is an important enabler to achieving economic growth and development. Air transport facilitates integration into the global economy and provides vital connectivity on a national, regional, and international scale. It helps generate trade, promote tourism, and create employment opportunities. The World Bank has financed aviation-related projects for over sixty years.

To improve operational efficiency and reduce launch costs for next-generation space transportation systems, rocket engines must be designed with high performance and low system complexity. With intense competition in the space transportation industry, current launcher systems, such as the European Ariane 5, utilize parallel staging. However, the main engine's operation over a wide range of altitudes results in off-design operation, causing a significant performance loss in conventional bell-type nozzles due to flow over- or under-expansion from fixed exit area ratios.

This can result in over 10% loss in specific impulse compared to an ideal contour nozzle. To address this issue, various altitude adaptive nozzle concepts have been proposed in the literature, with the most promising being the dual bell nozzle.

A rocket engine uses a nozzle to accelerate hot exhaust to produce thrust as described by Newton's third law of motion. The amount of thrust produced by the engine depends on the mass flow rate through the engine, the exit velocity of the flow, and the pressure at the exit of the engine. The value of these three flow variables are all determined by the rocket nozzle design.

A nozzle is a relatively simple device, just a specially shaped tube through which hot gases flow. Rockets typically use a fixed convergent section followed by a fixed divergent section for the design of the nozzle. This nozzle configuration is called a convergent-divergent, or CD, nozzle. In a CD rocket nozzle, the hot exhaust leaves the combustion chamber and converges down to the minimum area, or throat, of the nozzle. The throat size is chosen to choke the flow and set the mass flow rate through the system.

In this research, Ansys Fluent software is used as CFD (Computational Fluid Dynamics Software) to investigate and study the combustion products flow field in a dual bell Nozzle, as well as the evolution of the different thermodynamic parameters. This includes: the pressure, temperature, density, Mach number, etc.

Recently, the Ansys Fluent code has emerged as one of the most widely used tools for simulating all phenomena in the energy industry and research.

Rocket motor design relies heavily on Computational Fluid Dynamics (CFD). In traditional design methods, engineers utilize their experience to modify initial prototypes and then evaluate these modified configurations using CFD solvers. Typically, this process involves multiple iterations and a trial-and-error approach to arrive at the best design. This can be time-consuming and uncertain, and may involve sacrificing design reliability by using simplified models for flow analyses.

Our dissertation is structured as follows:

- A general introduction where we talk about energy problems encountered on a global scale
- In the first chapter, we refer to the different works carried out in the Combustion field and Rocket engine nozzle analysis
- Chapter two is devoted to general information on combustion.
- Chapter three is devoted to nozzle flow analysis.

Chapter I: Bibliographic search

I- Introduction:

In this chapter we present the previous numerical and experimental work carried out in the field of combustion as well as the Rocket Engine Nozzle analysis.

II- Previous works in Rocket engine combustion:

Edward et al. (2003) described the evolution of liquid fuels for past 100 years for aircraft and rockets as the engines and vehicles they fuel have undergone these significant increases in performance **[1]**.

Starting from the basic design aspects of a rocket combustion chamber and engine, **Haidn, O.J. (2008) [2]**. presented a detailed overview of the rocket engine, injection system, combustion chamber, its cooling, characteristics of different propellants based on their performance followed by the concept of advance nozzle design which are being used in the propulsion technology to enhance the performance of the launch vehicle. Various possibilities to improve thrust chamber cooling techniques involving new materials such as CuCrNb, ceramic matrix composites or effusion cooling were explained, the different aspects shown. Additionally, the advantages and the basic features of an advanced nozzle concept for a main stage engine, the dual bell nozzle was described and the current statues of technology explained.

The combustion analysis of H2/O2 flame structure under various flow conditions was carried out by **Guillaume Ribert et al. (2008) [3]**. During the combustion of H2/O2 counter flow specifically H2/O2 flames are investigated at pressures of 1–25 MPa and oxygen inlet temperatures of 100 and 300 K. Results concluded that the flame thickness and heat release rate correlate with the square root of the pressure multiplied by the strain rate. In his findings it was also concluded that considering three cases for the fluid formulation i.e. (i) ideal gas, (ii) partial real fluid and (iii) real fluid, the flame temperature for case (i) and (iii) was close to adiabatic flame temperature.

Daniel T. Banuti et. al (2010) [4] studied the effect of injector wall heat flux on cryogenic injection with the experiments at different combustion pressure and found that for cryogenic jets, a moderate change in temperature is accompanied by a drastic change in density.

Shabanian S. R. et al (2010) [5]. investigated the effect of operational and geometrical conditions for hydrogen/air premixed combustion in a micro scale chamber including; combustor size, wall conductivity, reactant flow rates and hydrogen feed splitting on combustion stability and outlet gas temperature. It was find out that the flame temperature increased sharply with increasing of feed flow rate at low flow rates due to the fact that the increase of inlet velocity. After a specific mass flow rate the temperature becomes constant and further feed lead to decrease in the temperature.

K. M. Panday et al. (2010) [6].worked on CFD analysis of pressure and temperature for a rocket nozzle with liquid Pantane and air as fuel and oxidizer with two inlets at Mach 2.1 and

concluded that the fuel and air enter in the combustion chamber and burning takes place due to high velocity and temperature and then temperature increases rapidly in combustion chamber and convergent part of the nozzle and after that temperature decreases in the exit part of the nozzle. Based on the result in his study, it was concluded that two inlet rocket nozzle is having better performance than single inlet.

D. Cecere et al. (2011) [7]. Have conducted a research work on hydrogen/air supersonic combustion in Hyshot II Scramjet. They have investigated in particular the fundamental physics of mixing, combustion and vorticity generation as well as the interaction between shock waves, boundary layer and heat release are analyzed by means of 3D Large Eddy Simulations (LES) using detailed chemistry. Results show very complex structures due to the interaction between the four sonic H2 crossflow injections and the airstream flowing at M = 2.79.

V.B. Betelin et al (2013) [8].have created a supercomputer modeling code of Hydrogen-oxygen combustion in Rocket engines. The code resolves hydrogen combustion chemistry in a sufficient way to model anomalous behavior of ignition delay times versus pressure. Within one and the same solver it was made possible to model establishing slow diffusion and kinetic combustion modes, as well as onset of detonation modes. Verification and validation of the code were carried out. Investigations showed that dependence of ignition delay time on pressure for hydrogen – oxygen mixtures is not monotonous and has three characteristic regions.

V.B. Betelin et al (2014) [9]. Have again worked on a Mathematical simulation of Hydrogen-Oxygen combustion in rocket engines using LOGOS code. Predictive modeling 3-D code was developed to simulate chemically reacting turbulent flows. The code was tested on simulating model combustion chamber fed by hydrogen and oxygen. Unstable regimes in rocket engines and their stabilization were studied. Chocking regimes in rocket engines were detected under definite initial conditions.

As investigated by **N.N Smirnov et al (14) (2007) [10]**. One of peculiarities of hydrogen–oxygen rocket engine is the following. On injecting liquid components fuel (hydrogen) having much lower critical temperature comes pre-evaporated and pre-heated in combustion chamber, while oxygen could be liquid then evaporating inside the chamber. Thus contrary to most types of engines, hydrogen engine has an inverse mixture entering combustion chamber, in which fuel is gaseous and oxidant is liquid.

Flame temperature in a combustion chamber is an important parameter to analyze the interaction between flow and combustion. **Liu et al.** (2019) **[11]** investigated the role of temperature on supersonic combustion and its ignition in a model scramjet combustor. The formation and development of fire nucleus was a controlling parameter for supersonic combustion ignition.

Zhi-Weei Huang et al (2016) [36] have studied the combustion oscillation, their study reports the combustion oscillation features in a three-dimensional (3D) rocket-based combined-cycle

(RBCC) engine combustor under flight Mach number (Mflight) 3.0 conditions both experimentally and numerically.

Combustion dynamics in liquid rocket engines is investigated by **A. Urbano et al (2016) [37]** by making use of a combination of Large Eddy Simulation and acoustic modal identification. Calculations are carried out in a model scale system comprising an ensemble of shear coaxial injectors feeding the thrust chamber with liquid oxygen and gaseous hydrogen.

Methane–oxygen burning is considered for many future rocket engines for practicality and cost reasons. As this combustion is slower than hydrogen–oxygen, flame ignition and stability may be more difficult to obtain. **Simon Blanchard et al** (2022) **[38]** have created a chemical model of methan oxygen combustion in Liquid Rocket Engine by using ARC (Analytically Reduced Chemistry), which is proposed for accurate chemistry description at a reasonable computational cost.

Combustion simulation was performed **by Min Son et al (2017) [39]** using gaseous methane and oxygen to determine the effects of injection conditions and geometries, especially the recirculation zone near the post, on the combustion characteristics of pintle injectors. A modified six-step JL mechanism and EDC were used to simulate turbulent combustion.

A new real gas/thermally perfect gas LES code using an axisymmetric approximation has been used by **M. Masquelet et al (2009) [40]** to simulate unsteady combustion and dynamics in a representative LOX-GH2 rocket engine consisting of three slot injectors that attempts to match the actual engine conditions. The purpose of this work was to prove the feasibility of such simulations and to assess their accuracy.

An Eulerian–Lagrangian computational approach for two-phase flows has been presented and applied by **Laurent Gomet et al (2014) [41]** to the modelling of turbulent combustion downstream of a liquid oxygen – gaseous hydrogen coaxial cryogenic injector. In this model the spray of LOx droplets is represented within a stochastic Lagrangian framework and a peculiar attention is paid to droplet vaporization and transient heating processes.

III. Previous works in Rocket engine nozzle design and simulation:

The basic configuration of the DBN was first proposed by **Foster et al. [12] in 1949**.

Genin et al. [13], **Schneider et al. [14],** and **Verma et al. [15]** used transient and steady numerical methods to study the different separation positions of the extension nozzle and the hysteresis during the transition and retransition.

However, it has received attention only in the past few decades with the increased interest in SSTO vehicles. For example, in 2010, **Taylor et al. [16]** conducted cold flow and hot gas experiments to study the flow and thrust characteristics of the EDN design. Taylor et al., in another study **[17]**, experimentally compared the thrust performance of EDN and DBN.

Rocket engines used in the first stage of space launchers work from sea-level to almost vacuum conditions. An example is represented by the Vulcain 2 liquid rocket engine used in the Ariane 5 launcher. The area ratio of its nozzle is limited by the necessity to avoid uncontrolled separation and dangerous side loads at lift-off. This limitation has a significant impact on the engine's performance when high altitudes are reached **[18]**.

G. Hagemann et al (1998) [19] have conducted a study on Expansion–Deflection nozzles. The reduction of Earth-to-orbit launch costs in conjunction with an increase in launcher reliability and operational efficiency are the key demands on future space transportation systems, like single-stage-to-orbit vehicles (SSTO). The realization of these vehicles strongly depends on the performance of the engines, which should deliver high performance with low system complexity. Their results were presented for dual-bell nozzles and other nozzles with devices for forced flow separation and for plug nozzles with external free stream expansion.

In order to avoid such limitations of classical bell nozzles, several alternatives have been proposed and studied: nozzles with fixed insert by **G. Luke et al (1992) [20]**, nozzles with temporary insert by **N.Goncharov et al (1992) [21]** nozzles with forced gas injection **V.V Semenov et al (2008) [22]**, plug nozzles by **R.A Wasko et al (2008) [23]**, dual-bell nozzles by **M. Horn et al (1993) [24]**. Among them, the dual-bell nozzle represents a promising solution because of its effectiveness and the minor changes it requires with respect to conventional nozzles.

Tomita et al. [25] conducted experiments on DBNs whose base nozzle and extension nozzle were designed by parabolic method with different extension wall pressure gradients.

High speed compressible flows in supersonic rocket engine nozzles have been the subject of a considerable amount of experimental and numerical studies since the second half of the twentieth century after the first operational application of the famous German V2 missile in 1943 following the work of the German Werner Von Braun. This research has continued and intensified until today in specific research laboratories in different countries such as:

•In the United States:

CHARLES E. TINNEY and AL (2012) from the University of Texas [26] .study that aims to investigate the impact of internal engine corrugated seals on the aerodynamic performance of a

convergent/divergent supersonic nozzle. The seals are designed to protrude into the flow to change the design pressure ratio of the nozzle, promoting mixing. The study measures axial thrust and uses optical flow measurements to visualize the effect of protrusion depth on shock strength and boundary layer thickness at the nozzle exit. The results indicate that the corrugated seals have a positive effect on the thrust coefficient, with an increase of up to 2%, and this effect is observed across a range of nozzle flow states.

JOSEF H. RUF (2010) [27] .study that tested two subscale nozzles for their side load characteristics during simulated nozzle start transients. The nozzles tested were a truncated ideal and a parabolic contour. The study presents measurements of side load moments using a strain tube approach in MSFC's Nozzle Test Facility and explains the processing techniques used to convert the strain gage signals into side load moment data. The study also presents nozzle wall pressure profiles for separated nozzle flow at various nozzle pressure ratios and discusses the effect of the test cell diffuser inlet on the parabolic nozzle's wall pressure profiles. The results show that the peak side load moment for the truncated ideal contour was 45% of that of the parabolic contour. The study also discusses the impact of facility vibration and a minor fabrication flaw in the nozzle contours.

TEN-SEE Wang (2009) (NASA Marshall Space Flight Center) [28]. Investigation of Flow Characteristics inside a Dual Bell Nozzle with and without Film Cooling Mayank Verma, Nitish Arya, Ashoke study where a simulation was performed to understand the film cooling process in a dual bell nozzle. The secondary stream was injected at different locations on the nozzle wall, and the impact of injection location on film cooling was evaluated. The cooling effect was demonstrated through temperature and pressure distributions on the nozzle wall and downstream of the injection point, where the mixing of the main flow and secondary flow was observed. The inflection region was identified as the most promising location for injection, and the effect of Mach number of the secondary stream was investigated. The study showed that the separation point in a dual bell nozzle can be controlled with the help of secondary injection, allowing for optimization of thrust.

DIMITRI PAPAMOSSCHOU and AL (2009) from the University of California [29].discusses the separation of supersonic flow in a convergent-divergent nozzle, which is a fundamental fluid phenomenon with a wide range of applications. When a supersonic nozzle is operated at pressure ratios below its design point, flow downstream of the shock wave separates from the nozzle walls. Although flow separation is usually seen as an undesired occurrence, it can have some interesting applications in fluid mixing. Past research at the University of California, Irvine has shown that flow exiting an over expanded nozzle has a strong instability that can enhance the mixing of the flow itself and be used as a fluidic actuator to enhance the mixing of an adjacent flow. While much literature on nozzle flow separation focuses on predicting separation location in rocket nozzles.

Craig A.HUNTER (1998) (NASA Langler Research Center) [30]. Describes the implementation of a new porous condition in the PAB3D solver to simulate the flow over porous surfaces. The condition is used to compute the flow field of a convergent-divergent nozzle with porous cavities for shock-boundary layer interaction control. The study compares the flow fields of a nozzle with and without porosity for different nozzle pressure ratios. The results show that porous configurations can control off-design separation in the nozzle and stabilize the exhaust

flow. The article also discusses various computational simulation results, such as wall centerline pressure, mach contours, and thrust efficiency ratio, and indicates that the computed results are in good agreement with experimental data.

Junhui Liu and Yu Yu Khine (AIAA 2020-2561) 8 Jun 2020[31].this stusy discusses nozzle boundary-layer separation in highly over expanded jets and its adverse effects on noise reduction devices around the nozzle lip. Large-eddy simulations are used to study this phenomenon and it is found that accurate predictions require a grid resolution that captures local elongated turbulence structures prior to the separation. Upstream turbulences have a slight effect on the thickness of the boundary layer in the divergent section and shift the separation location downstream if the boundary layer is laminar. However, if the boundary layer is already turbulent, upstream turbulences do not affect the separation location. Surface roughness does not affect the separation location but allows for a coarser grid resolution to predict the separation. The favorable pressure gradient inside the convergent and divergent nozzle reduces the effect of upstream turbulences on the nozzle boundary-layer development.

The European Union

•In Germany:

GERALD HAGEMANN, RALF STARK, MANUEL FREY, MICHAEL TERHARDT, ANDREAS GROSS, C. WEILAND, NURNBERGER-GENIN, (DLR Lampoldshausen Laboratory) [32]. Discusses the Cold Gas Subscale Test Facility (SSTF) P6.2 located at the German Aerospace Center DLR in Lampoldshausen. The facility is used to test nozzles, diffusers, and ejectors using gaseous nitrogen in an easy, quick, reliable, and effective way. The article showcases some experimental setups with nozzles, diffusers, and ejectors and additional visualization techniques with an infrared camera and color Schlieren of the SSTF. The SSTF was established in late 1998, and its objective was to have a relatively cheap and easy-to-handle configuration to perform tests and study gas dynamic behavior in the field of altitude simulation and flow separation of nozzles. The article also mentions the relation between the model and the original through the Reynolds Number Analogy and Mach number. If the Reynolds Number is similar to the model, one can transform the results from the SSTF directly to the original.

• In Sweden (Sweden):

JAN OSTLAND and AL (Volvo Aero Corporation) June 2004[33]. The article discusses the challenges in developing rocket nozzles with higher performance due to flow separation and resulting side-loads. The article explains how different methods have been suggested to control separation, but none have been implemented in full-scale due to uncertainties in predicting flow phenomena. The article describes the methods used in investigating the causes of flow separation and side-loads, including sub-scale testing of model nozzles operated with air. The article also provides a comprehensive review of supersonic flow separation and side-loads in internal nozzle flows and discusses different approaches for predicting these phenomena. The article concludes by discussing future directions of research, including active and passive flow control in rocket

nozzles. The work was performed at VAC's Space Propulsion Division within the framework of European space cooperation.

•In Italy:

MARCELLO ONOFRI, FRANCESCO NASUTI and all (University of Rome: La sapienza) [34].discusses the use of dual-bell nozzles for improving the performance of large liquid rocket engines for launcher first stages. The study focuses on the impact of the second bell shape on the side loads that can occur during the transition between the two main operating modes of the nozzle. The analysis is performed using a validated turbulent Navier-Stokes solver and geometries generated by the method of characteristics. The design of the second bell profile is critical and results obtained from suitable test cases are used to discuss the design. The results reveal that different geometries designed by the method of characteristics result in modest performance changes but severe differences in behavior during the transition phase.

•In Spain:

JOSE A. MORINIGO (2004), JOSE J. SALVA [35].discusses the importance of understanding the two different separation modes in TOC (Thrust Optimized Contour) nozzles for rocket engines used in space launchers. The transitions between these modes can cause strong lateral forces that may lead to engine failure and risk for the vehicle. The simulation methodology used for this investigation involves solving the compressible three-dimensional Reynolds averaged Navier-Stokes equations on multiblock structured grids. The results confirm the existence of two stable separation modes and show the hysteresis loop in the sub-scale J2S nozzle, which is consistent with reported experimental data and numerical studies. The effect of the contour shape on the cap-shock structure has been explored, and the analysis identifies the direct contact of the inner shock with the Mach disk as the mechanism that produces the sudden transition towards the cap-shock.

CHAPTER II: COMBUSTION

II.1. Definition:

Nearly 90% of the world's energy needs (transportation, production, electricity, heating...) is provided by combustion. The study of combustion phenomena is obviously important in an enclosed fire or natural environment, but Better understanding of the phenomena involved in the combustion process also optimizes unit operation and energy efficiency industry, especially by restricting consumption. In the end, this is what we care about more specifically, knowledge of these phenomena allows predict the formation and evolution of pollutants to better control them Emissions and their discharge into the atmosphere.

Combustion is a chemical reaction that occurs when oxygen in the air, fuel, and a heat source combine. Combustion is an exothermic reaction (exothermic reaction). It is manufactured in an "open" system or a "closed" system (i.e. no heat and mass exchange with the external environment). Overall, this is a chemical reaction that only occurs when chemical species interact or are willing to modify each other. Combustion is also a reaction in which combustible substances are oxidized by oxygen (combustibles), the products of which are called smoke or unburned. [42]

Two important combustion regimes can be distinguished [43].

II.1.1.Deflagration (Very Fast):

This is a fast process that requires less than 1ms for 80% completion. It is characterized by the presence of a flame which propagates through the unburned mixture. A flame can be defined as a rapid chemical change occurring in a very thin fluid layer, involving steep gradients in temperature and species concentrations, and accompanied by luminescence. From a macroscopic point of view, the flame front can be considered as an interface between the burnt gases and the unburned mixture.

Compared to the unburned mixture, the burnt gases are much higher in volume and temperature, and much lower in density. The waves of

Deflagration in air-fuel mixtures normally propagate at speeds below 1 m/s. All flame processes that occur in the combustion chambers of gas turbines fall into this category. [43]

II .1.2.Detonation (instant)

The characteristic of the detonation is a shock wave which is connected and supported by a zone of chemical reaction. Detonation waves travel at supersonic speeds, ranging from 1 to 4 km/s. They cannot occur in conventional air-fuel mixtures used in gas turbine combustors, but the possibility could arise in situations where oxygen injection is used to aid ignition and acceleration. Of the motor. Currently, pulse detonation engines are of interest to the military and these engine combustion chambers use detonation waves. [43]

II .2.The Fire Triangle

Fire Triangle is a diagram which represents the three components that creates a fire such as Oxygen or Air, Fuel and Heat (source of ignition). Absence of any of the components, fire would not occur.

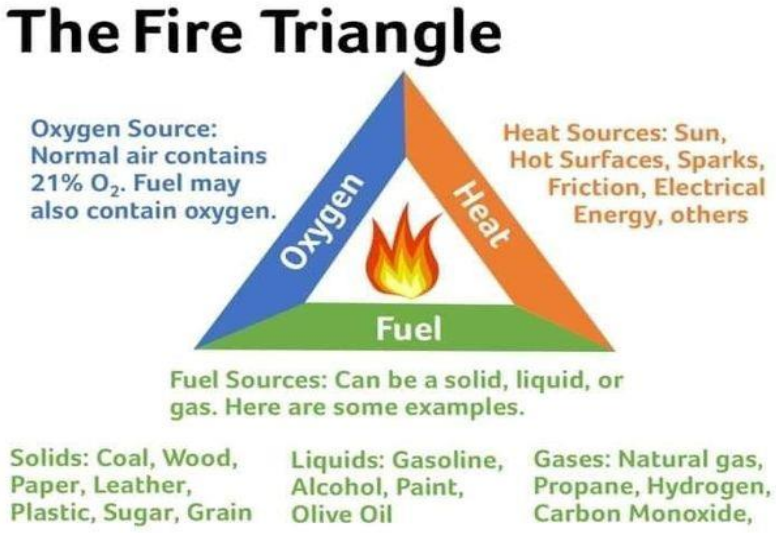

***Figure (*II*. 1)**: the fire triangle showing the association of the three essential elements for chemical combustion*

II .2.1.The fuel

It is a substance that can burn in the presence of an oxidizer, is often an organic product, that is to say composed mainly of carbon and hydrogen (eg: methane, gasoline, alcohol ...), In our study we will use methane CH4 as fuel. [43]

II.2.2.The oxidizer

In general, ambient air, especially oxygen, is a good oxidizer. [43]

II.2.3.Source of ignition:

Generally heat or a flame, for example that produced by a spark. [43]

II .3.Different types of Combustion:

II .3.1-Fast Combustion:

Flash fire is a form of combustion in which a large amount of heat and energy is released in the form of light, causing a fire. It is used in some machines, such as internal combustion engines or thermo baric weapons. [43]

II .3.2-Slow Combustion:

Smoldering is a reaction that results in low heat release, little temperature rise, and no flame. [43]

II .3.3-Complete combustion:

During complete combustion, the reagents react with the oxidizing agent to form products that can no longer be oxidized by the oxidizing agent: these products have reached a level of stability that cannot be altered by the combustion reaction. [43]

II .3.4-Incomplete combustion (lack of air):

Incomplete combustion occurs when there is not enough oxidizer to completely react the fuel or when the contact time at temperatures where combustion is possible is too short. It therefore produces combustion residues, smoke in the form of ash, some of which are highly toxic to humans and the environment, such as carbon monoxide (a deadly gas), pure carbon particles (soot, tar, and ash), nitrogen oxides, hydrocarbon (carcinogens such as benzene, or highly toxic substances such as polycyclic aromatic hydrocarbons), and volatile organic compounds. [43]

II .3.5-Stoichiometric combustion:

Under these conditions, stoichiometric combustion occurs when the amount of oxygen introduced into the reactor is exactly equal to that required for complete combustion of methane (CH4); the products of complete combustion are mainly carbon dioxide, nitrogen and water vapour. [43]

II .4.Parameter and characterization of a flame

The notion of flame encompasses different processes and can be characterized using different parameters which have the advantage of allowing classification. The three main parameters are:

-The nature and number of reagents;

- The mode of introduction of the reagents;

-The gas flow regime in the reaction medium. [43]

II .5.Classification of flames

There are several classifications of flames, but in our work we are interested in two main classifications

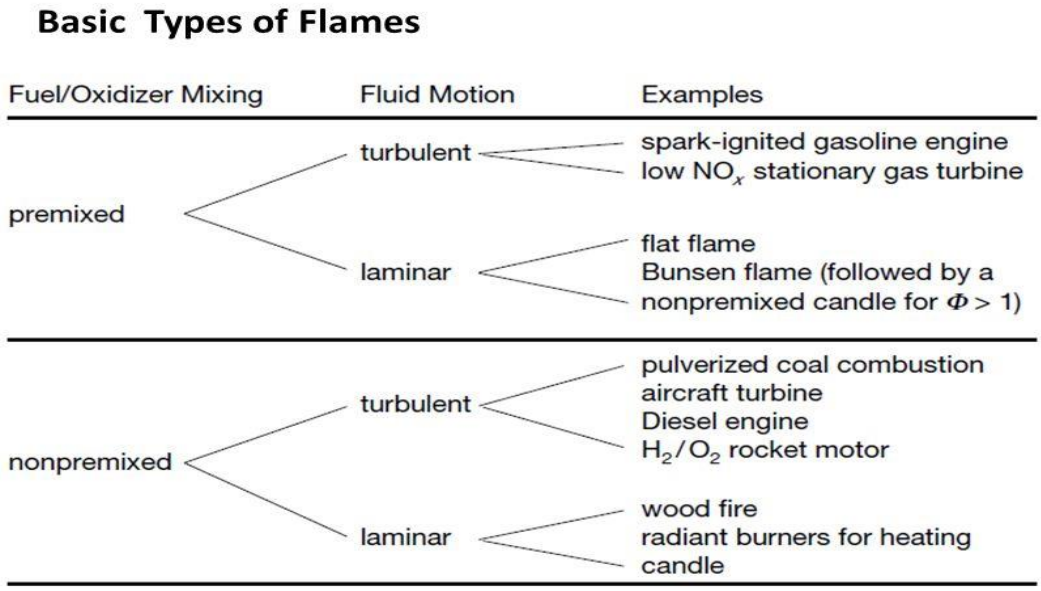

Figure (II. 2): *types of flame*

II.5.1-Classification according to mixtures:

Two situations generally encountered are identified depending on the procedure used to introduce the reactants into the flame zone. They are shown schematically in figure (2).

II .5.1-1-The premixed combustion

Fuel and oxidizer are pre-mixed before reaching the flame front. This mode is often used in a lean mixture, thus increasing efficiency and reducing the production of NOx. This type of flame increases the risk of explosion which comes from the storage mode of the reactive mixture. [44]

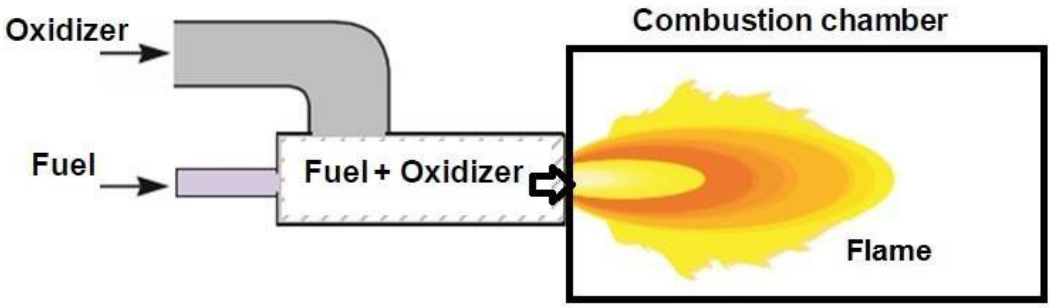

Figure (II. 3): *Premixed combustion*

Let us define a dimensionless scalar variable or progression variable c such that c = 0 on the unburned mixture side and c = 1 on the burnt gas side. For example, if Tu is the unburnt gas temperature and Tb is the burnt gas temperature, then the dimensionless temperature can be defined as follows:

$$c = \frac{T - T_u}{T_b - T_u} \qquad \textbf{(II.1)}$$

The progression variable could be any scalar, i.e. we could have chosen the concentration of a reactant as the progression variable. Since the reaction sheet is infinitely thin, at any point in the flow field, we can find that the value of c is either unity or zero. The transition from zero to unity occurs instantly at the reaction sheet. Therefore, the probability density function for the progression variable is given by:

$$P(c, x, t) = \alpha(x, t)\,\delta(c) + \beta(x, t)\,\delta(1 - c) \qquad \textbf{(II.2)}$$

By definition, the normalization condition leads to: $\alpha(x, t) + \beta(x, t) = 1$ **(II.3)**

It can be seen that the mean progression variable,

$$\bar{}(x,t) = \int_0^1 \mathrm{cP(c,x,t)dc} = (x,t) \qquad \textbf{(II.4)}$$

is nothing but the probability of finding burnt gas at location x and time t. The density function is completely described by the average advancement variable, as we can write (removing the variables x and t):

$$P(c) = (1-\bar{c})\delta(c) + \bar{c}\delta(1-c) \qquad \textbf{(II.5)}$$

Assuming constant pressure and constant molecular weight, it can be shown that the ideal gas law reduces to this:

$$\frac{\rho}{\rho_u} = \frac{\mathrm{T_u}}{\mathrm{T}} = \frac{1}{1+\mathrm{rc}} \qquad \textbf{(II.6)}$$

Where r is the heat release parameter. Using the relationship above, the average density can be calculated as follows:

$$\frac{\bar{\rho}}{\rho_u} = 1 - \beta + \frac{1}{1+\mathrm{r}} \qquad \textbf{(II.7)}$$

The Favre mean of the progression variable is given by:

$$\boldsymbol{c} \equiv \frac{\bar{\rho}\mathrm{c}}{\bar{\rho}} = \frac{\rho_u}{\bar{\rho}}\frac{\beta}{1+\mathrm{r}} \qquad \textbf{(II.8)}$$

Combining the two expressions, we get:

$$\bar{\mathrm{c}} = \beta = \frac{(1+\mathrm{r})\tilde{c}}{1+\mathrm{r}\tilde{c}} \qquad \textbf{(II.9)}$$

And so:

$$\alpha = \frac{1-\tilde{c}}{1+r\tilde{c}} \qquad \textbf{(II.10)}$$

The average density is:

$$\rho = \frac{\rho_u}{1+\mathrm{r}\tilde{c}} \qquad \textbf{(II.11)}$$

[48]

II .5.1-2-The Non-premixed combustion (Scattering flames)

The fuel and the oxidizer are injected differently; the resulting flame front is positioned in the meeting zone of the two currents. Easier to master. These flames have the disadvantage of producing a large quantity of pollutants because the temperatures reached on the flame fronts are generally high. [44], the instantaneous thermochemical state of the fluid is related to a conserved scalar quantity known as the mixing fraction. The mixing fraction can be written in terms of mass fraction as follows [48]

$$f = \frac{Z_i - Z_{i,ox}}{Z_{i,fuel} - Z_{i,ox}} \quad \textbf{(II.12)}$$

Where: Zi is the elemental mass fraction for the element, i. The subscript ox indicates the input value of the oxidizer current and the subscript $fuel$ indicates the input value of the fuel current. If the diffusion coefficients of all species are equal, this equation is the same for all elements, and the definition of the mixing fraction is unique, f. The mixture fraction is therefore the elementary mass fraction that comes from the fuel flow.

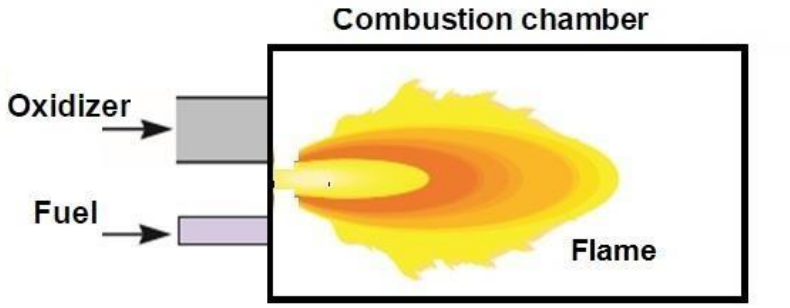

Figure (II.4): *Non-premixed combustion*

Assuming equal diffusivities, the species equations can be reduced to a single equation for the mixing fraction, f. The reaction source terms in the species equations cancel (since elements are conserved in chemical reactions), and so f is a conserved quantity. While the assumption of equal diffusivities is problematic for laminar flows, it is generally acceptable for turbulent flows where turbulent convection overwhelms molecular diffusion. The equation for Favre's average mixing fraction (average density) is:

$$\frac{\partial}{\partial t}(\rho f) + \nabla.(\rho \vec{v} f) = \nabla.\left(\frac{\mu_t}{\sigma_t}\nabla f\right) + S_m + S_{user} \quad \textbf{(II.13)}$$

The source term Sm is due solely to mass transfer into the gas phase from liquid fuel droplets or reacting particles (e.g. coal).

$Suser$ is any user-defined source term.

In addition to solving the average Favre mixture fraction, a conservation equation for the mixture fraction variance, $\overline{f'^2}$

$$\frac{\partial}{\partial t}(\rho\overline{f'^2}) + \nabla.(\rho v\overline{f'^2}) = \nabla.\left(\frac{\mu t}{\sigma t}\nabla\overline{f'^2}\right) + c_g u_t(\nabla\overline{f}')^2 - c_d\rho\frac{\varepsilon}{k}\overline{f'^2} + Suser \quad \textbf{(II.14)}$$

Where $f' = f - \overline{f}'$. The default values of the constants σt, Cg, Cd are respectively 0.85, 2.86 And 2.0 and $Suser$ is any user-defined source term.

II .5.1-3-Partially premixed combustion

In terms of mixing, there are two extremes: Premixed combustion where the fuel and oxidizer are completely mixed before they enter the combustion chamber and non-premixed combustion where the fuel and oxidizer enter separately. We have dealt with these two cases in the two preceding paragraphs. In technical applications, however, the optimum is often somewhere between the two extremes, trying to take advantage of the advantageous characteristics of both while avoiding their negative effects. If the fuel and the oxidizer enter separately, but partially mix under the effect of turbulence, the combustion takes place in a stratified medium, once the mixture is ignited. Such a mode of combustion is traditionally called partially premixed combustion. [44]

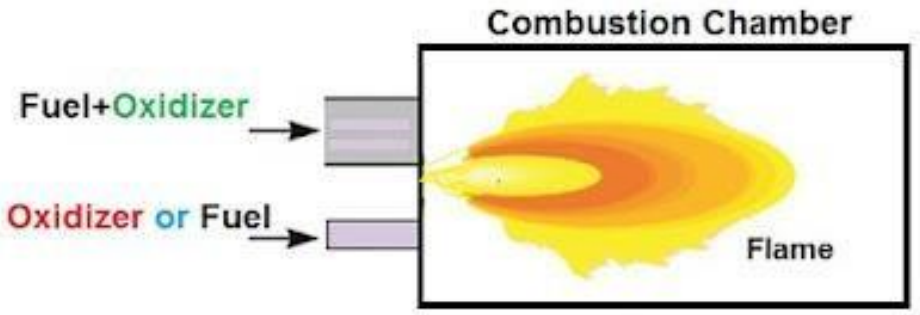

Figure (II. 5): *Partially premixed combustion*

Methods of introducing reagents:

Depending on the mode of introduction of the fuel/oxidizer mixture, a distinction is made between:

• The premix flames for which the reactants are previously mixed before the introduction and initiation of combustion at the level of the burner. In these flames controlled by chemical and thermal processes, the rate of propagation is determined by the oxidation reactions that occur in the flame front;

• The diffusion flames for which the meeting of the fuel with the oxidizer is at the burner outlet. In these process-managed flames physics of material transfer, the speed of propagation is controlled mainly by molecular diffusion phenomena. [44]

II .5.2-Classifications according to flow types:

The gas flow regime in the reaction medium also makes it possible to classify flames into two categories, laminar flames and turbulent flames. The transition between the two types of flow is observed for a certain value of the number Of Reynolds (Equation. (1.1)):

$$\mathcal{R}e = \frac{\rho V X}{\mu}$$

(II.15)

-ρ: the density of the gas mixture (g.m -3);

- V: gas flow velocity (m. s -1)

- X: the critical dimension of the system (in the case of a flow in a cylindrical pipe; x is the diameter of the tube (m));

- μ: the dynamic viscosity (g.m -1. S -1).

✦ The flow is said to be laminar when the Reynolds number is less than 2300. In this type of flame, the reaction zone depends on the coupling between the phenomena of convection, chemical kinetics and molecular transfer processes.

✦ The flow is said to be turbulent if the Reynolds number is greater than 2300. The increase in the flow velocity, and therefore in the Reynolds number, generates friction forces on the walls which cause the formation of "turbulence". Consequently, in a flame of this type, the reaction medium can no longer be considered homogeneous. [45]

The flow is said to be laminar when the Reynolds number is less than 2300.

In this type of flame, the reaction zone depends on the coupling between the phenomena of convection, chemical kinetics and molecular transfer processes. The flow is said to be turbulent if the Reynolds number is greater than 2300. The increase in speed flow, and therefore the Reynolds number, generates friction forces on the walls which cause the formation of "turbulence". Consequently, in a flame of this type, the reaction medium can no longer be considered homogeneous. [46]

To fix ideas, figure (2) summarizes these four generic situations and Associated with some industrial applications.

II.6-The Power and Challenges of Computational Fluid Dynamics in Combustion Analysis:

Computational models can help predicting flame composition, regions of high and low temperature inside the burner, and detailed composition of exit by-products. Detailed computational results can also help better predict the chemical structure of flames and understand flame stabilization processes. These capabilities make Computational Fluid Dynamics (CFD) an excellent tool to complement experimental methods for understanding combustion and thus help in designing and choosing better fuel composition according to the specific needs of a burner. With the advent of more and more powerful computing resources, better algorithms, and the numerous other computational tools in the last couple of decades, CFD has evolved as a powerful tool to study and analyze combustion. However, numerous challenges are involved in making CFD a reliable and robust tool for design and engineering purposes. The numerical simulation is a useful tool because it can easily apply various conditions by simply changing the parameters. Methane is the simplest hydrocarbon fuel available; several studies have focused on methane-air flames. [45]

II.6.1-Role of the combustion chamber:

✓ Increase the total energy of the air by combustion.

✓ Ensure the transformation of the chemical energy contained in the air-fuel into thermal energy.

✓ Cool the burnt gases before the turbine. [47]

II.6.2-Combustion problems:

The combustion chamber is very difficult to design and build because the modeling numerical data of the aerodynamic and thermal phenomena that take place in the room are very tricky to implement. [47]

II.6.3-Construction constraints of the combustion chamber:

✓ Reduce pollutants leaving the room.

✓ Reduce carbon emissions (smokes).

✓ Reduce the weight and size of the chamber.

✓ Increase the resistance to thermal stresses of the chamber and reduce the load losses.

✓ Ensure good efficiency and good combustion stability.

✓ Obtain combustion whatever the altitude and operating speed of the engine.

✓ Reduce the temperature of the burnt gases. [47]

Figure (II.6): Comparison of different types of combustion chambers [47]

Type	Advantages	Disadvantages
Tubular	1. Mechanically robust. 2. Fuel flow patterns and of air are easily matched. 3. Platform testing does not require only a small fraction of the total engine air mass flow. 4. Incurs a light problem round.	1. Bulky and heavy. 2. High pressure loss. 3. Requires interconnects.
Annular	1. Minimum length and weight. 2. Minimum engine frontal area. 3. Minimum pressure loss. 4. Easy light ride.	1. Serious buckling problem on the exterior coating. 2. Platform tests require air mass flow engine complete. 3. Difficult to match fuel flow patterns and of air. 4. Difficult to maintain a stable outlet temperature.
Can-annular	1. Mechanically robust. 2. Fuel flow patterns and of air are easily matched. 3. Platform testing does not require only a small fraction of the total engine air mass flow. 4. Low loss of pressure. 5. Shorter and lighter than tubular combustion chambers.	1. Less compact than annular. 2. Requires interconnects. 3. Incurs a light problem round

II.7-The fuel equations:

The combustion of the fuel being the source of motricity in the engine. The origin of this kinetics being the combustion of the fuel which results in a chemical reaction. This chemical reaction makes it possible to first estimate the quantities of toxic products emitted into the atmosphere and also between the calculations that can lead to the determination of the performance of the engine. [48]

II.7.1-Methane:

Methane is a chemical compound with the chemical formula CH4 discovered and isolated by Alessandro Volta between 1776 and 1778. It is the simplest hydrocarbon, and the first term in the family of alkanes. Under normal conditions of temperature and pressure, methane is a colorless and odorless gas. About twice as light as air, it is explosive in a confined environment (firedamp). In an unconfined environment it dilutes in the air and escapes to the upper atmosphere, where it has fewer tendencies to form explosive clouds than gases heavier than air (propane, butane); however, it is a greenhouse gas. Methane is a fuel that makes up to 90% of natural gas. Its auto-ignition temperature in air is 540°C.

Chemical formula of methane: CH4

Molar mass: 16.04g/mol; C=74.87%, H=25.13% [48]

The combustion of methane:

$$CH_4+2(O_2+3.76N_2) \rightarrow CO_2+2H_2O+7.52\ N_2 \qquad \textbf{(II.16)}$$

II.7.2-Hydrogen:

First element in the periodic table. Under normal conditions it is a colorless, odorless and tasteless gas, made up of diatomic molecules, H2. The hydrogen atom, symbol H, consists of a nucleus with one unit of positive charge and one electron. Its atomic number is 1 and its atomic weight 1.00797. It is one of the main compounds of water and all organic matter, and it is widely distributed not only in the earth but also in the entire universe. Hydrogen is the most flammable of all known substances. At normal temperature it is not a very reactive substance but at high temperatures it is strongly reactive. [48]

The combustion of hydrogen:

$$2H_2+O_2 \rightarrow 2H_2O \qquad \textbf{(II.17)}$$

II.7.3-Kerosene:

Kerosene is a flammable liquid mixture of chemicals that are produced in the distillation of crude oil. To produce kerosene, crude oil is distilled in a distillation tower in a process similar to that used to produce diesel and gasoline. It is a medium weight distillate in the refining process,

and can be produced by distilling crude oil (here it is known as straight run kerosene) or by hydrocarbon cracking heavier petroleum (here it is known as cracked kerosene). The chemical composition of kerosene is fairly complex, and it is a complex mixture of paraffins (55.2%), naphthenes (40.9%), and aromatic hydrocarbons (3.9%). Kerosene tends to contain hydrocarbons that have anywhere from 11 to 13 carbons in the chains. Liquid kerosene fuels contain potentially harmful compounds, including hexane and benzene. [49]

The combustion of Kerosene:

$$4C_{12}H_{23} + 71O_2 \rightarrow 48CO_2 + 46H_2O \qquad \textbf{(II.18)}$$

II.8-Technologies and applications:

The uses of combustion and flame phenomena can be classified into five general categories:

• heating devices:

Heating devices for the production of steam (steam, etc.), in metallurgy and in industry in general, use the combustion of gas, wood, coal and liquid fuels. The control of the combustion process to achieve optimum efficiency is ensured by an appropriate ratio and distribution of fuel and oxidizer in the oven, stove, furnace, etc., by the choice of conditions for transporting the heat of the products of combustion towards the heated bodies and by appropriate aerodynamics of the gas flows in the furnace. Radiation contributes to some extent to heat exchange. Since combustion in kilns is a very complex process, only general ideas can be given by combustion theory, so the optimum conditions and kiln design are usually decided empirically. [48]

• Explosives:

Combustion and detonation of explosives are widely used in all kinds of works with mechanical action or explosion as their final goal. The practical applications of explosives are based on the theory of their combustion and detonation.

Combustion of condensed explosives occurs mainly in the gas phase due to their evaporation, sublimation or decomposition and can be treated in terms of the combustion theory of gases, which predicts the rate of combustion, its dependence on temperature and pressure, as well as the parameters determining the combustion regime and the nature of the explosive. The control of combustion and detonation in their practical applications is made possible by the use of theory, as well as the results of experimental research on combustion and detonation. [48]

Figure (II. 7): *Image of explosive*

• Rocket propulsion:

The combustion products of gaseous, liquid or solid propellants in rockets are ejected from the combustion chamber through the nozzle (de Laval) at high speed. Knowledge of the kinetics of chemical processes in the nozzle is essential to determine the required thrust. Thrust decreases with increasing average molecular weight of combustion products. Mixtures of low molecular weight and high heat of combustion are therefore used for rockets. [48]

Figure (II. 8): *Propulsion of a rocket*

• Chemical reactions:

Flames are used in various ways to produce chemical reactions. An example is the bead test in analytical chemistry. The reducing power of a flame that does not contain enough oxygen is used to a limited extent. The soot produced by some flames is commercially useful, and the making of coke and charcoal depends on careful combustion and flame control. [48]

II.9-HISTORY OF PROPULSION FOR AVIATION

Throughout man's history there has been a constant need for power to move. Whether to hunt for food, to escape predators or enemies, to plow a field, to take goods to trade, to go to war; there has always been a need to get from one place to another. [50]

II.8.1-ANIMAL POWER

Initially the only power available was your own muscles or the muscles of some beast of burden. One could go faster by riding a horse. More power could be had by using teams of horses or oxen or hundreds or even thousands of people, but there were certainly limitations as to what could be done and how fast it could be done. [50]

II.8.2-WATER AND WIND

Water travel allowed for more speed and greater loads, but one had to either row, sail, or go with the current. Men did learn how to sail against the wind, but the wind does not always blow. They built canals to go where they wanted, but speed was a limitation. [50]

II.8.3-STEAM ENGINES

The first steam engine was called an aeolipile ("wind ball") and was invented by a Greek, Hero of Alexandria, in the 1st century AD. Steam entered a ball and exited from one of two bent pipes. This caused the ball to spin, but it was only used as a toy. The first steam device to do actual work wasn't invented until 1698: An engine developed by Thomas Savery in England was used to pump water out of flooded mines. Refinements to the engine were made by Thomas Newcomen in 1712 and James Watt in 1769. [50]

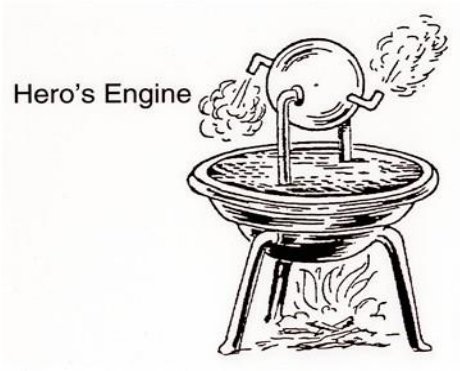

Figure (II. 9): *Aeolipile.*

These engines worked by introducing steam into a cylinder and then cooling it, causing the steam to condense. This created a rapid decrease in the volume of gas present and thus caused a piston to move. Watt's improvement, condensing the steam outside the working cylinder, was so efficient that he is often wrongly credited with the invention of the steam engine. His work brought on the Industrial Revolution. Factories and mills no longer had to be located on a source of water power, and the waywas opened to create self-propelled vehicles.

This new technology was first applied to a vehicle by Nicolas-Joseph Cugnot, a French military engine- near, in 1769. His three-wheeled steam "wagon" was designed to carry cannons, and it ran at almost 3 milesper hour (mph). It was heavy and hard to control, andafter smashing into a wall it quickly lost support.

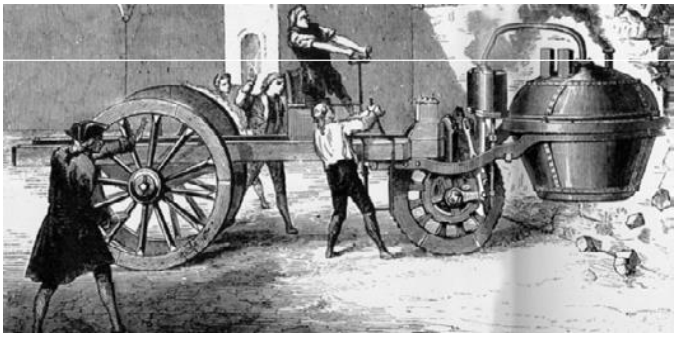

Figure (II.10): *Cugnot steam engine.*

By 1840, however, steam power was in regular use in steam coaches, railroads, and steamboats. Man's greatest dream, to fly through the air like the birds, wasjust starting to appear on scene. Hot air balloons got man into the air, but at the whim of the wind. To usesteam power in a practical way to power an aircraft wasan impossible dream. Steam engines were heavy and required both fuel and water. However, inventors were not deterred, and experimental aircraft using steam engines to turn large fans for propulsion appeared as early as 1882. French engineer Clement Ader built a series of light, steam-powered aircraft. One of these, the E'tole, weighted only 653 pounds (lb), including the operator. Witnesses said that the craft made a few hops, the longest being 165 feet (ft). Ader, however, had nomeans to control the craft. [50]

In the late 1880s American expatriate and inventor of the machine gun, Hiram Maxim, became interested in aviation and actually became the first person to pilot a self-propelled heavier-than-air craft. Spending

£20,000 of his own funds, Maxim had a huge biplane craft constructed. It was about 200 ft from front to rearwith a wingspan of 104 ft. Two 18-ft propellers were each turned by a separate steam engine that produced180 horsepower (hp) and were run from a common boiler. The craft carried four people and weighed an astounding 8000 lb. On July 31, 1894, the craft moveddown its 1800-ft launch rail and actually lifted off. [50]

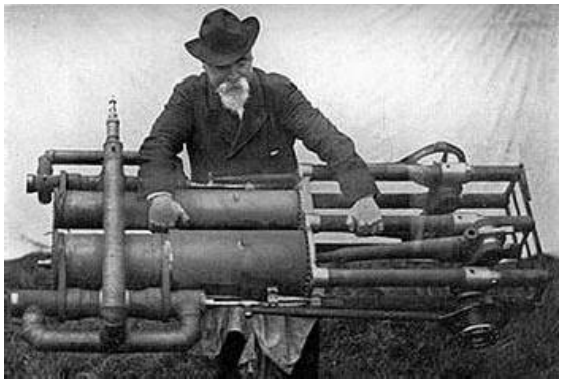

Figure (II. 11): *Hiram Maxim holds one of his steam engines.*

A second restraining rail—set at a height of 9 inches (in.)and designed to keep the craft from gaining altitude—broke, and the craft rose almost 5 ft in the air for a distance of almost 1000 ft before a part of the structurebroke and it crumpled to the ground. Although it lacked any form of adequate control in the air, Maxim's planeshowed that an engine with sufficient horsepower—even steam engines—could make very heavy aircraft fly. [50]

About this time another aviation pioneer, Samuel P. Langley, entered the race for powered flight. In 1897he developed a steam-powered model aircraft that weighed 26 lb and had a 5-ft wing span that flew for over a half mile (mi). Langley's efforts to scale up thisaircraft to be large enough to carry a pilot, however,proved to be very difficult. [50]

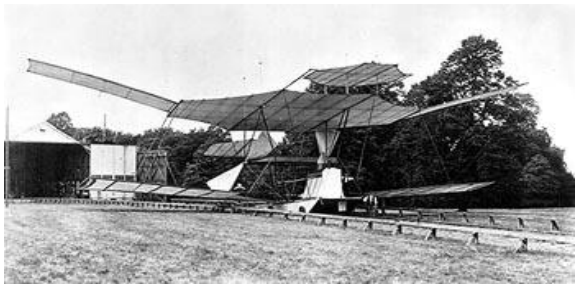

Figure (II. 12): *Maxim's aircraft.*

II.8.4-INTERNAL COMBUSTION PISTON ENGINES

During the period of time from 1860 to 1900 a number of creative people developed a variety of reciprocation piston engines that burned fuel within cylinders. The first patent for such an engine was by Samuel Morey of the United States in 1826. In 1858, Belgium-born Jean Lenoir patented a double-acting piston engine that ran on coal gas. He applied it to a three-wheeled vehicle that he drove 50 miles in 1862.The French inventor Alphonse deRochas created a piston engine that compressed the gas within the cylinderbefore ignition and placed it on a wheeled vehicle in 1862. Siegfried Marcus in Austria did the same in 1864.When removed from a museum cellar in 1950 Marcus'svehicle was still drivable! [50]

In Germany in 1876, Nikolaus Otto patented the Otto cycle four-stroke engine consisting of intake, compression, ignition, and exhaust. Most cars still usethe Otto cycle today. Gottlieb Daimler invented the first"modern" gasoline engine with vertical cylinders and acarburetor, which he patented in 1887. Karl Benz soldhis first gasoline-powered cars in 1887. [50]

During this same time, Samuel Langley had constructed a one-quarter-scale model of his previously steam-powered airplane but with a gasoline engine. Itflew successfully in 1901 and was the first gasoline- powered aircraft. [50]

In 1899, Wilbur and Orville Wright began constructing kites and gliders and unlocking the secrets of aerial control. In 1902 they developed a 32-ft gliderthat could be controlled along all three axes—pitch, roll,and yaw. In just 6 weeks during the winter of 1902–03,along with their mechanic Charlie Taylor, they built alightweight four-cylinder aluminum block engine. They used their own wind tunnel data to design the first true aircraft propellers, which had an airfoil cross section and an efficiency of 66 percent, a great improvement over Maxim's flat blades. On December 17, 1903, theymade the first controlled flight of a powered airplane at Kitty Hawk, North Carolina. [50]

During this same time, Samuel Langley made a full-scale version of his successful quarter-scale model with a 5-cylinder, air-cooled radial engine that produced a remarkable 52 hp. Unfortunately, in two launchattempts in October and December of 1903, his air- craft's structure failed at launch. [50]

During 1904 and 1905, the Wrights built larger engines with increased horsepower. They also furtherimproved their propeller design and by October of 1905 they could remain in the air until they ran out of gas.

Figure (II. 13): *Wright flyer.*

Period of over 30 min. For the next 3 years the Wright brothers stopped flying and concentrated on developing engines and securing patents.

By 1911 the Europeans, some of whom did not honor the Wrights' patents, had made a number of advances in aircraft design and developed many new aircraft. They found tractor propellers (front mounted) to be more efficient than pusher propellers. Theytried 4-, 8-, and 12-cylinder engines as well as 3- and5-cylinder rotary engines. Propellers with two, three,and four blades were also tried as well as propellers with variable pitch, but most engines of the day wereonly powerful enough to drive two-blade propellers. Planes were able to fly over 1100 mi in distance and above 13,000 ft in altitude, and they could stay aloftfor over 28 hours (hr). [50]

In 1913 Igor Sikorsky developed the first fourengine aircraft that could carry 13 passengers. It would eventually create 600 hp and be used as a bomberin World War I. In January of 1914 he flew it from St. Petersburg to Kiev and back, a distance of 1600 mi. The war accelerated aircraft development among theEuropean powers until by 1918 aircraft had reached speeds of up to 140 mph and effective altitudes (op- erating ceilings) of over 20,000 ft. The British SopwithDolphin carried a 300-hp Hispano-Suiza engine, while deHaviland was using a 400-hp American-made Liberty engine in its DH–4 aircraft. [50]

The years after the war saw a number of young former military pilots looking to replace the thrill of combat flying. Some became barnstormers and members of aerial "circuses" while others got involved in air races. The races, especially the Schneider Cup sea- plane trophy races, led various countries to accelerate the development of improved aircraft, particularly in the area of propulsion. Superchargers, which increased thepressure of the air entering the engine cylinders, firstshowed up in 1919 and greatly increased performanceat higher altitudes. These were both mechanical and turbo powered. Another significant development was an engine block with built-in water cooling rather thanexterior tube cooling. This improved the power-to-weight ratio from 1:2 down to 1:1.5, resulting in lighter,more powerful engines. [50]

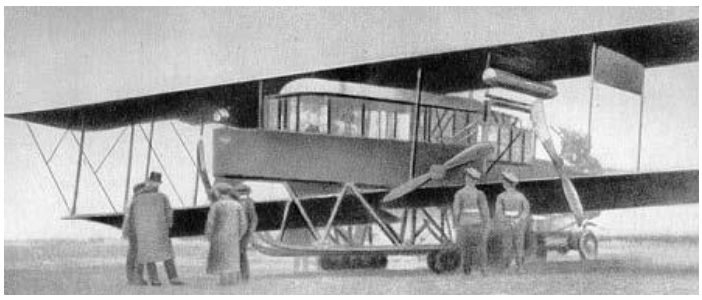

Figure (II. 14): *Sikorsky's four-engine aircraft.*

Advances were made in air-cooled radial engines, which had a much better weight-to-horsepower ratio than in-line engines. The development of the Nation-al Advisory Committee for Aeronautics (NACA) cowl helped to eliminate the drag caused by the large frontal area of a radial engine. Propellers were designed with controlled pitch and constant speed gearing to get maximum power under different load conditions: high-revolutions-per-minute (rpm) fine pitch at takeoff and low-rpm coarse pitch at cruise conditions

By the end of the World War II, speeds of 440 mph andoperation ceilings of 42,000 ft had been reached withpiston-driven engines, producing up to 2200 hp.

Figure (II. 15): *P–51 Mustang.*

II.8.5-TURBINE ENGINES

By the middle of World War II, nearly every variation of piston engines had been investigated. To get more power required more cylinders; this meant more cooling would be needed, and there was also a limit to the speed at which propellers could turn. As the tips approached the speed of sound, shock waves develop,which cause a loss of performance. Thus propellers had to actually be geared down as engine revolutions per minute (rpm) increased. [50]

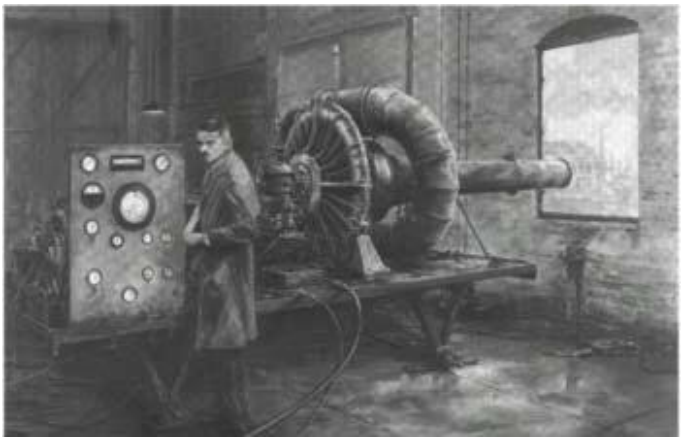

Figure (II. 16): *Frank Whittle demonstrating the first jet engine.*

In 1928 a young Royal Air Force (RAF) cadetnamed Frank Whittle designed a gas turbine engine and took out a patent in 1930. No interest was shown in his ideas because strong enough metals had not yet been developed. By 1937 the alloys were available so Whittle renewed his patent and ground tested his engine. In 1941 it propelled a Gloster E28/39 fighter plane at over 400 mph.During this same time a young German engineer, Hans von Ohain, independently patented a gas turbine engine, and on August 27, 1939, it flew in a Heinkel He178 aircraft. Improvements were made, including attempts at turboprops.

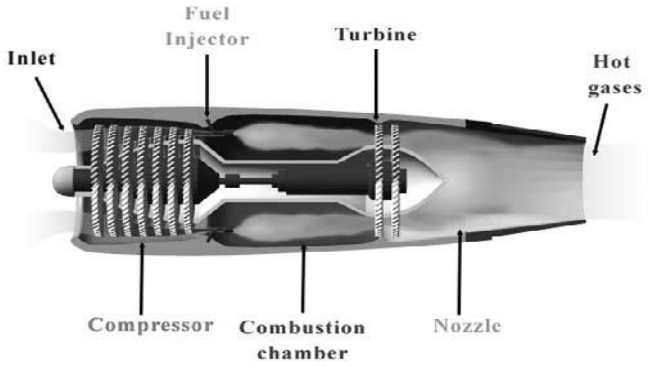

Figure (II. 17): *Turbojet engine.*

Turbine-powered planes (jet planes or turbojets) entered combat near the end of World

War II, but they did not have much of an impacton the outcome of the war.

After the war, development of turbine engines greatly accelerated since they had a much better power-to-weight ratio than piston engines and could run many more hours before maintenance. The first turboprop airline service began in 1948, and the first turbojet airline began in 1952 with the De Havilland Comet. In the 1950s Rolls-Royce introduced the first turbofan engine, the Conway, a low-bypass turbine with a ratio of 0.3:1.0, where 0.3 liters (L) of air went around (bypassed) the engine for every 1.0 L that went through the core for combustion. Today's high-bypassengines will run up to a ratio of 17:1 for bypass air. [50]

II.8.6-ROCKET ENGINES

During World War II, the Germans developed a rocket-propelled plane called a Komet. It was very fast but ineffective mainly due to high fuel consumption. After the war, the Bell Aircraft Company built the rocket-powered Bell X–1. Launched from a B–29 bomber at 23,000 ft, the "Glamorous Glynnis" piloted by Chuck Yeager reached a speed of Mach 1.06, or 1.06 times faster than the speed of sound. This broke the sound barrier for the first time. [49]

Figure (II. 18): *Bell X–1*

In the 1960s theNorth American X–15, a rocket plane, became the firstaircraft to go Mach 6 and fly above 100,000 ft.

Figure (II. 19): *X–15 rocket plane.*

II.8.7-SOLAR POWERED ELECTRIC MOTORS

A NASA program researched high-altitude long- duration flights based on solar power. In 1977 the firstsolar-powered airplane, the "Solar Challenger," flew six miles. In 2001 the 247-ft wingspan solar plane "Helios" built by NASA achieved a height of 98,000 ft. Only rocket planes have gone higher.

Figure (II. 21): *Solar Challenger.*

II.8.8-EXOTIC ENGINES

As man seeks to fly faster, higher, and further into space, new engines have been developed. Ramjets and scramjets fly in the atmosphere in the hypersonic range, scooping oxygen from the atmosphere to avoidcarrying it like rockets. On November 16, 2004, NASA's X–43A unmanned scramjet achieved an astoundingspeed of nearly Mach 10! Ion propulsion engines pro- duce a small amount of thrust by accelerating charged particles. Over a long period of continuous operation they efficiently accelerate spacecraft to extremely highspeeds for deep-space travel. [50]

Figure (II. 22): *NASA X–43A scramjet.*

Figure (II. 23): *Ion propulsion engine.*

II.9-TYPES OF ENGINES

II.9.1-Internal combustion (piston) engines:

For the 40 years following the first flight of the Wright brothers, airplanes used internal combustion engines to turn propellers, which generate thrust. Today, most general aviation or private airplanes are still powered by propellers and internal combustion engines, much like your automobile engine.

As the name implies, the combustion process of an internal combustion engine takes place in an enclosed cylinder where chemical energy is convertedto mechanical energy. Inside the cylinder is a moving piston which compresses a mixture of fuel and airbefore combustion and is then forced back down the cylinder following combustion. On the power stroke the piston turns a crankshaft, which converts the linear (up and down) motion of the piston into circular motion. The turning crankshaft is then used to turn theaircraft propeller. The motion of the piston is repeatedin a thermodynamic cycle called the Otto Cycle, whichwas developed Dr. N. A. Otto of Germany in 1876 and is still used today. For a complete discussion of piston engine operation look at the following Web site [51]

INTAKE:

The first stroke of this four-stroke process is called INTAKE. As the piston moves down from the top of the cylinder, called "top dead center," the intake valve opens and a mixture of air and a very fine mist of fuel, usually gasoline, are drawn into the cylinder at constant pressure. The ideal mixture is about 14.7 parts air to one part fuel. This means that 1 lb of gasoline uses 115 lb of air! In your car engine this fine mist of fuel is sprayed directly into the intake Intake starts back up the cylinder, the EXHAUST stroke begins. The exhaust valve opens residual by a fuel injector. The fine mist of liquid fuel provides a great deal of surface area that can react quickly with the oxygen in the air. [51]

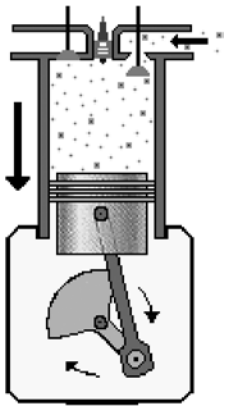

Figure (II. 24): *Intake*

COMPRESSION

The second stroke is COM- PRESSION. When the piston reaches “bottom dead center” the intake valve closes, sealing the cylinder, and the piston moves back up the cylinder. As the volume is decreased, the piston does work on the gas mixture. The fuel- air mixture is compressed to about one-ninth of its volume, raising its temperature and increasing its pressure. Now the gas particles are very close together so they will be able to react quickly when ignited. [51]

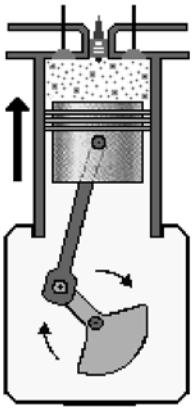

Figure (*II. *25): *Compression*

POWER

As the piston nears top dead center, a surge of high-voltage cur- rent is sent to the spark plug. This produces a high-energy spark, which ignites the compressed air-fuel mixture. The fuel rapidly combines with the oxygen (burns) and produces carbon dioxide gas and water vapor. These hot gases expand and exert tremendous force on the piston, driving down the cylinder and turning the crank- shaft. This is called the POWER stroke, and work is done by the gases. [51]

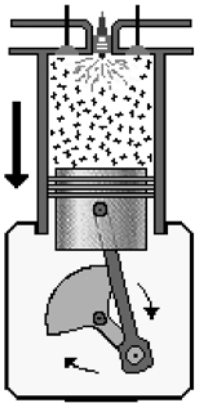

Figure (*II. *26): Power

EXHAUST

Once bottom dead center is reached and the piston Compression Power heat is exchanged (released), and pressure returns to atmospheric conditions. The piston pushes the waste gases out of the cylinder, and the process is ready to begin again. [51]

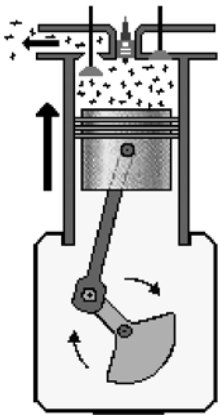

Figure (II. 27): *Exhaust*

The amount of power derived from this type of engine depends on a number of factors. There is no work done by either the intake or exhaust cycle, so half of the strokes of the engine do nothing to add to or subtract from the engine's performance. The remaining strokes determine the work available from the engine.

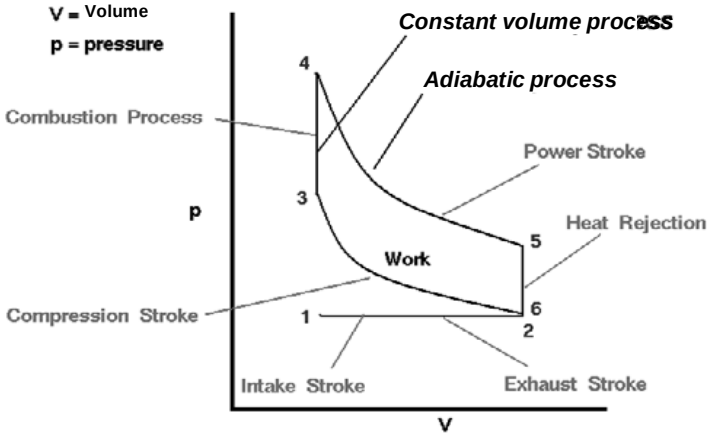

Figure (II. 28): *Ideal Otto cycle. [51]*

In an ideal Otto cycle, as shown on this diagram,the area enclosed between the compression stroke (2–3) and the power stroke (4–5) is the work done by theengine. To increase the amount of work done this area needs to be made larger. Increasing the volume of thecylinder, having more cylinders, raising the pressure, decreasing the volume during compression, or forcing

more air into the cylinder (supercharging) are all waysthis can be accomplished. With aircraft engines these changes cause some problems. Increasing the number or size of the cylinders adds weight to the engine and creates more heat that must be dissipated. Someaircraft engines are air-cooled to save weight, and radial arrangements of cylinders as shown below allow for more cooling but increase drag. Others are water cooled, requiring the additional weight of a radiator and water. Raising the pressure in the cylinders creates more heat, stresses metal, and requires special fuel toprevent knocking. Engineers are always trying to maximize the balance between the positive and negative forces in any processes. [51]

Figure (II. 29): *Radial engine.*

Also note that the Otto cycle is labeled "ideal." In actual operation, gasoline engines are in the range of 30 percent efficient because gases don't burn instantly at constant volume, there are losses due to friction, and much of the heat generated goes to waste in the radiator and exhaust rather than to power.

In turbine engines, air is drawn in and compressed, fuel is added and burned, and the hot gases expand out the rear of the engine, pushing the aircraft forward. Some of these exhaust gases turn a turbine, which drives the compressor. A number of different types of gas turbine engines have been developed for use depending upon the specific needs of a particular type of aircraft.

II.9.2-BASIC TURBINE ENGINES OR TURBOJETS

Turbojets were the first type of turbine engines developed. All the thrust of these engines comes through the turbine and nozzle, which is called the core of the engine. These are what people commonly refer to as jet engines. [49]

The turbojet engine, developed for aircraft in the years prior to World War II, was a departure in thinking from the standard piston engine. Instead of burning fuel in a confined space that is dependent upon precise timing of ignition, the turbojet engine is essentiallyan open tube that burns fuel continuously. According to Newton's Third Law (see "Newton's Laws" in chapter 4, "Physics and Math"), as hot gases expand out from the rear of the engine, the engine is accelerated in the opposite direction. The engine consists of three main parts, the

compressor, the Burner, and the turbine, Along with the inlet, shaft, and nozzle, as shown. [49]

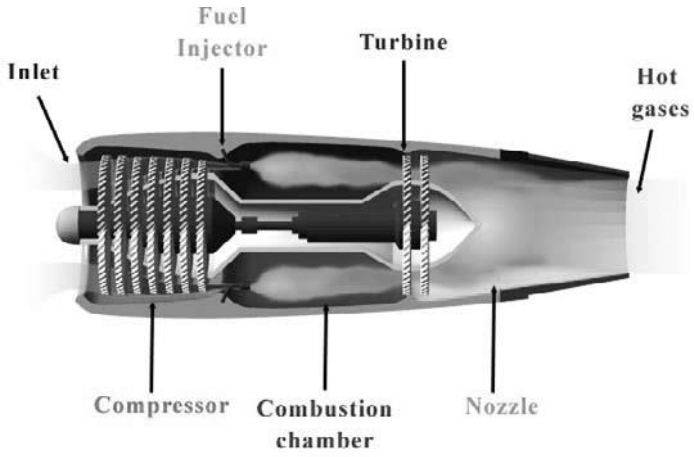

Figure (II. 30): *Cutaway view of turbojet engine.*

A large mass of air enters the engine through the INLET and is drawn into a rotating COMPRESSOR. There are two types of compressors, centrifugal and axial. The axial type is shown above. The compressorraises the pressure of the air entering the engine bypassing it through a series of rotating and stationary blades. As the gas is forced into smaller and smallervolumes, the pressure of the gas is increased.

II.9.3-TURBOFAN

A turbofan is a modified version of a turbojet engine. Both shares the same basic core of an inlet, compressor, burner, turbine, and nozzle, but the turbofan has an additional turbine to turn a large, many-bladed fan located at the front of the engine. This is called a "two-spool" engine. One spool is used to power the compressor and another spool to turn the large fan. Some of the air from this large fan enters the engine core where fuel is burned to provide some thrust, but up to 90 percent of it goes around or "bypasses" the core of the engine. As much as 75 percent of the total thrust of the engine comes from the bypass air. [49]

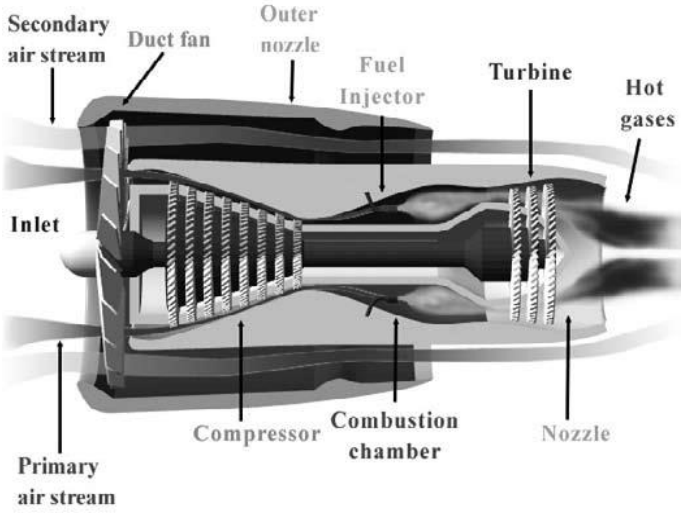

Figure (II. 31): *Cutaway view of turbofan engine.*

Although there is less energy added to this bypass air compared with that going through the core, by moving a very large amount of air the turbofan gets a large boost in thrust for very little additional fuel. It is thus a very fuel-efficient engine and good for cruising. Also, since the fan has many blades and the air is ducted, turbofans can operate faster and more efficiently than simple propeller aircraft. The pressure ratio of a 50-blade ducted fan may be 1.4 to 1.6 (i.e., the pressure is increased by a factor of 1.4 to 1.6), where- as a propeller may have a pressure ratio of only 1.02. This is why large passenger planes using turbofans are able to cruise at high subsonic speeds and still use fuel efficiently. Even jet fighters will often use low-bypass turbofan engines, where a smaller amount of air bypasses the core, so they can conserve fuel while in cruising mode. [50]

II.9.4-TURBOPROP

This engine is a hybrid of a turbojet and a propeller engine. It has at its heart a turbojet core to produce power, but with two turbines. The first turbine powers the compressor while the second powers the propeller through a separate shaft and gear reduction. The gears are necessary to keep the propeller from going super- sonic and losing efficiency. [49]

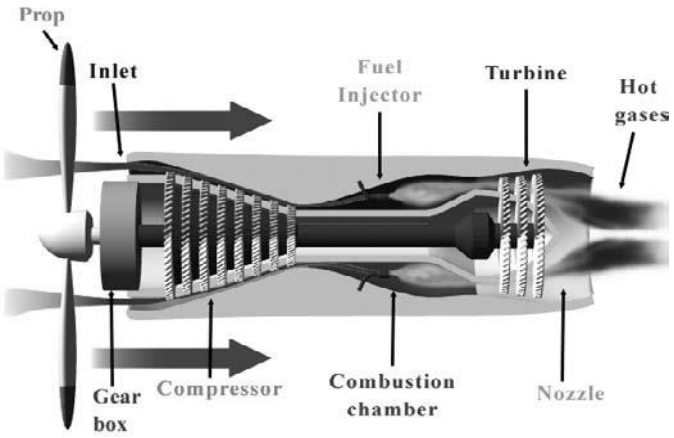

Figure (II. 32): *Cutaway view of turboprop engine.*

Unlike a basic turbojet, the second turbine removes most of the remaining energy from the flow to power the propeller and less than 10 percent of actual thrust is produced by the core. Turboprops operate well in the low subsonic range, with much more power than a piston-driven propeller aircraft. This is why turbojets are used by long-range military cargo planes. Another version of the turboprop is the turbo- shaft engine. Instead of driving a propeller, the shaft is used to power such things as helicopters, tanks, train engines, and even race cars. [49]

II.9.5-AFTERBURNING TURBOJET

This engine is a turbojet with the added capability of injecting fuel into the hot gases after they have passed through the turbine. The fuel ignites to produce additional thrust of over 50 percent.

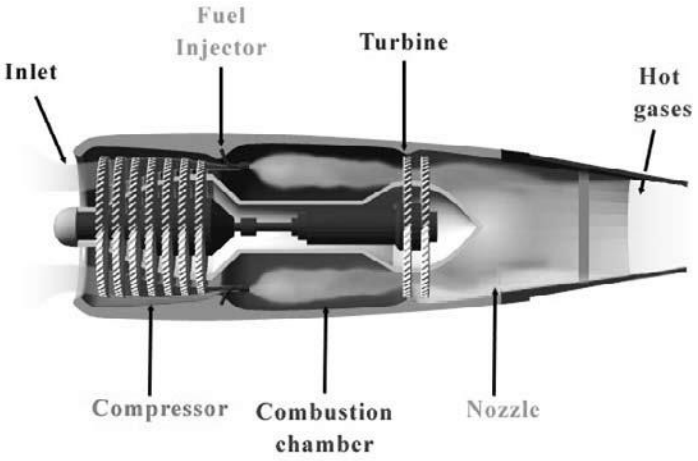

Figure (II. 33): *Cutaway view of afterburning engine.*

Since most of the compressor air has not been used for burning in the combustor, there is sufficient hot oxygen available to burn this added fuel. Stabilizerrings hold the flame and keep it from getting blown out the back of the engine. A variable nozzle is used to change how the gas leaves the engine, producing maximum thrust when the afterburners are used. [50]

The afterburner does not burn fuel as efficiently as the combustors, so its operation dramatically increases fuel consumption. Thus, it is generally only employedon fighter aircraft to gain short bursts of speed such as in short takeoffs and in dog fighting. Otherwise, the aircraft would quickly run out of fuel.

II.10- Thermodynamics in Combustion:

II.10.1 Introduction:

The principal energy laws that govern every organization are derived from two famous laws of thermodynamics. The second law, known as Carnot's principle, is controlled by the concept of entropy.

Today the word entropy is as much a part of the language of the physical sciences as it is of the human sciences. Unfortunately, physicists, engineers, and sociologists use indiscriminately a number of terms that they take to be synonymous with entropy, such as disorder, probability, noise, random mixture, heat; or they use terms they consider synonymous with antientropy, such as information, neguentropy, complexity, organization, order, and improbability.

The two principal laws of thermodynamics apply only to closed systems, that is, entities with which there can be no exchange of energy, information, or material. The universe in its totality might be considered a closed system of this type; this would allow the two laws to be applied to it.

The first law of thermodynamics says that the total quantity of energy in the universe remains constant. This is the principle of the conservation of energy. The second law of thermodynamics states that the quality of this energy is degraded irreversibly. This is the principle of the degradation of energy.

The first principle establishes the equivalence of the different forms of energy (radiant, chemical, physical, electrical, and thermal), the possibility of transformation from one form to another and the laws that govern these transformations. This first principle considers heat and energy as two magnitudes of the same physical nature

About 1850 the studies of Lord Kelvin, Carnot, and Clausius of the exchanges of energy in thermal machines revealed that there is a hierarchy among the various forms of energy and an imbalance in their transformations. This hierarchy and this imbalance are the basis of the formulation of the second principle. [51]

II.10.2 Definitions:

System: In thermodynamics, a system refers to a defined portion of the physical universe that is being studied or analyzed. It can be a single substance, a mixture of substances, or a region of space that is being studied.

State of a Thermodynamic System:

In thermodynamics, a state of a system refers to the set of thermodynamic properties that fully describe the system at a given point in time. The state variables can include temperature (T), pressure (P), volume (V), internal energy (U), and entropy (S), among others. The state of a system can be mathematically expressed as:

$$S = S(U, V, n) \qquad \textbf{(II.19)}$$

Where S is the entropy, U is the internal energy, V is the volume, and n is the number of particles in the system. This equation is known as the state postulate, which states that the state of a system can be uniquely determined by its thermodynamic properties.

The state of a system can also be represented on a thermodynamic diagram, such as a pressure-volume (PV) diagram, where each point on the diagram corresponds to a specific state of the system. The behavior of the system can be analyzed by examining the changes in the state variables as the system undergoes various thermodynamic processes. [52]

The first Law of Thermodynamics:

The first law of thermodynamics, also known as the law of conservation of energy, states that the energy of a closed system is conserved, and cannot be created or destroyed, but can only be transferred between the system and its surroundings in the form of heat and work. Mathematically, the first law of thermodynamics is expressed as:

$$\Delta U = Q - W \quad \textbf{(II.20)}$$

Where ΔU is the change in internal energy of the system, Q is the heat added to the system and W is the work done on the system. A positive value of Q indicates that heat is added to the system, while a positive value of W indicates that work is done on the system. The equation can be rewritten as:

$$\Delta U = Q - P\Delta V \quad \textbf{(II.21)}$$

Where P is the pressure of the system, and ΔV is the change in volume of the system.

The first law of thermodynamics is a fundamental principle of thermodynamics and has wide-ranging applications in various fields, including physics, chemistry, and engineering.

When the system performs an open transformation, the algebraic sum of the work and the quantity of heat exchanged with the outside is constant, the state function is therefore:

$$\Delta E = E_B - E_A = Q + W \quad \textbf{(II.22)}$$

Isochore Transformation (at a constant volume):

$$dV = 0 \quad ; \quad Q = \Delta E \quad \textbf{(II.23)}$$

Isobar Transformation (at a constant pressure):

$$Q = \Delta E + P(V_B - U_A) \quad \textbf{(II.24)}$$

Then, the Enthalpy State Function is introduced:

$$H = E + PV \quad \textbf{(II.25)}$$

Second Law of Thermodynamics:

The second law of thermodynamics is a fundamental principle of nature that governs the behavior of thermodynamic systems. It has two statements, known as the Kelvin-Planck statement and the Clausius statement.

The Kelvin-Planck statement of the second law states that it is impossible to construct a device that operates in a cycle and produces no effect other than the transfer of heat from a colder body to a hotter body.

The Clausius statement of the second law states that it is impossible for a heat engine to operate in a cycle and transfer heat from a colder body to a hotter body without any external work input.

Mathematically, the second law of thermodynamics is expressed in terms of the following equations and variables:

1- Entropy (S):

Entropy is a thermodynamic property that measures the degree of disorder or randomness in a system. It is denoted by the symbol S and is related to the number of microstates that correspond to a given macrostate. The change in entropy of a system is given by:

$$\Delta S = \int \frac{dQ}{T} \quad \textbf{(II.26)}$$

(I.6)Where ΔS is the change in Entropy dQ is the amount of heat transferred to the system, and T is the temperature at which the heat is transferred.

2- Entropy Production (ΔS_{gen}):

Entropy production is a measure of the amount of irreversibility in a process. It is given by:

$$\Delta S_{gen} = \sum i \left(\frac{dQ_i}{T_i}\right) \quad \textbf{(II.27)}$$

Where ΔS_{gen} is is the entropy production, dQ_i is the amount of heat transferred in each step of the process, and T_i is the temperature at which the heat is transferred.

3- Carnot efficiency (η_c):

The Carnot efficiency is the maximum possible efficiency of a heat engine that operates between two given temperature reservoirs. It is given by:

$$\eta_c = 1 - \frac{T_c}{T_h} \quad \textbf{(II.28)}$$

Where $T_c$is the temperature of the colder reservoir and T_h is the temperature of the hotter reservoir.

4- Clausius inequality:

The Clausius inequality is a statement of the second law of thermodynamics that states that the entropy change of a closed system is always greater than or equal to zero. Mathematically, it is expressed as:

$$\Delta S \geq \int \frac{dQ}{T} \quad \textbf{(II.29)}$$

Where ΔS is the change in entropy and the integral is taken over a reversible path.

These equations and variables are fundamental to understanding the behavior of thermodynamic systems and have wide-ranging applications in physics, chemistry, and engineering. [53]

II.10.3 Thermochesmitry:

Thermochemistry is the study of the heat transfer that occurs during chemical reactions. Several variables and formulas are used in thermochemistry to quantify the energy involved in chemical reactions, including the following:

1- Mass of a component :

$$m_i = n_i M_i \quad \textbf{(II.30)}$$

2- Total Mass (m):

Total mass refers to the sum of the masses of all the components in a system. It is denoted by the symbol m and is given by the formula:

$$m = \sum m_i \quad \textbf{(II.31)}$$

Where m_i is the mass of each component in the system

3- Mole Fraction (X):

Mole fraction is the ratio of the number of moles of a component to the total number of moles in a system. It is denoted by the symbol χ and is given by the formula:

$$X = \frac{n_i}{\Sigma n} \quad \textbf{(II.32)}$$

Where n_i is the number of moles in the ith component in the system and Σn is the total of number of moles in the system.

4- Mass Fraction (Y):

Mass fraction is the ratio of the mass of a component to the total mass of a system. It is denoted by the symbol w and is given by the formula:

$$Y_i = \frac{m_i}{\sum m} \quad \textbf{(II.33)}$$

Where m_i is the mass of the ith component in the system and Σm is the total mass of the system.

5- Molar concentration:

$$C_i = \frac{n_i}{V_T} \quad \textbf{(II.34)}$$

Where C_i is the molar concentration, n_i is the number of moles of the ith component, and V_T is the total volume of the component.

6- Density:

$$\rho_i = \frac{m_i}{V_T} \quad \textbf{(II.35)}$$

Where ρ_i is the density, n_i is the number of moles of the ith component, and V_T is the total volume of the component.

II.10.4 Air/Fuel Ratio:

The air/fuel ratio (AFR) is defined as the ratio of the mass or volume of air to the mass or volume of fuel in a combustion reaction. AFR is typically expressed as a dimensionless ratio or as a mass or volume ratio. The ideal AFR for complete combustion of a hydrocarbon fuel is called the stoichiometric ratio, which varies depending on the specific fuel being burned.

The stoichiometric air/fuel ratio can be calculated using the following general equation:

$$AFR = (A\ /\ F)_S = \frac{m_{air}}{m_{Fuel}} \quad \textbf{(II.36)}$$

For hydrocarbon fuels, the stoichiometric AFR can be calculated based on the chemical reaction:

$$C_nH_m + (n+\frac{m}{4})(O_2 + 3.76N_2) \longrightarrow nCO_2 + \left(\frac{m}{2}\right)H_2O + \left(n+\frac{m}{4}\right)3.76N_2 \qquad \textbf{(II.37)}$$

>here n and m are the number of carbon and hydrogen atoms in the fuel molecule, respectively.

The stoichiometric AFR for hydrocarbon fuels is typically in the range of 14.7:1 to 15.5:1 for gasoline, 14.6:1 to 14.8:1 for diesel fuel, and 17.2:1 to 17.4:1 for natural gas.

For our calculations we have chosen three mixtures: CH_4(Fuel) / O_2(Oxidizer), H_2 (Fuel)/ O_2(Oxidizer), $C_{12}\ H_{23}$ (Fuel) / O_2 (Oxidizer).

Our Stochiometric reactions will be:

$$\left.\begin{array}{c} C_{12}H_{23} + 17.75O_2 + 66.74N_2 \longrightarrow 12CO_2 + 11.5H_2O + 66.74N_2 \\ CH_4 + 2O_2 + 7.52N_2 \longrightarrow CO_2 + 2H_2O + 7.52N_2 \\ 2H_2 + O_2 \longrightarrow 2H_2O \end{array}\right\} \qquad \textbf{(II.38)}$$

The Equivalence ratio will then be introduced when dealing with non-stohiometric mixtures, this will be defined as the ratio between the actual Air/fuel ratio and the Air/fuel stoichiometric (Φ):

$$\Phi = \frac{\left(\frac{A}{F}\right)_s}{\left(\frac{A}{F}\right)_a} \qquad \textbf{(II.39)}$$

$0<\Phi<1$ fuel-lean

$\Phi = 1$ Stoichiometic condition

$1<\Phi<\infty$ Fuel-rich

II.10.5 Ideal Gases:

In this study, the gases are considered as Ideal Gases.

An ideal gas is a theoretical gas composed of a large number of small particles that follow the laws of classical mechanics. In an ideal gas, the particles are assumed to have negligible volume and to not interact with each other except through perfectly elastic collisions. The behavior of an ideal gas is described by the ideal gas law, which relates the pressure, volume, temperature, and number of particles of the gas [54]:

$$PV = nRT \qquad \textbf{(II.40)}$$

Where P is the pressure of the gas, V is its volume, n is the number of moles of the gas, R is the universal gas constant, and T is the temperature of the gas in Kelvin.

Other important formulas for ideal gases include:

Boyle's law: PV = constant at constant temperature

Charles's law: V/T = constant at constant pressure

Gay-Lussac's law: P/T = constant at constant volume

Avogadro's law: V/n = constant at constant temperature and pressure

Dalton's law of partial pressures: The total pressure of a mixture of ideal gases is the sum of the partial pressures of each gas component.

It's important to note that while ideal gases provide a useful theoretical framework for understanding the behavior of real gases, no gas in the real world is truly ideal.

II.10.6 Equations of state:

State Equations for a reactive fluid are the conservation equations for total mass, mass of each species, momentum and energy. [55, 56]

Equation of continuity:

The continuity equation is a fundamental principle in physics that describes the conservation of mass in a fluid. It states that the mass flowing into a control volume must equal the mass flowing out of the control volume, plus any net increase or decrease in mass within the control volume.

It is given by:

$$\frac{\partial \rho}{\partial t} + \nabla \cdot (\rho v) = 0 \qquad \textbf{(II.41)}$$

Equation of chemical species continuity:

$$\frac{\partial \rho Y_i}{\partial t} + \frac{\partial u_k Y_i}{\partial x_k} = -\frac{\partial F_i^k}{\partial X_k} \qquad \textbf{(II.42)}$$

Where Y_i is the mass fraction and F_i^k is the Diffusion Flux of the i-th specie.

According to Fick's law:

$$F_i^k = -\rho D_i \frac{\partial Y_i}{\partial X_k} \qquad \textbf{(II.43)}$$

Where D_i is the Binary Diffusion coefficient of the i-th specie.

So, the equation of chemical species is written as:

$$\frac{\partial \rho Y_i}{\partial t} + \frac{\partial u_k Y_i}{\partial x_k} = -\rho D_i \frac{\partial Y_i}{\partial X_k} + \omega_i \qquad \textbf{(II.44)}$$

Where ω_i is the chemical reaction rate.

Specific enthalpy of the mixture:

$$h = \sum h_i Y_i \qquad \textbf{(II.45)}$$

With: $h_i = \int_{T_0}^{T} Cp_i \, dT + Q_{p,i}^0$

Where Cp_i is the heat capacity of the i-th specie at a constant pressure and the Formation Heat of the i-th specie at a constant pressure and a reference temperatureT_0.

Specific Enthalpy will then be defined as:

$$h_i = \int_{T_0}^{T} Cp_m \, dT + \sum Q_{p,i}^0 Y_i \qquad \textbf{(II.46)}$$

Where Cp_m is the Heat Capacity of the mixture per mass unit.

II.10.7 Characteristic parameters:

Kinematic viscosity and dynamic viscosity are both important concepts in fluid mechanics, and they are closely related. Here are definitions of both terms along with their formulas and units:

Kinematic viscosity: Kinematic viscosity is a measure of a fluid's resistance to flow under gravity, defined as the ratio of the dynamic viscosity of the fluid to its density:

$$\nu = \frac{\mu}{\rho} \quad \textbf{(II.47)}$$

Where:

ν is the kinematic viscosity (in m^2 / s)

μ is dynamic viscosity (in Pa.S)

ρ fluid density (in Kg / m^3)

Dynamic viscosity: Dynamic viscosity is a measure of a fluid's internal resistance to flow, or its "thickness." It is defined as the ratio of the shear stress applied to the fluid to the resulting shear rate.

$$\tau = \mu \left(\frac{du}{dy}\right) \quad \textbf{(II.48)}$$

Where:

τ is shear stress (in Pa)

$\frac{du}{dy}$ is the velocity gradient (in s^{-1})

Both kinematic and dynamic viscosity are important parameters in fluid mechanics, and they are often used in the design of fluid handling systems, as well as in the study of fluid dynamics and heat transfer [57].

The Prandtl number is a dimensionless number that is used in fluid mechanics to describe the ratio of momentum diffusivity (viscosity) to thermal diffusivity. It is named after the German physicist and engineer Ludwig Prandtl.

$$p_r = \mu \frac{C_P}{\lambda} \quad \textbf{(II.49)}$$

The Lewis number is a dimensionless number that is used in fluid mechanics and combustion to describe the ratio of thermal diffusivity to mass diffusivity. It is named after the British chemist and physicist Gilbert N. Lewis.

$$L_e = \frac{s_c}{p_r} \quad \textbf{(II.50)}$$

Chapter III: General information on nozzles

Introduction:

The thrust of an engine depends mainly on the velocity of the combustion products through the outlet section of the nozzle that propels it. During their passage through a De Laval nozzle, the exhaust gases are accelerated from subsonic to supersonic speeds.

The optimization of the choice of a propulsion nozzle must take into account in addition to the gas dynamics calculations of interest such as the material used, the wall construction, the cooling requirements and the permissible sizing limits etc.

III.1. Definition of the nozzle:

A nozzle is a passive mechanical device that connects two tanks at different pressures. It is one of the most important elements in turbomachines and turbojet engines, and 40% of the total thrust of the latter is produced by nozzles.

According to the expansion rate, the nozzles will be either simply convergent (Figure III.1.a) for high expansion rates, otherwise will be convergent divergent (Figure III.1.b), according to the geometry we find the nozzles with plane geometry (Figure III.2.a) or axisymmetric (Figure III.2.b).

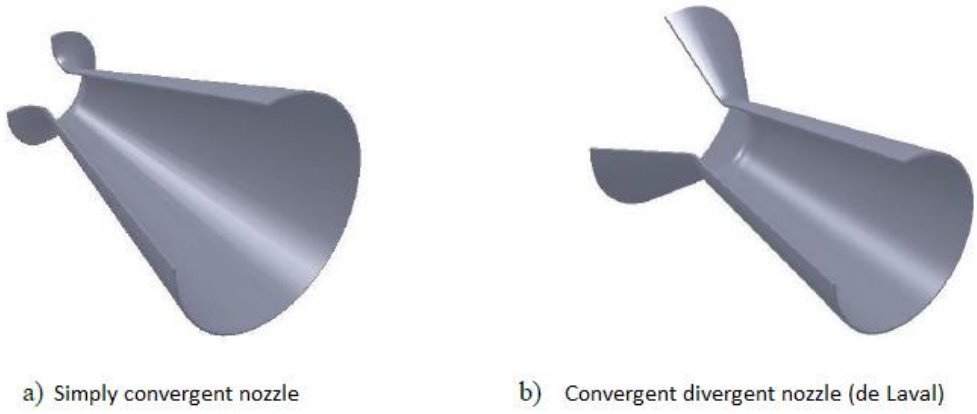

Fig. III.1: Nozzle Profiles

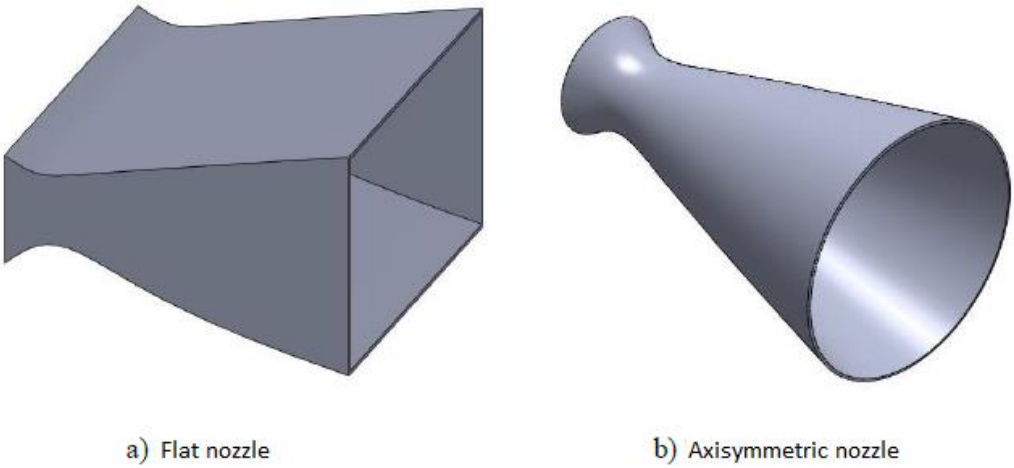

Fig. III.2: Different geometric shapes of nozzles [07].

III.2. Role and use of the nozzle:

Supersonic nozzles are used in many aeronautical and aerospace structures such as rocket and missile engines, aircraft engines and in the manufacture of supersonic wind tunnels for the modeling and experimental realization of supersonic flows.

III.2.1. Rocket engine:

In the rocket engines, the nozzle organ constitutes the essential part, because it makes it possible to accelerate the gases at the exit of the combustion chamber up to a certain speed whose purpose is to obtain a force of thrust as a resultant of this acceleration. Let us note here that the structure of a missile is constituted by the combustion chamber and the nozzle and that the latter constitutes approximately 70% of the total mass of a propulsive chamber.

Fig. III.3: Nozzle of the European engine Vulcain 2 of ARIANE 5

III.2.2. Aircraft engine:

The major progress that has been made in aviation during this century is undoubtedly the advent of supersonic flight, which at its beginning did not cause an immediate change of attitude in the manufacturers, because the primary concern for the first military supersonic aircraft is to ensure good conditions of subsonic or transonic flight so that the use of a divergent was practically proscribed to avoid the regimes of overexpansion at these moderate speeds. The profitability of such projects is ensured only if the optimal performances are obtained from all the elements of the engine, in such projects the role assigned to the nozzle is defined in the following way:

- Must ensure optimal expansion of combustion gases. That is to say, the maximum thrust of the regime of cruising. This problem is delicate, because the section of exit must be connected to the master torque of the engine; or the structure of the plane by fairing.
- The nozzle must ensure the blocking of the flow at the various speeds of operation by the variation of the surface to the neck according to the flow and the conditions of temperatures and pressure of gases to be evacuated.
- In the intermediate flight regime, the nozzle must not cause too high thrust losses because of its inadequacy.
- It must contribute to the braking of the aircraft during the landing phase and to the noise attenuation.

Fig. III.4: Nozzle of a fighter aircraft

III.2.3. Wind Tunnel:

A wind tunnel creates an artificial air flow. There are several types of wind tunnels, but generally speaking a wind tunnel consists of three main parts:

- ❖ The collector or the convergent
- ❖ The experience room
- ❖ The diffuser or divergent: that the air crosses at its exit of the chamber of experiment, in direction of ventilator which aspires it and rejects it then outside. The diffuser has the shape of a truncated cone whose section increases, so the speed of the air flow is gradually reduced to the fan blade driven by an electric motor.

One of the roles of a wind tunnel is to simulate real flows but on reduced scale prototypes. To achieve this, it is necessary to model the flow at the exit of the nozzle which must be uniform and parallel like the free air of the atmosphere [40].

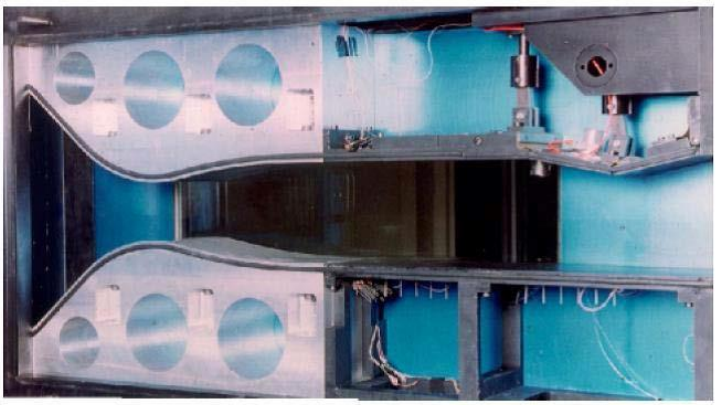

Fig. III.5 - The S8ch supersonic wind tunnel at the Onera Meudon Center [3].

III.3. THE QUASI-MONODIMENSIONAL APPROACH:

The quasi one-dimensional approach is an approximation of the flow in a variable area of the stream tube. In three dimensions the exact solution must be found with numerical methods such as: finite differences, finite volumes and the method of characteristics, however, for a wide variety of engineering problems, such as the study of the flow in wind tunnels or in rocket engines, the quasi one-dimensional results are frequently sufficient. The quasi one-dimensional approach allows the cross-sectional area of the flow tube to vary as opposed to the one-dimensional approach, at the same time, one continues to assume that all properties of the flow are uniform across a given cross-section, hence these properties are a function only of "x" and time "t" if the flow is non-steady. Each flow where A = A(x), P = P(x), ρ = ρ(x) and V = u = u(x) in addition to being permanent (no variation with respect to time) is defined as a quasi one dimensional flow.

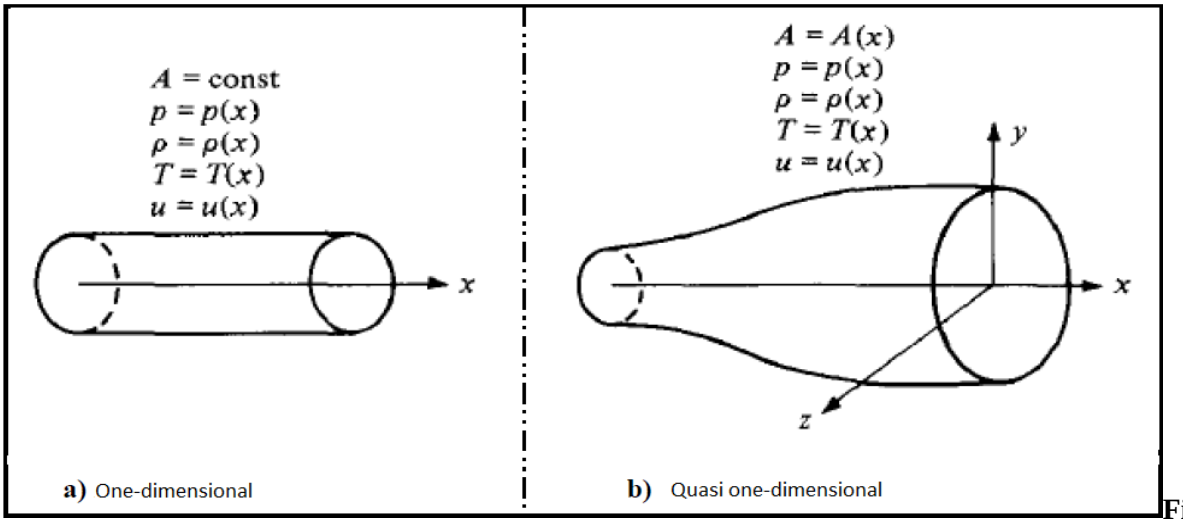

Fig. III.6: The difference between the Monodimensional approach and the Quasi-Monodimensional approach.

III.3.1. Reminder on Gas Dynamics:

To calculate analytically the different parameters of the flow in any section of the channel section of the channel, we use the relations of gas dynamics with the quasi one-dimensional approach.

Temperature ratio:

$$\frac{T_0}{T} = 1 + \frac{\gamma-1}{2} M^2 \qquad \textbf{(III.1)}$$

Where:

T0: Stagnation temperature

T: Static temperature

M: Mach number

$$\gamma = \frac{C_P}{C_V}$$

Cp: Heat capacity at constant pressure

Cv: Heat capacity at constant volume

Pressure ratio:

$$\frac{P_0}{P} = \left(1 + \frac{\gamma-1}{2} M^2\right)^{\gamma/\gamma-1} \qquad \textbf{(III.2)}$$

Where:

P0: Stagnation pressure

P : Static pressure

The density ratio:

$$\frac{\rho_0}{\rho} = \left(1 + \frac{\gamma-1}{2} M^2\right)^{1/\gamma-1} \qquad \textbf{(III.3)}$$

With:

$\rho 0$: Reference density

ρ : Density

Notes:

- the total quantities (***ρ0, P0, T0***) represent the parameters of the flow when it is brought to a stagnation in an isentropic way.

- The parameters are noted at the speed of sound by an Asterisk **M*=1**, **U*=a***, **At=A*** and the above formulas then become:

❖ **Temperature ratio :**

$$\frac{T^*}{T_0} = \frac{2}{\gamma+1} \qquad \textbf{(III.4)}$$

Where:

T^*: Static temperature at the speed of sound

❖ **Pressure ratio :**

$$\frac{P^*}{P_0} = \left(\frac{2}{\gamma+1}\right)^{\gamma/\gamma-1} \qquad \textbf{(III.5)}$$

Where:

P^*: Static pressure at the speed of sound

❖ **Density ratio :**

$$\frac{\rho^*}{\rho_0} = \left(\frac{2}{\gamma+1}\right)^{1/\gamma-1} \qquad \textbf{(III.6)}$$

Where:

ρ^*: Density at the speed of sound

For the standard conditions where $\gamma = 1.4$ we get:

$\frac{T^*}{T_0}$ **= 0.833,** $\frac{\rho^*}{\rho_0}$ **= 0.634,** $\frac{P^*}{P_0}$ **= 0.528**

III.3.2. Section ratio formulas:

Speed of sound:

For a non-viscous, adiabatic flow, there are no energy dissipation mechanisms such as friction, thermal conduction or diffusion, in which case the flow is considered isentropic. Hence, any change in pressure dp in the flow is accompanied by an isentropic change in density dρ [16]. Relation (III.7) shows the relationship between pressure and density for isentropic flow.

$$\frac{dP}{d\rho} = \left(\frac{\partial P}{\partial \rho}\right)_s = a^2 \qquad \textbf{(III.7)}$$

For a perfect calorific gas:

$$H = C_P T \qquad \textbf{(III.8)}$$

$$a = \sqrt{\gamma r T} \qquad \textbf{(III.9)}$$

Where:

a : Speed of sound

r : Gas constant (for the Air r=287 j/kg.k)

Speed-section relationship (Hugoniot relationship):

$$\frac{dA}{A} = (M^2 - 1)\frac{dU}{U} \qquad \textbf{(III.10)}$$

This equation shows us some very important results:

- If $0 \leq M \leq 3$, this corresponds to incompressible flow.
- If $0.3 \leq M \leq 1$ (subsonic flow): an increase in velocity ($dU > 0$) is associated with a decrease in cross-section ($dA < 0$) and vice versa (see figure III.7.a).
- Si (supersonic flow): an increase in velocity is accompanied by an increase in cross-section and vice-versa (figure III.7.b).
- If M=1 (sonic flow): equation (III.10) gives, $\frac{dA}{A} = 0$, which mathematically corresponds to the minimum or maximum cross-section. The minimum cross-section is the only one that has any physical significance.

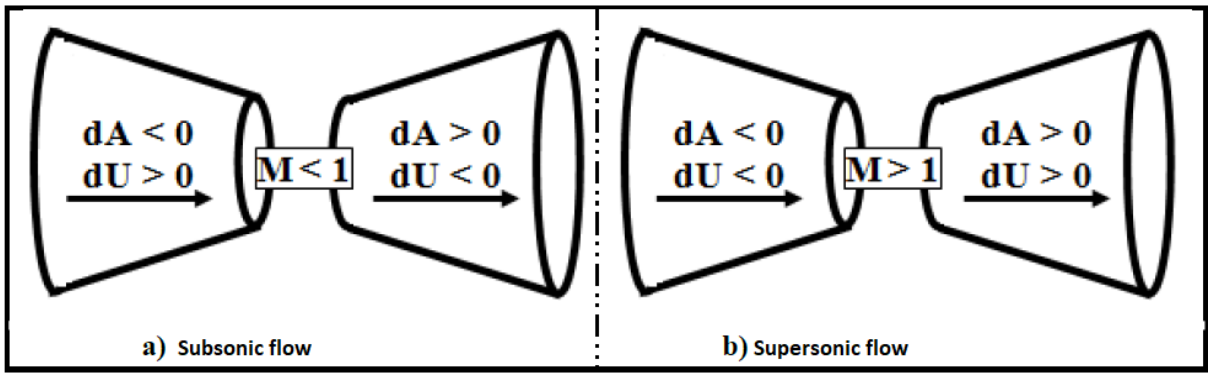

Fig. III.7: Speed-section relations.

The above results clearly show that for a gas to expand isentropically from subsonic to supersonic velocity, it must flow through a convergent-divergent channel, as shown in figure (III.8). In addition, the minimum cross-section separating the convergent and divergent sections must have a sonic flow; this cross-section is called the throat.

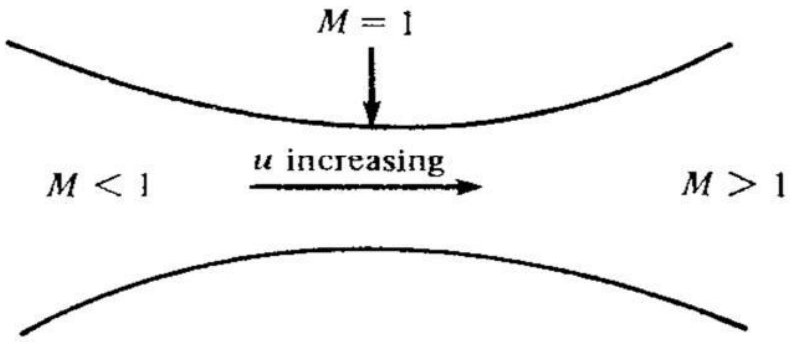

Fig. III.8 : Convergent divergent channel.

Section ratio:

The relation (III.8) is known as the Mach section-number relation, and presents a remarkable result. It shows that **M= *f*(A/A*)**, i.e. the Mach number at any nozzle position in any nozzle position is a function of the ratio of the local cross-section to that of the throat.

$$\left(\frac{A}{A^*}\right)^2 = \frac{1}{M^2}\left[\frac{2}{\gamma+1}\left(1+\frac{\gamma-1}{2}M^2\right)\right]^{\frac{\gamma+1}{\gamma-1}} \qquad \textbf{(III.11)}$$

Where:

A: Chanel section

A*: Channel section wehre M=1

III.3.3. Theoretical operation of the supersonic nozzle:

The one-dimensional approach to the flow of thermally perfect, non-viscous gases makes it possible to describe the different operating regimes of a supersonic nozzle. Consider the system shown in figure III.9, consisting of a De-Laval nozzle. The nozzle communicates with a reservoir containing a gas at an assumed fixed generating pressure Pc. The nozzle opens out into a quasi-infinite enclosure whose static pressure Pa is variable.

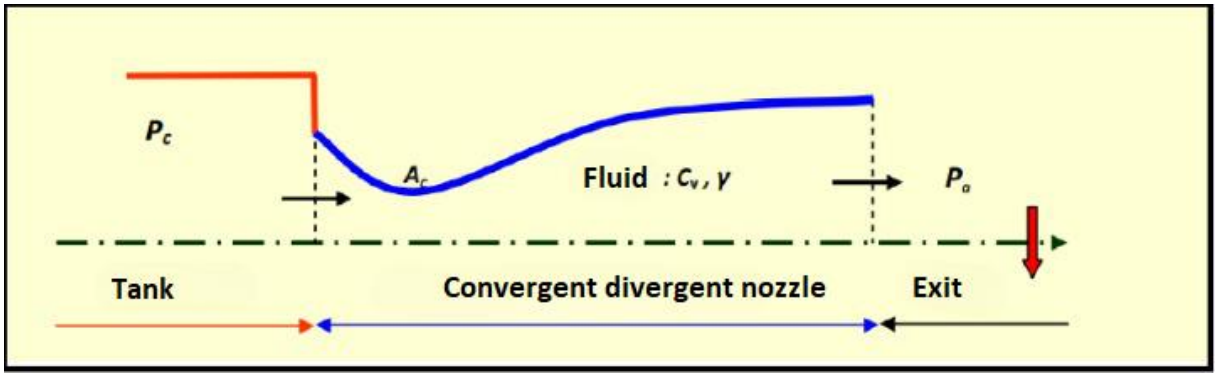

Fig. III.9 : Schéma de la tuyère supersonique.

If the pressure of the external environment is equal to the chamber pressure, the fluid is completely at rest (Fig. III.10, curve (a)). If the ambient pressure Pa falls progressively below the assumed constant pressure Pc, a flow rate is generated, and five particular flow regimes are distinguished [38], [15], [34].

Subsonic flow:

At the start of the flow, the flow rate increases as the ambient pressure decreases.

Flow is subsonic throughout the nozzle [Fig. III.10, curves (b) and (c)]. In the convergent section, velocity increases and pressure decreases until a minimum value is reached at the throat. In the divergent section, velocity decreases and pressure rises to the pressure of the external environment. Pressure is therefore minimal in the neck section, where velocity passes through a maximum value.

Adapted sonic flow:

If ***Pa*** continues to decrease until a characteristic value is reached (***Pac1***), the flow at the neck becomes sonic and the flow rate reaches a maximum limit value [Fig. II.22, curve (d)]. The flow is said to be sonically adapted. Again, except at the throat, the flow is subsonic. At the nozzle throat, pressure reaches the critical value ***P**** and velocity reaches the speed of sound.

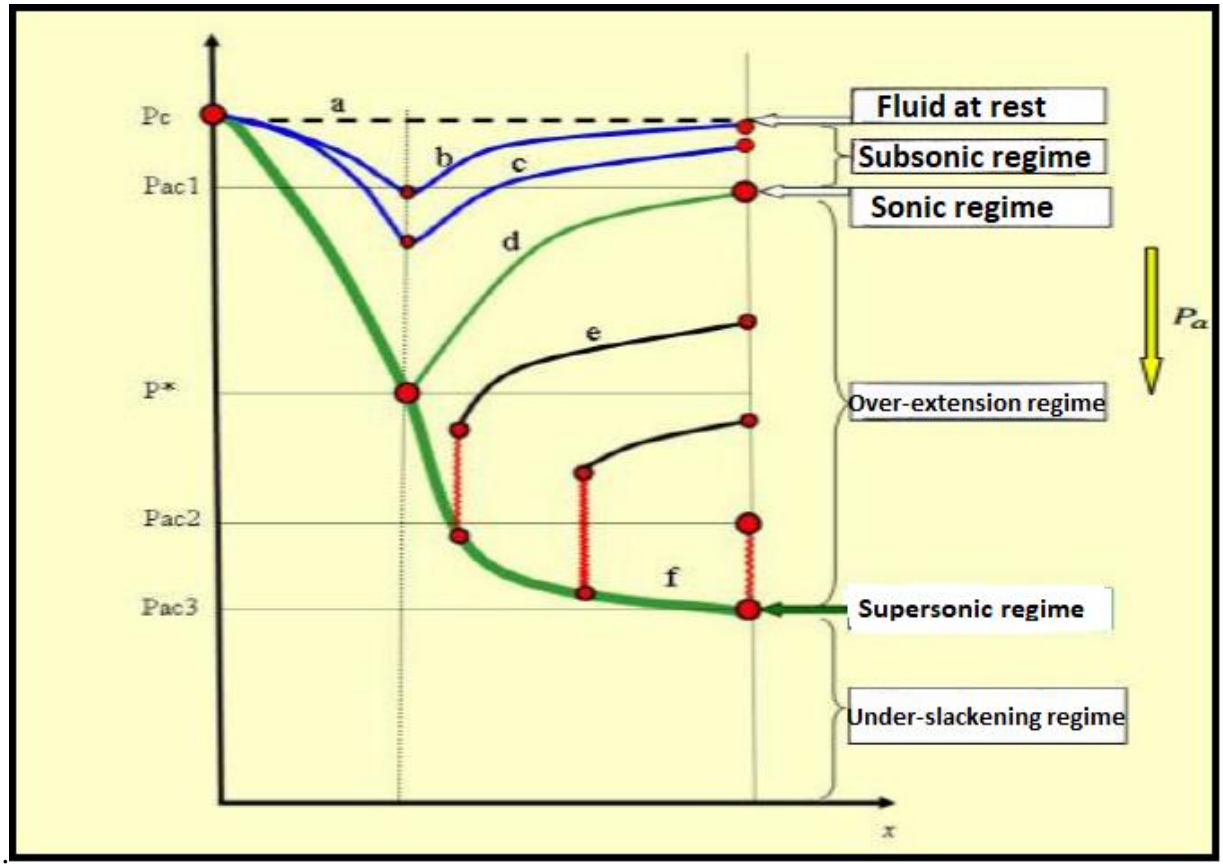

Fig. III.10: Flow regimes in a supersonic nozzle (Pressure evolution along the nozzle).

Non-adapted sonic flow:

If ***Pa*** drops below ***Pac1***, the neck remains sonic. In the divergent flow, an irreversible phenomenon known as a shock wave appears, and the flow is said to be sonic and non-adapted, or over-expansion. The evolution of gas flow is represented by curve (e) in figure III.10.

In the convergent section, the flow remains unchanged, but in the divergent section a stationary shock wave normal to the nozzle axis divides the flow into two parts (Fig. II.23). In the first part of the divergent flow, the velocity continues to increase and the pressure decreases. Through the shock wave, pressure rises abruptly, and velocity falls abruptly. The shock wave is positioned in such a way that the recompression that takes place brings the outlet pressure down to the ambient pressure Pa. In the second part of the divergent flow (after the shock wave), pressure rises again and velocity gradually decreases, the flow is once again subsonic.

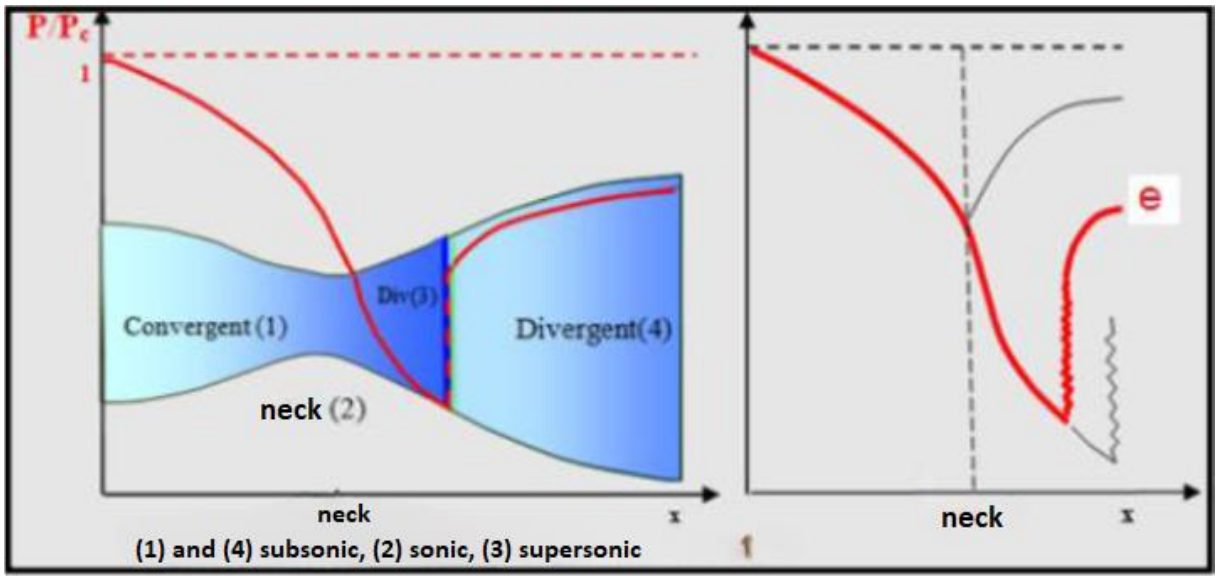

Fig. III.11: Overexpansion in 1D.

The shock wave moves towards the outlet as ***Pa*** decreases. Let ***Pac2*** be the ambient pressure at which the shock wave moves to the nozzle outlet.

By further reducing the pressure ***Pa*** below ***Pac2***, the flow in the divergent nozzle is fully supersonic, and the reduction in ***Pa*** no longer modifies the flow inside the nozzle. Pressure adaptation between the nozzle outlet pressure and the ambient pressure takes place outside the divergent nozzle, via oblique shock waves.

Adapted supersonic flow:

If ***Pa*** continues to decrease, there will come a time when the flow will be entirely supersonic throughout the nozzle. The shock wave phenomenon disappears and there is no longer any external recompression, so the nozzle is perfectly adapted. The evolution of the gas is represented by curve (f) in figure III.10. Let ***Pac3*** denote the ambient pressure at which this phenomenon occurs. ***Pac3*** is called the adaptation pressure.

Non Adapted Supersonic flow:

When the pressure ***Pa*** falls below ***Pac3***, the flow is said to be supersonic non-adapted. The flow in the Laval nozzle remains unchanged. The nozzle and the ambient pressure must take place outside the nozzle via a series of oblique expansion waves.

Comments and results:

✓ The one-dimensional approach to the flow of non-viscous thermally perfect gases enables us to describe the different operating regimes of a supersonic nozzle.

✓ A supersonic nozzle therefore only functions correctly for the pressure ratio ***Pac3/Pc***, where ***Pac3*** is called the adaptation pressure.

✓ To limit the range of each flow regime, we need to determine the characteristic values of the ambient pressure for a fixed chamber pressure ***Pc***. These values are ***Pac1, Pac2, Pac3***.

✓ The one-dimensional approach enables us to study the effect of cross-section variation, normal shock waves, oblique shock waves and relaxation waves.

✓ The one-dimensional approach provides an initial estimate of the operating parameters of supersonic nozzles.

III.3.4. Real operation of the supersonic nozzle:

The one-dimensional approach to flows of calorically perfect, non-viscous gases assumes the complete absence of viscous effects. In real flows, the nozzle has a boundary layer which is very sensitive to pressure variations, making the physical phenomena in the nozzle more complex. When the nozzle throat is sonic, the flow in the nozzle depends solely on the pressure at the nozzle outlet (***Pe***) and the pressure of the surrounding environment (***Pa***). Depending on the difference between these two pressures, three cases are encountered:

- If Pe = Pa, the nozzle is adapted.
- If Pe > Pa, the nozzle is said to be under-extended.
- If Pe < Pa, the nozzle is said to be over-extended.

Adaptation regime:

In the adapted mode, gas expansion is fully completed in the nozzle. The gas expands from the chamber to the nozzle outlet. On leaving the nozzle, no pressure adaptation is required, since the ambient pressure ***Pa*** is equal to the outlet pressure ***Pe***. The gas exits the nozzle as a quasi-uniform supersonic jet. An isobaric boundary separates the supersonic jet from the ambient fluid. As it leaves the nozzle, the jet's boundary layer comes into contact with the ambient fluid, dragging it along in its wake. This interaction forms a mixing layer (Figure .III.12).

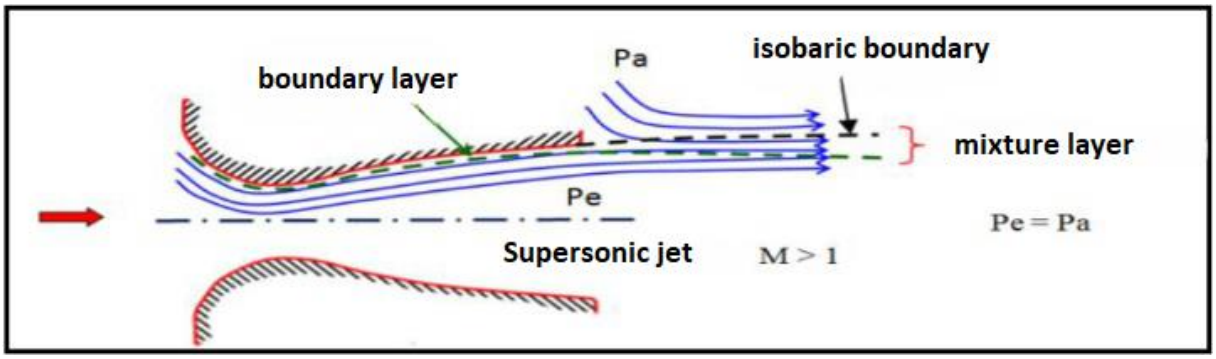

Fig. III.12: Organization of the adaptation flow.

Under-expansion regime:

This supersonic non-adaptation regime is known as the under-expansion regime. It occurs when the ambient pressure ***Pa*** is lower than the adaptation pressure. Expansion in the nozzle is incomplete. On leaving the nozzle, the gas continues its expansion from the outlet pressure ***Pe*** to the lower ambient pressure ***Pa***. Further expansion of the gas is achieved at the nozzle outlet by an expansion wave bundle. Since the outlet pressure is higher than the ambient pressure, a widening of the supersonic jet is observed at the nozzle outlet. The isobaric boundary separating the supersonic jet from the ambient fluid takes on a divergent shape (Figure III.13).

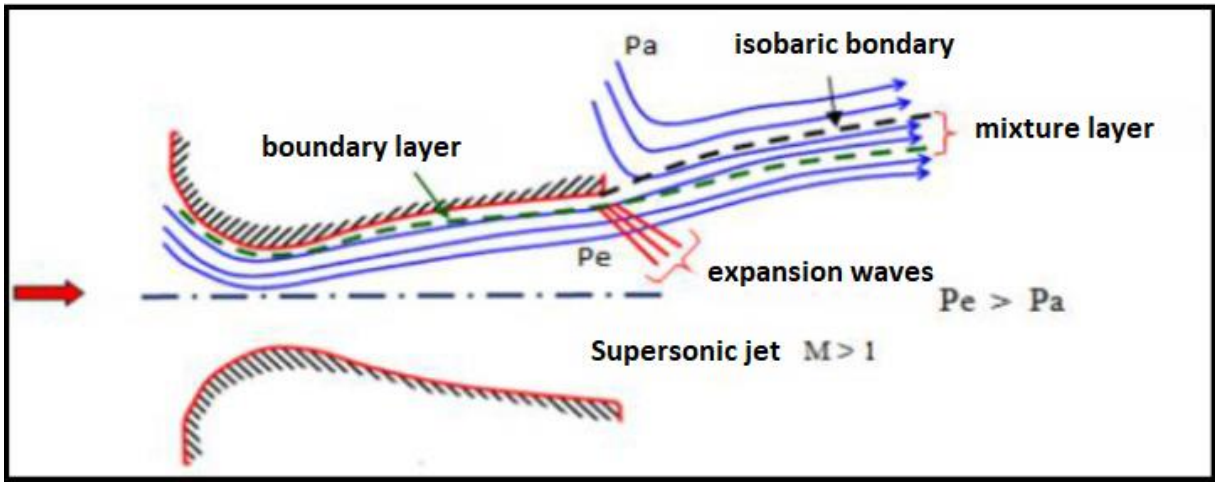

Fig. III.13: Flow organization in the underflow regime.

Figure III.14 shows the parietal pressure profile along the nozzle at adaptation and under expansion. The flow follows a strictly decreasing pressure distribution from chamber pressure to outlet pressure.

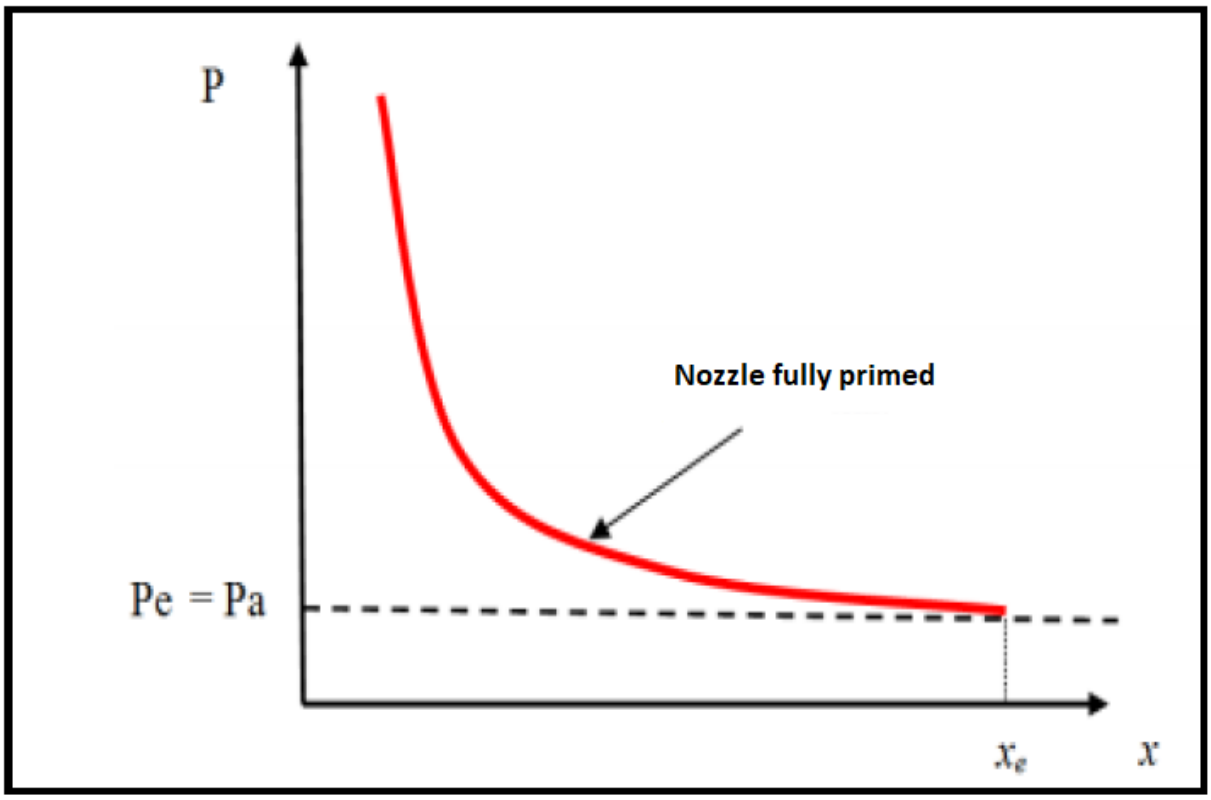

Fig. III.14: Parietal pressure profile along the nozzle at adaptation and under expansion.

Over-expansion regime:

The second non-adaptive supersonic regime is the so-called over-expansion regime. This regime occurs when the ambient pressure ***Pa*** is higher than the nozzle's the nozzle's adaptation pressure. The gases in the nozzle expand to a static pressure ***P1***, which is lower than the ambient pressure ***Pa***. The boundary layer of the jet in this situation undergoes back pressure, and a shock of intensity ***P2/P1*** is formed in the flow. Pressure ***P2*** is the pressure after the shock, and is almost equal to ambient pressure. Depending on the intensity of the shock, two cases are encountered: the over-expansion regime with incipient disbonding, and the over-expansion regime with extended disbonding.

❖ **Overspreading with incipient detachment :**

For moderate adverse pressure gradients, the subsonic boundary layer detects or senses the counter pressure at a point O called the interaction origin just a little ahead of the nozzle outlet. The boundary layer lifts off the nozzle at the lip, and an oblique shock forms at the nozzle exit. In this regime, there is no point of separation. This over-expansion regime is referred to as over-expansion with incipient debonding (Figure.III.15).

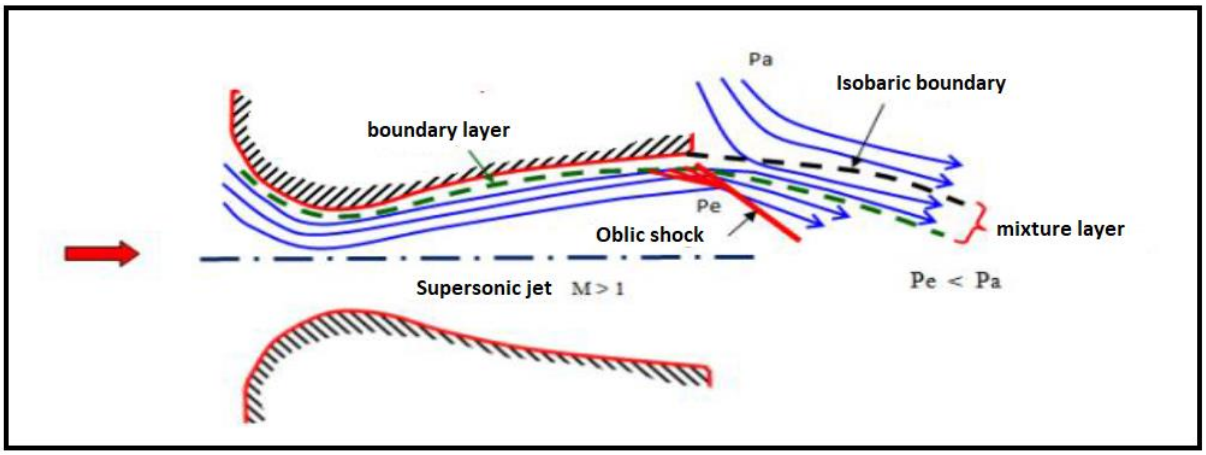

Fig. III.15: Over-extended nozzle with incipient boundary layer disbonding.

❖ **Overspreading with extensive detachment:**

The boundary layer cannot withstand any amount of back pressure. Above a certain critical value, the boundary layer lifts off the inside of the nozzle. This disbonding leads to a profound change in the flow, as shown in figure (III.16), [36], [17].

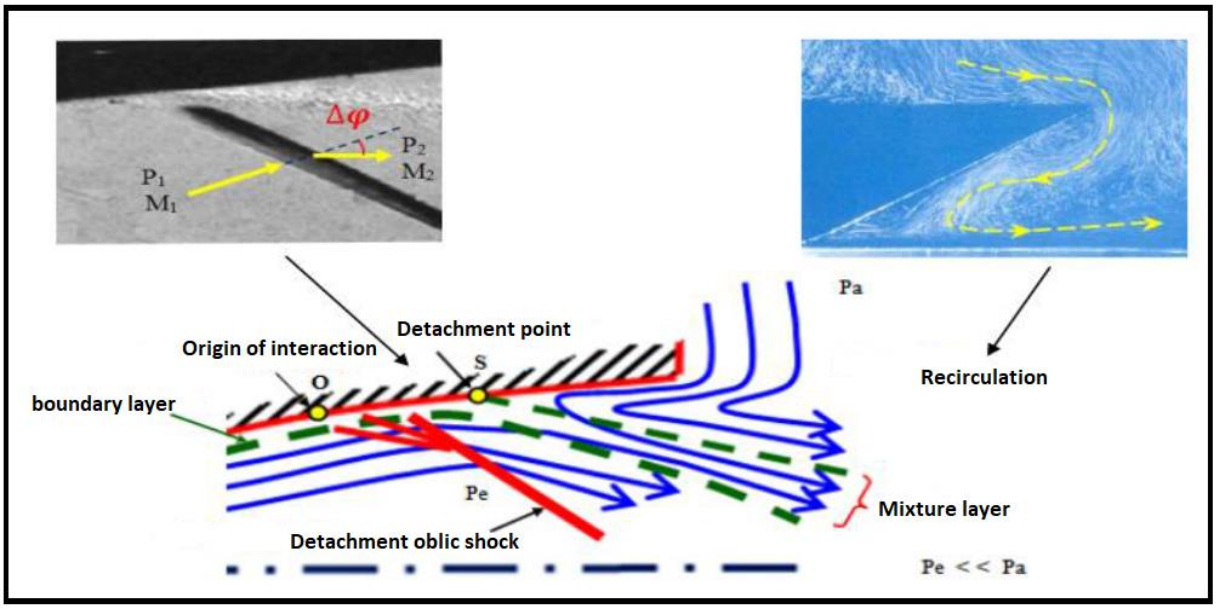

Fig. III.16: Over-extended nozzle with extensive boundary layer disbondment.

The resulting disbond occurs at a point ***S*** inside the nozzle. At this disbonding point, the nozzle's internal flow is rapidly compressed from pressure ***P1*** (undisturbed pressure immediately prior to disbonding) to pressure ***P2*** (pressure downstream of the disbonding point). This rapid back pressure causes the formation of an oblique shock through which the flow is slowed down and deflected by an angle **Λ**, and its Mach number rises from ***M1*** to ***M2***. From ***S*** starts a mixing layer, a viscous zone ensuring a continuous transition in the properties of the detached flow

between the high-velocity jet located near the axis of symmetry and the region close to the wall, where the fluid is almost stagnant. The fluid in the external environment is drawn into the nozzle by the entrainment effect, then discharged into the mixing layer. This regime is very dangerous for the nozzle. The flow topology in this regime is strongly influenced by the nozzle profile and the pressure ratio ***Pc/Pa***

III.3.5 Peformance parameters :

- **Thrust :**

The thrust delivered by a nozzle depends not only on the ejection velocity of the combustion gases, but also on the difference between the outlet and ambient pressure. In the one-dimensional theory of a permanent, non-viscous flow, the thrust is as follows;

$$\boldsymbol{F = \dot{m}V_e + (P_e - P_a)A_e} \qquad \textbf{(III.12)}$$

F : Thrust (N)
A_e : Nozzle exit section
$\dot{m}$: Mass flow rate (kg/s)

- **Thrust coefficient :**

The thrust coefficient is a dimensionless ratio, defined as the ratio of the thrust $\boldsymbol{F}$ to the product of the total pressure in the chamber and the air in the cross-section at the throat.:

$$\boldsymbol{C_F = \frac{F}{P_0 A^*}} \qquad \textbf{(III.13)}$$

This coefficient is characteristic of gas expansion in the divergent section of the nozzle.

- **Mass flow rate :**

For sonic conditions at the neck section A_c the mass flow rate $\dot{m}$ is locked at its maximum value for a given value of P_i :

$$\boldsymbol{\dot{m} = \frac{P_i A_c \delta(\gamma)}{\sqrt{C_P T_i}}} \qquad \textbf{(III.14)}$$

$$\boldsymbol{\delta(\gamma) = \frac{\gamma}{\sqrt{\gamma - 1}} \left(\frac{\gamma + 1}{2}\right)^{\frac{1-\gamma}{2(\gamma-1)}}} \qquad \textbf{(III.15)}$$

γ : Ratio of specific heats at constant pressure and volume

C_P : Heat capacity at constant pressure

- **Flow coefficient:**

Since the actual flow does not perfectly comply with the flat-slice assumption, and does not behave like a non-viscous, calorically perfect gas, the actual flow $\bar{m}$ is then corrected with a coefficient C_D approaching unity

$$C_D = \frac{actual\ current\ flow}{current\ isentropic\ flow} \quad \textbf{(III.16)}$$

$$\bar{\dot{m}} = C_D \dot{m} \quad \textbf{(III.17)}$$

- **Effective speed:**

The effective speedV_{eff}, is the exit speed of the adapted nozzle. It is defined by the ratio of thrust to flow:

$$V_{eff} = \frac{F}{\dot{m}} \quad \textbf{(III.18)}$$

Where:
F : Thrust

- **Specific impulse:**

The specific impulse, noted I_s is defined as the ratio of thrust to the product of mass flow and gravitational acceleration.

$$I_s = \frac{F}{\dot{m}g} \quad \textbf{(III.19)}$$

Where:

g : Acceleration due to gravity

- **Total impulse:**

Total impulse, noted as the integral of thrust over the entire operating time:

$$I_{totale} = \int_0^t F dt \quad \textbf{(III.20)}$$

III.4 Nozzle with altitude compensation:

For most of these studies, the objectives are to describe and characterize disbonding zones, define design criteria and improve existing ones in order to produce nozzles capable of operating on the ground, in over-expansion conditions, without jet disbonding. An exhaustive compilation of all the proposed criteria (mostly empirical or semi-empirical) has been compiled by Stark, [75]. All these studies underline the major role played by ambient pressure in the occurrence of jet disbonding in supersonic nozzles. The ratio between the static pressure level at the wall and the ambient pressure is often used as a good correlation parameter to predict its occurrence. However, most of the control techniques proposed in these studies have only been tested in the laboratory, on small surfaces and under very low enthalpy flow conditions. Unfortunately, these conditions are not representative of those encountered in rocket engines. The control techniques proposed often appear to be inapplicable to these engines, as they are too complex and

inappropriate to their operating conditions. Below, we outline the various ideas put forward to control, avoid, master or reduce the effects of disbonding.

III.4.1 Controlled detachment nozzle:

This category includes the following types of concepts:

Nozzle with controlled internal roughness:

This concept [76], which includes angular sectors of increased roughness on the inner surface of the nozzle, is intended to limit the lateral loads induced by the possible asymmetry of the disbond line, without however limiting or preventing the disbond itself. It should be noted that there are no documents in the literature attesting to the effectiveness of such a device. What's more, steady-state operation with a well-established separation line inside the nozzle would have prohibitive consequences for the thermomechanical strength of the structure.

Expandable or divergent nozzles:

It's also known as a dual position nozzle (Figure III.17). There are several numerical studies in the literature on this type of nozzle. Recently, Sato et al [77] carried out a test campaign on a reduced-scale model, in order to evaluate the lateral loads acting on the moving part during deployment in flight. These loads represent a major constraint for the mechanical dimensioning of the motor (in particular for the deployment system and for the divergent section itself) [78]. The impossibility of verifying the motor sizing on the ground under conditions representative of flight remains a stumbling block to the use of this type of concept, without compromising the launcher's reliability.

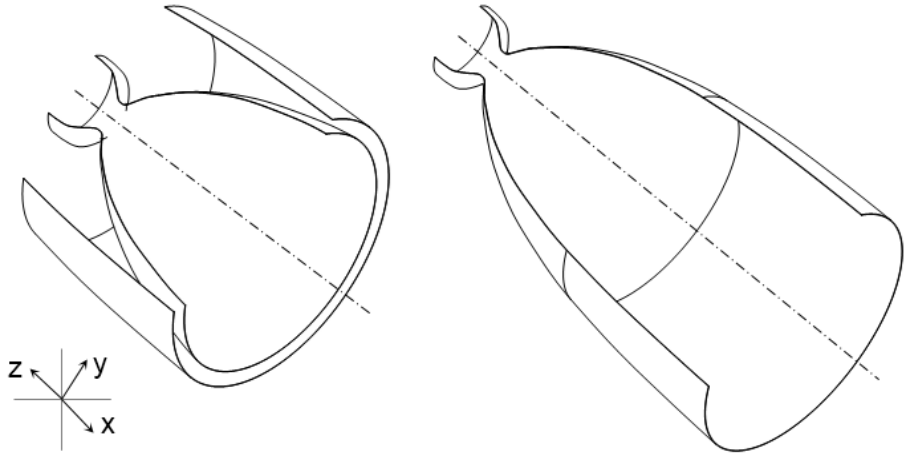

Figure III.17: Deployable nozzle.

Trigger ring nozzle:

This type of nozzle can be divided into two sub-categories, depending on how the trigger ring operates. These are:

Nozzle with fixed trigger ring:

In order to control boundary layer separation, a trigger is attached to the inner wall of the divergent nozzle, which disturbs the boundary layer and causes it to separate symmetrically under over-expansion conditions, Figure III.18a. At very high altitude (very low ambient pressure), the flow recollects itself behind the actuator and thrust is higher, using the entire cross-section ratio. The transition between the two modes (low altitude, high altitude) depends on a number of parameters, including the size of the actuator [79]. This nozzle has more or less the

same performance as the double-curve concept [25]. However, problems relating to high-temperature resistance, precise trigger attachment and uncertainty of the transition between the two modes of operation seem to affect its performance, and interest in the concept has waned since the 1970s [79, 80].

Temporary trigger ring nozzle:

This concept features a temporary insert to control low-altitude lift-off. This insert is removed in no-load mode. This trigger can be either ejectable, [81], or ablative, [82], Figure III.18b and III.18c respectively. The trigger can be a total secondary nozzle or a partial insert fixed internally to the nozzle wall. This type of actuator results in a slight loss of performance in low-altitude mode compared with a curved nozzle with the same cross-section ratio [82-84]. Hot tests of the ejector nozzle [83] have demonstrated the feasibility of this concept. However, it should be stressed that this concept is highly dependent on a reliable mechanism that provides abrupt, symmetrical detachment of the insert. Unsymmetrical ejection would result in the generation of side loads. In addition, there is the risk of collision downstream of the nozzle wall, since inserts can also experience transverse movement towards the wall. These limitations of ejectable inserts have led to consideration of the use of ablative inserts (i.e. in solid consumable fuel), [79, 82, 85]. As the launcher ascends, the size of the insert is continuously reduced until it is completely consumed, resulting in a curved nozzle for improved performance in high-altitude operation. However, the main uncertainties of this concept are the rate of consumption and the stability of the insert. In addition, a homogeneous, symmetrical and well-defined consumption time must be guaranteed, despite possible local fluctuations in pressure and temperature near the nozzle walls. With current technology, this objective is highly uncertain.

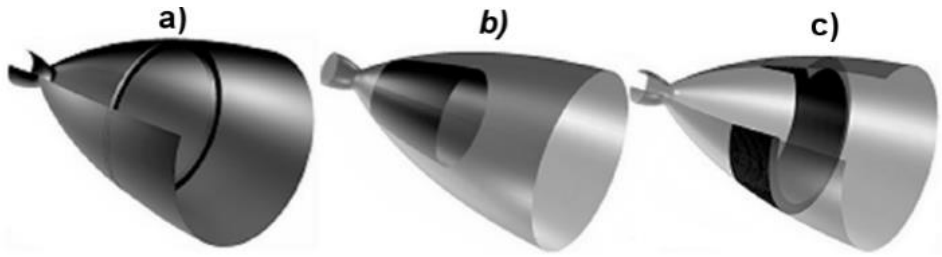

Figure III.18: Trigger ring nozzles, a) fixed, b) ejectable, c) ablative, [25].

Secondary flow injection nozzle:

Passive secondary injection nozzle:

This concept is based on the possibility of controlling the position of the jet detachment by secondary injection of a fluid jet, Figure III.19a, taken directly from the external atmosphere and introduced inside the nozzle through slots made directly on the metal wall, hence the name "Vented Nozzle", [25]. These slots close in high-altitude mode, enabling the nozzle to be operated in a regime adapted to different flight altitudes, thus improving the engine's overall performance. Parsley and Van Stelle [86] carried out hot tests to characterize the performance of this concept. The test results showed that this nozzle operates similarly to a TIC profile nozzle at low altitude. However, no study of the flow behavior during the transition between the two modes was carried out. In 2007, Semenov et al [87] carried out a campaign of experimental measurements. These experiments showed that the gain in performance remained limited (of the order of 1-3%). In addition, the existence of side loads in the low-altitude mode, and a significant outward leakage of hot gases in the high-altitude mode, are prohibitive limitations for the application of this concept on a launcher.

Active secondary injection nozzle:

A gas at a defined pressure is injected into the main nozzle flow, either normally or at an angle, from the wall. The overstretched flow can then be forced to separate at a desired location, Figure III.19b. An experiment by [88], based on this concept, shows that a large amount of gas is required to induce significant flow separation. Furthermore, no increase in net yield is achieved when considering the additional mass flow.

Another alternative to this concept has been proposed by [89], Figure III.20a. The main idea of this device is to reduce the external pressure level at the nozzle outlet section. This requires a secondary nozzle to be positioned close to the main divergent outlet. This device is probably the most promising, although the definition proposed in [89] (curved secondary nozzle) has not demonstrated any real effectiveness: the Vulcain 1 engine does indeed incorporate one of the variants proposed by the author, but its sensitivity to jet disbondment is no different from that of other engines in the same class. Recently, Boccaletto [90] proposed the installation of an aerospike at the end of the main nozzle, Figure III.20b, and named the resulting profile BOCCAJET. Experimental measurements with cold gas and numerical simulations have shown a potential improvement in performance, but no results in fire operation have been discussed.

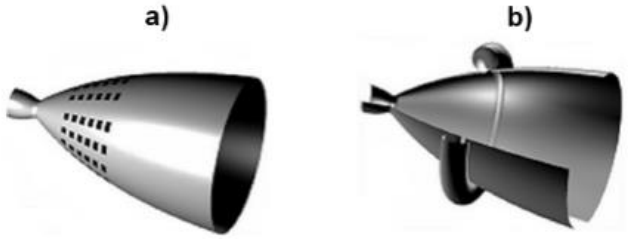

Figure III.19 : Secondary flow injection nozzle, a) Passive injection, b) Active injection, [25].

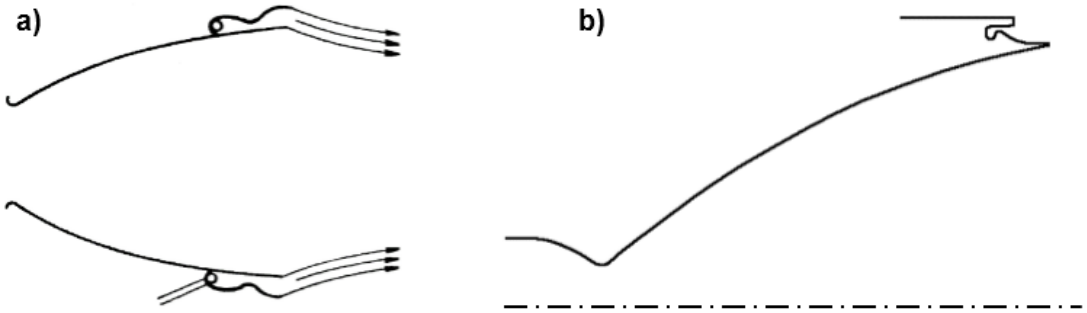

Figure III.20: Secondary flow injection nozzle near the outlet, secondary nozzle a) curved, b) aerospike (Boccajet)

Dual bell nozzle:

Several theoretical and numerical studies have been carried out on this type of nozzle: Horn & Fisher [3], Miyazawa et al [9], Nasuti et al [91], Miyazawa & Otsu [92]. Several scaled-down test campaigns have been carried out, both in cold gas; Génin & Stark [11, 19, 20], Östlund & Bigert [93], Verma et al. [14], Niu et al. [94], Tomita et al. [95], Reijasse et al. [16] and in conditions representative of rocket engine operation; Hagemann et al. [10], Hasegawa et al. [96]. The concept is based on the possibility of operating the nozzle at two different speeds. At low altitudes, only the first louver operates under "full flowing" conditions, while the second

louver is completely lifted off. At higher altitudes, the entire nozzle operates under full flowing conditions, Figure III.21. At the moment of transition between the two operating regimes, high lateral loads can be generated, as shown in Alziary de Roquefort et al. [97].

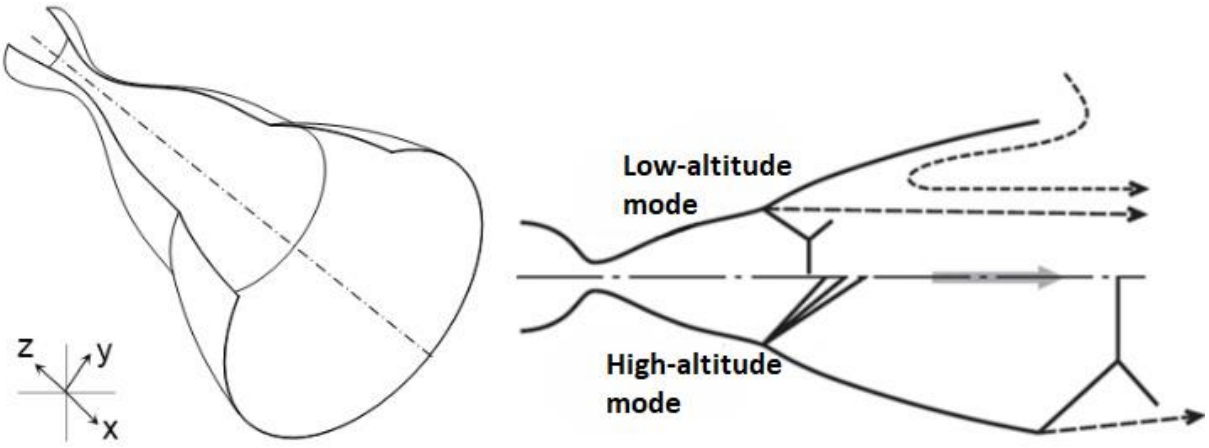

Figure III.21: Dual bell nozzle.

III.4.2 Vortex generator nozzle

To reduce lateral loads, two non-axisymmetrical designs are proposed.

Corrugated wall divergent:

The basic idea behind this concept, [98], is to increase the resistance to disbonding by generating vortices using a wavy contour at the nozzle outlet, Figure III.23a. The corrugated contour makes it possible, probably, to slow down the lateral movement of the disbond line by (i) increasing drag in the critical region, (ii) inducing longitudinal vortices which fix the structure of the circumferential flow, Figure 1.22.

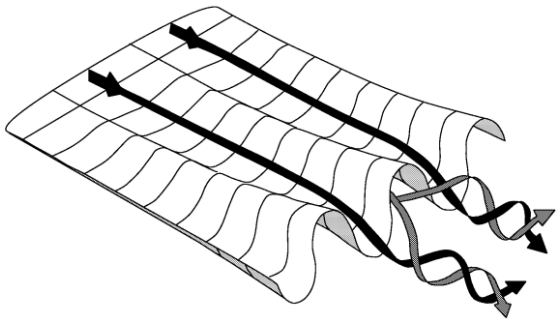

Figure III.22: Schematization of vortex structures on a corrugated surface, [99].

Cold gas tests on subscale models [99] have shown that the corrugated contour significantly reduces, and in some cases totally eliminates, shock-induced disbonding in the overstretched flow. However, due to the high parietal stress on the corrugated surface and an increase in overstretch losses, disbond control is achieved at the cost of significant performance losses, ranging from 3.6%□6.4% compared to the fully disbonded case. In addition, the complexity of design and manufacture increases significantly when moving from a geometry of revolution to a three-dimensional geometry.

Polygonal divergent

The main idea is to control jet disbonding by introducing ridges along the divergent section, while achieving a gradual transition, from the throat to the outlet, from a circular to a polygonal cross-section of the nozzle, [100]. Experimental work on this type of concept was

carried out by the FSCD working group - Östlund J. & Bigert M. [93]. However, the results obtained were not considered convincing.

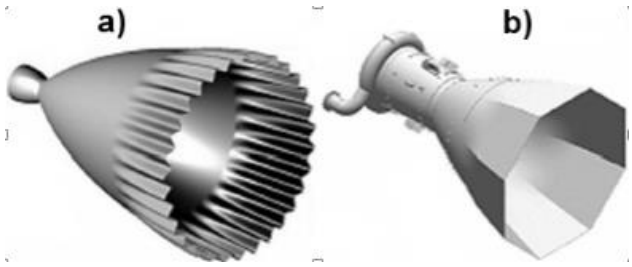

Figure III.23: Nozzle with vortex generators, a) Corrugated-wall diverter, b) Polygonal diverter, [25].

III.4.3 Dual-mode nozzle

Dual throat nozzle:

This concept envisages two completely concentric combustion chambers, Figure III.24a. At low altitude, both chambers operate in parallel at a moderate expansion ratio. In high-altitude mode, only the inner chamber remains in operation. This results in a higher expansion ratio than in the first mode, and thus a gain in performance in high-altitude mode. Fire tests [101] have demonstrated the presence of disbonding in low-altitude mode at high outer nozzle/inner nozzle pressure ratios. This disbond results from high thermal loads on the inner nozzle. In addition, profile discontinuity in high-altitude mode induces performance losses of the order of 0.8-4%, depending on the cross-sectional ratio of outer to inner throat [5].

Dual concentric engines:

This concept, [102], envisages two concentric motors, the smaller of which is enclosed within the larger, Figure III.24b. Unlike the previous type, the inner chamber is not completely enclosed within the outer chamber, so the latter is annular in shape with an independent inner wall. In principle, the two operating modes are comparable to those of a dual throat nozzle, [5]. Numerical simulations [103,104] have shown the presence of compression waves close to the outlet lip of the inner nozzle, in the low-altitude mode, causing flow inhomogeneity in the common mixing zone between the inner and outer nozzles. These compression waves are reflected back into the flow field after interaction with the outer wall.

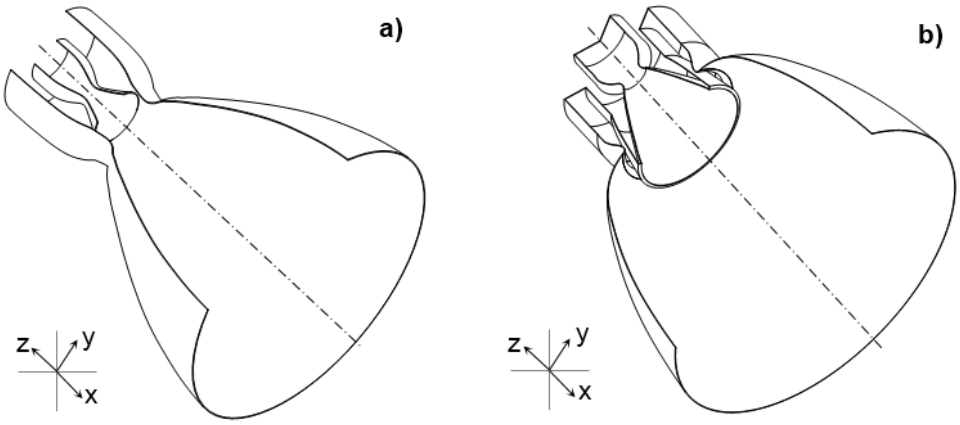

Figure III.24: Dual mode nozzle, a) Dual throat nozzle, b) Dual concentric engines.

During the high-altitude mode, expansion waves are noticed at the outlet of the outer nozzle when the cross-section ratio suddenly increases and the flow is directed towards the axis of symmetry. Close to the axis, a shock occurs and static pressure rises significantly in the central jet region. This pressure increase induces subsonic and supersonic recirculation zones in the inner nozzle. According to [5], losses due to inhomogeneity and compression shock remain comparable to those in curved (conventional) nozzles. To date, no experimental measurements have been made on this type of nozzle, either with cold gas or fire.

III.4.4 Self-adjusting nozzle:

This category of nozzles will be classified according to operational type, i.e. expansion is achieved by internal or external flow.

Self-adapting internal flow nozzle

- **Variable surface divergent :**

This concept, [105], involves varying the nozzle's cross-section ratio by extending its previously folded surface (Figure III.25). This would enable the nozzle outlet pressure to be adapted to all flight altitudes. Although from a theoretical point of view this solution is the most appropriate for eliminating the problem of jet separation and maximizing nozzle performance, its feasibility has yet to be fully demonstrated. Nevertheless, similar technological solutions (superimposed petal nozzles) have been used on ballistic missiles and some military aircraft nozzles. This technology allows rather modest rates of change in cross-section ratio, and cannot easily be integrated into nozzles requiring active cooling of the metal wall.

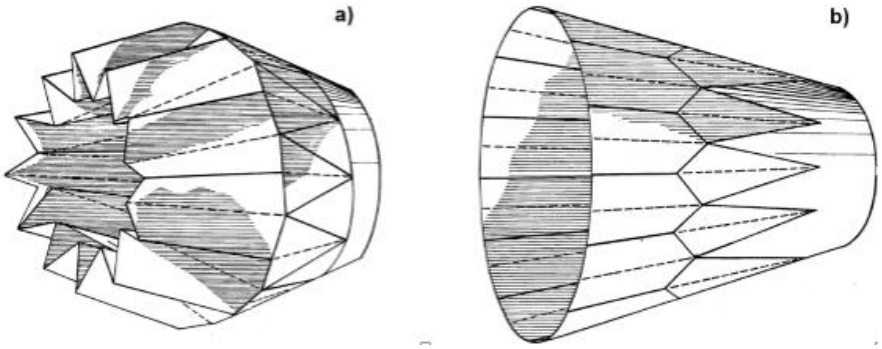

Figure III.25 : Variable surface divergent : [105].

- **Variable-area throat :**

This concept, shown in Figure III.26, uses a conventional curved nozzle with a fixed outlet cross-section and a mechanical needle in the combustion chamber and throat area to vary the throat area and, consequently, the cross-section ratio. The annular neck section between the needle and the outer wall is varied by axially displacing the needle.

The needle concept has been used in solid rocket motors as a means of providing variable thrust. In principle, it allows continuous variation of the throat cross-section and, consequently, optimum cross-section ratios throughout the mission. However, it requires a sophisticated actuator and control system. The concept raises questions of motor weight, design complexity, needle and neckwall cooling, and reliability. The performance losses of this type of nozzle are in the range of 1 to 2.5% compared with a curved nozzle for the same cross-section ratio [106]. These performance losses vary according to the position of the needle.

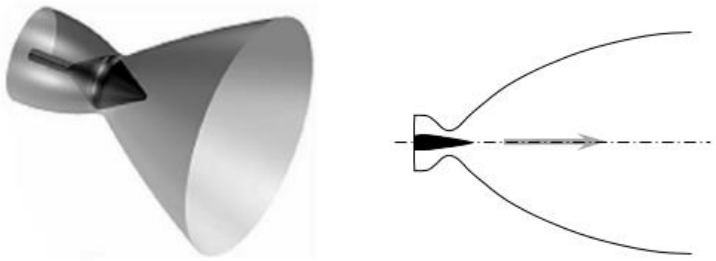

Figure III.26: Nozzle with variable cross-section throat, the figure on the left is taken from [25].

– **Expansion/deflection nozzle :**

These concepts, shown in Figure III.27, are primarily aimed at reducing the overall motor footprint, particularly in the longitudinal direction. Several variants of this concept have been proposed. The best known is where the combustion chamber (and other engine components) are embedded in the middle of the nozzle [107]. In this concept, the combustion gases reach sonic velocity in correspondence with the zone where their flow direction undergoes a strong deviation, to be directed into the supersonic nozzle, without generating shock waves. Indeed, focusing a compression wave on the metal wall of the throat would be prohibitive for the thermomechanical strength of the structure.

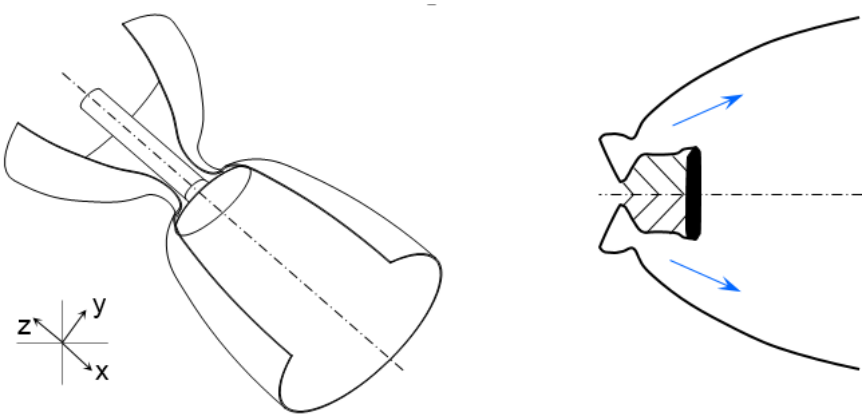

Figure III.27: Expansion/deflection nozzle

Defining the profile of the sonic region of the combustion chamber, as well as its cooling, represent the most critical points for the realization of this concept. Nevertheless, a prototype has been built in Russia (RD-0126E engine) and fire tests were carried out in the 1990s, demonstrating that it worked well [47]. However, this type of nozzle is mainly intended for use in a vacuum, as it offers no improvement over the problem of jet disbonding.

Self-adapting external flow nozzle:

Self-adaptation results in the jet's outer boundary adjusting to the external pressure pa. The advantage of plug nozzles over conventional nozzles arises in over-expansion regimes, as the outer boundary is adapted to the jet, which is channelled through an effective cross-sectional area ***Aeff*** that varies according to the external pressure. A central-body nozzle therefore operates with an effective cross-section ratio ***Aeff/Ac*** that adapts to altitude. The result is a self-controlled expansion of the propellant gases, which explains why there is no jet separation on the spine.

Several variants of this type of concept have been proposed in the literature: linear or axisymmetric, ideal or truncated spine with or without gas injection at the base, fed by a single or multi-chamber combustion chamber (modular chambers). Numerous theoretical, numerical and experimental studies have been carried out to evaluate the optimal spine geometry - Dunn & Coats [108] - and to assess the performance and limitations of the various possible architectures - Calabro et al. [109], Le Bozec et al. [110], Wisse [111, 112], Onofri [113]. In the following, we shall confine ourselves to an overview of a few variants. Readers interested in this type of nozzle can refer to the above references and to reference [5].

- **Nozzle with ideal central body:**

This concept calls for an ideal axisymmetric central body (full-length plug nozzle) with a conical or curved profile, Figure III.28. The profile calculation is based on Rao's method [37], or to take into account kinematics and boundary layer effects, on the TDK (Two-Dimensional Kinetics) method, [108]. From a point of view similar to that of an ideal nozzle with internal flow, the profile of an ideal spine is very long and therefore much heavier than that of a conventional ideal nozzle. This type of nozzle offers better performance in low-altitude mode and the same performance in high-altitude mode as a conventional nozzle for the same cross-section ratio [5]. However, its weight and length make it difficult to integrate on a launcher. In addition, it requires a high-tech cooling system, especially at the tip of the spine.

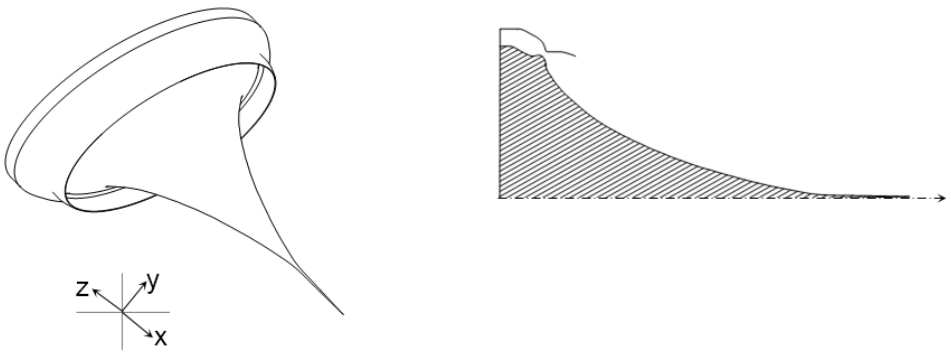

Figure III.28: Nozzle with ideal profiled central body

– **Nozzle with truncated central body:**

This concept has advantages over the previous one, given its mass and moderate length. In fact, it results in a behavior of the flow field deferent. In low-altitude mode, the bottom region generates an open wake at a pressure very close to atmospheric pressure. In high-altitude mode (at the design pressure ratio), the wake closes and its length is independent of atmospheric pressure. The transition between the two modes generates negative thrust, due to the fact that when the wake closes, the pressure at the base is slightly lower than atmospheric pressure. This loss of thrust is highly dependent on the percentage of truncation. At low altitude, this nozzle

gives almost the same performance as the ideal central body nozzle. At high altitudes, however, it is characterized by a loss of performance due to the drag of the base [5].

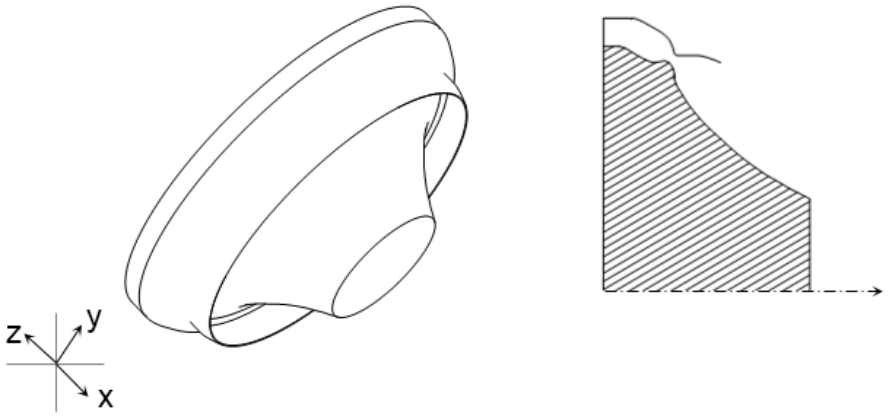

Figure III.29: Nozzle with truncated central body

– **Flat nozzle with truncated central body:**

Linear Aerospike Nozzles (LANs), which were the subject of numerous studies in the years 1980□2000. The best-known example is probably the NASA XRS-2200 prototype, Figure III.30, fire-tested in August 2001 at NASA's Stennis Space Center. However, following the cancellation of the X-33 project, for which this engine was intended, work was halted.

By design, this type of nozzle enables the engine to operate with a constantly attached supersonic flow, as the jet is constantly in pressure equilibrium with the atmosphere (whatever the flight altitude).

However, when the nozzle is operating at high altitude, the static pressure of the surrounding environment is low, and its propulsive performance diminishes sharply. It is also important to emphasize that several difficulties still need to be resolved before this technology can be applied in flight. Firstly, control of the shock network (and associated thermomechanical loads) generated by the interaction of the propulsive jet with the atmosphere and the metal surface of the spine, under all engine operating conditions and at all flight altitudes. On the other hand, the need to properly cool the spine, particularly its tip, imposes design and manufacturing constraints that are difficult to meet.

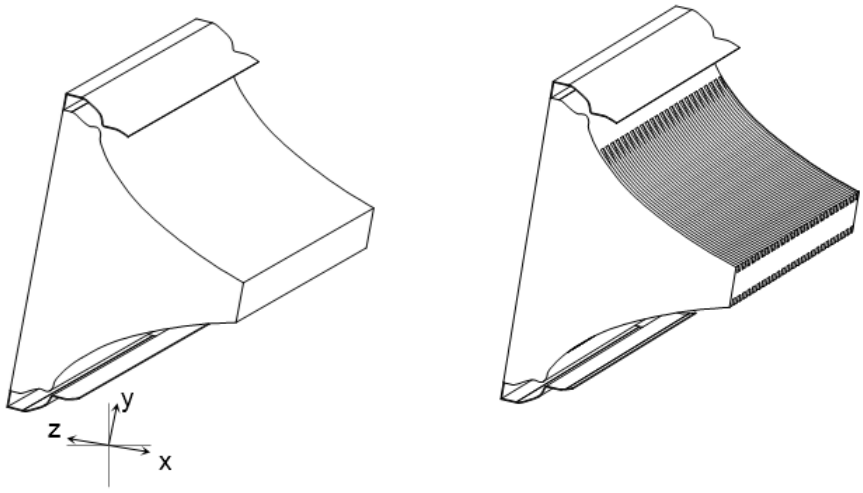

Figure III.30: Flat nozzle with truncated central body.

CHAPTER IV: RESULTS AND DISCUSSIONS

IV-1.INTRODUCTION

This chapter is devoted to the simulation of supersonic flows in Dual bell nozzle using Fluent-ANSYS simulation software.The results obtained presented in the form of curves and contours for the different parameters (Mach, pressure, temperature, etc.) will be compared, analyzed and discussed.

IV-1-1. Overview of Physical Models in ANSYS FLUENT

Ansys Fluent provides comprehensive modeling capabilities for a wide range of incompressible and compressible, laminar and turbulent fluid flow problems. Steady-state or transient analyses can be performed. In Ansys Fluent, a broad range of mathematical models for transport phenomena (like heat transfer and chemical reactions) is combined with the ability to model complex geometries. Examples of Ansys Fluent applications include laminar non-Newtonian flows in process equipment; conjugate heat transfer in turbo machinery and automotive engine components; pulverized coal combustion in utility boilers; external aerodynamics; flow through compressors, pumps, and fans; and multiphase flows in bubble columns and fluidized beds. [58]

To permit modeling of fluid flow and related transport phenomena in industrial equipment and processes, various useful features are provided. These include porous media, lumped parameter (fan and heat exchanger), stream wise-periodic flow and heat transfer, swirl, and moving reference frame models. The moving reference frame family of models includes the ability to model single or multiple reference frames. A time-accurate sliding mesh method, useful for modeling multiple stages in turbo machinery applications, for example, is also provided, along with the mixing plane model for computing time-averaged flow fields. [58]

Another very useful group of models in Ansys Fluent is the set of free surface and multiphase flow models. These can be used for analysis of gas-liquid, gas-solid, liquid-solid, and gas-liquid-solid flows. For these types of problems, Ansys Fluent provides the volume-of-fluid (VOF), mixture, and Eulerian models, as well as the discrete phase model (DPM). The DPM performs Lagrangian trajectory calculations for dispersed phases (particles, droplets, or bubbles), including coupling with the continuous phase. Examples of multiphase flows include channel flows, sprays, sedimentation, separation, and cavitations. [58]

Robust and accurate turbulence models are a vital component of the Ansys Fluent suite of models. The turbulence models provided have a broad range of applicability, and they include the effects of other physical phenomena, such as buoyancy and compressibility. Particular care has been devoted to addressing issues of near-wall accuracy via the use of extended wall functions and zonal models. [58]

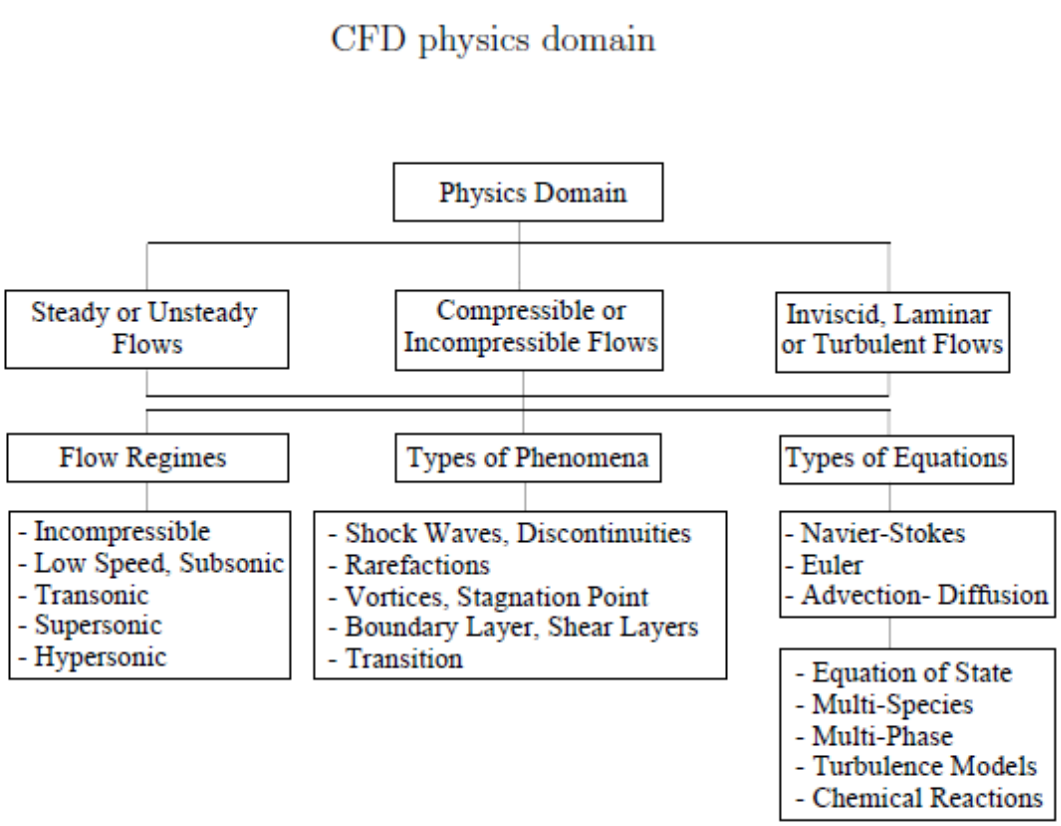

Figure(IV.1):CFD Physics Domain

IV -1-2.Calculation codes on cfd

Like any CFD software, it is composed of three elements: the preprocessor, the solver and the postprocessor.

- The definition of the problem to be solved is done using the ANSYS Design Modeler and Meshing preprocessor. It makes it possible to represent the geometry, discretize the domain by several meshing algorithms and name the different components and/or materials (fluid or solid).

- The solver makes it possible to numerically define the operating conditions under which the simulation will be carried out, as well as the specification of the boundary conditions. Finally, it allows to choose the iterative process by proposing various numerical schemes for spatio-temporal discretization and for velocity/pressure coupling.

- The postprocessor is the element that displays the results obtained. It makes it possible to view velocity vector fields, pressure and turbulence fields as well as all other quantities on a segment, a section or the entire domain. It also allows you to draw curves.[59]

IV -2.Numerical simulation

IV-2 -1.Preprocessing

IV-2 -1-1.Geometry (computational domain) creation

Creation of the axisymmetric geometry (or the computational domain) using the DesignModeler module in Ansys workbench.

IV -2-1.1.1-Combustion Chamber

For optimum performance, the combustion chamber is built with particular dimensions. Its length of 0.06 meters offers enough room for the combustion process to proceed well. The chamber's 0.014-meter width permits a controlled flow of the fuel and air mixture. These measures were meticulously chosen to guarantee that the combustion chamber performs to its fullest capability, enhancing combustion stability and overall engine performance.

This is a representation of a species transport combustion chamber (as shown in Figure IV.2).

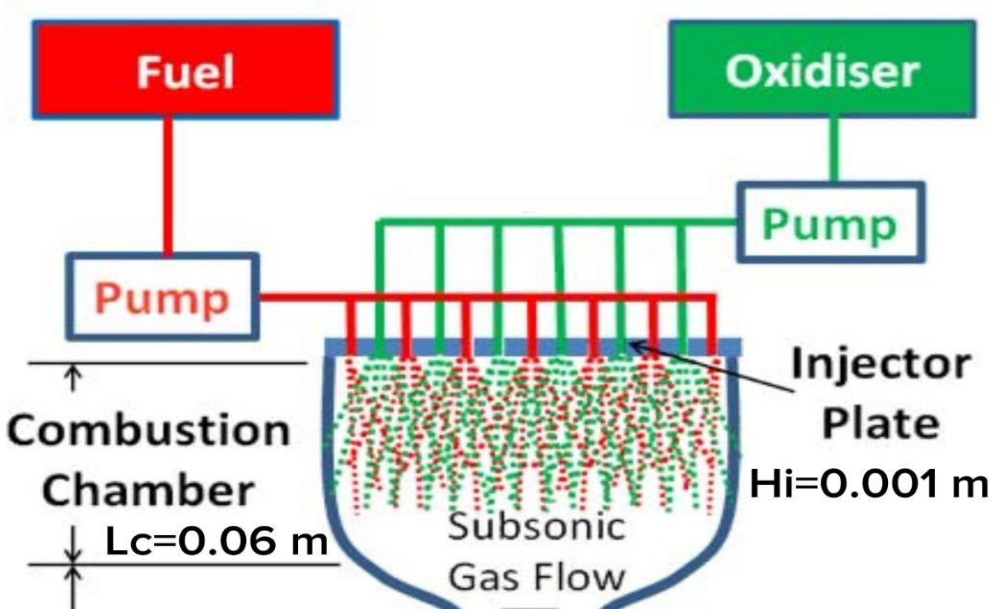

Figure(IV.2):multiple fuel and oxidizer inlets

The use of multiple inlets for fuel and oxidizer modelisation in the combustion chamber helps in:

1.Improving mixing: By supplying fuel and oxidizer through several inlets, the mixing of the two streams can be improved, resulting in more effective combustion and a more even distribution of temperature inside the combustion chamber. This can enhance combustion stability and lower pollutants.

2. Increasing turbulence: More turbulence in the combustion chamber can improve the mixing of fuel and oxidizer and increase combustion efficiency. Multiple inlets can increase turbulence in the combustion chamber.

3.Increasing flexibility: Multiple inlets allow for greater flexibility in the design of the combustion system. For example, by varying the number and location of inlets, it is possible to

optimize the combustion process for different operating conditions, such as changes in altitude, temperature, or fuel type.

4.Enhancing combustion stability: Multiple inlets can also help to promote combustion stability. By injecting fuel and oxidizer from several locations, it is possible to create more uniform and stable combustion conditions throughout the combustion chamber. This can reduce the risk of flame blowout or other combustion instabilities.

5.Higher combustion efficiency: With multiple inlets, it is possible to achieve more complete combustion of the fuel. This is because the fuel and oxidizer can be more effectively mixed, leading to a more uniform and complete combustion process.

It is important to take into account how specific parameters can affect the combustion process. One crucial element is mixing, where the size of the combustion chamber is significant. Increased mixing time between the fuel and oxidizer is made possible by a longer chamber, which improves combustion efficiency. However, insufficient mixing can lead to uneven combustion, which can result in areas of rich or lean combustion and the generation of contaminants.

Another important element impacting combustion is turbulence. It improves mixing and increases the effectiveness of combustion. Turbulence levels are influenced by the combustion chamber's length; longer chambers often produce more turbulence. However, too much turbulence might result in unstable combustion and higher emissions.

The combustion chamber's length also affects heat transfer. Longer chambers offer more surface area for heat transfer, which can aid in dissipating heat from combustion products and preventing damage to the chamber. However, excessive heat transfer might cause combustion products to burn incompletely by lowering their temperature below the acceptable threshold.

The pressure drop across the system is also impacted by the combustion chamber's length. A longer chamber frequently results in a greater pressure drop, which can lower the combustion process's overall efficiency. On the other hand, if the pressure drop is too low, insufficient mixing and combustion may occur.

To ensure effective and clean energy conversion, the combustion process must be optimized taking into account these factors and how they interact.

Next, we show the axisymmetric dual-bell nozzle with its design parameters:

IV -2.1.1.2-The Dual-Bell Nozzle:

To increase the effectiveness and performance of rocket engines, a twin bell nozzle is a particular kind of rocket nozzle design. It is divided into two distinct sections, a convergent section and a divergent section. While the diverging part further expands the exhaust gases to produce more thrust, the convergent section quickens the flow of exhaust gases.

DBN length = 23.79 × Rth, DBN exit radius = 4.98 × Rth, with Rth (throat radius) = 0.01 m, exit Mach number DBN: Me, stagnation temperature and pressure (total parameters in the combustion chamber): T_0 = 300 K, P_0 = 30 bars.

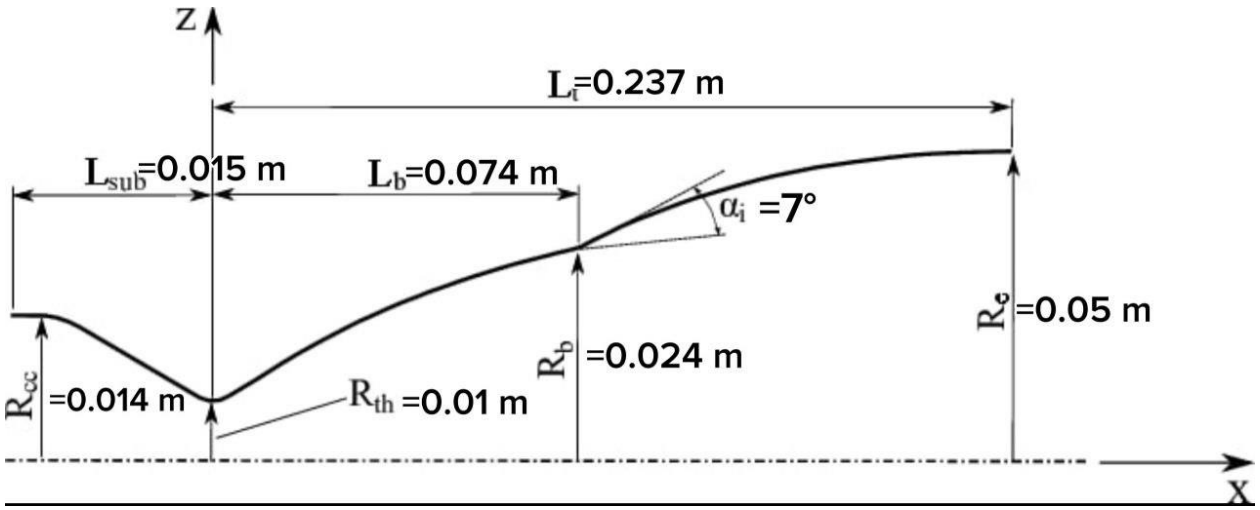

Figure (IV.3): The Axisymmetric Dual-Bell Nozzle

IV-2 -1-2.Meshing

IV-2 1-2-1.Discretization of computational domain

The discretization of computational domain involves the transformation of the initial transport equations into algebraic equations approximating them by defining the relations of the dependent variables in the selected regions in time and space. One of the most common approach to discretization applies the use of the mesh method. As a result of discretization, the differential equations (in which each one is linearized) is replaced by a system of algebraic equations, whose consequence takes the form a linear algebraic equations. This process occurs by discretization of a computational mesh. Each of the elements of this mesh corresponds to a control volume throughout the calculations. Depending on the discretization method, the mesh is composed of nodes, elements or volumes. The level of the precision gained from the solution of numerical problems is largely relative to the type and density of such a mesh. Depending on the applied geometrical form, meshes can be classified into triangular and quadrilateral (for two-dimensional models). In turn, for three-dimensional models, the most common meshes are tetrahedral (with a base in the form of a triangle), pyramid-shaped prisms with a triangular base, and hexagonal prism with a base in the form of a triangle. The use of hexagonal cells results in the limitation of the number of the mesh elements in the computational domain and provides a better accuracy of calculations. However, the generation of this type of meshes requires a considerable input in terms of amount of required effort. In turn, tetrahedral meshes are applied with regard to models with considerable curvatures and in cases when numerous details need to be accounted for.[60]

In such as case a number of post-processors have the capability of generating this type of mesh. The classification in terms of the arrangement of the cells in a mesh, we can distinguish structured, unstructured and hybrid meshes. In the first type, cells are characterized by regular connectivity. The generation of this mesh type requires more effort; hence, they are recommended for the case of simple geometries. The unstructured type is applied most commonly for the case of complex geometries. In this case, any shape of each mesh cell can be used. In many cases, the third type of cell arrangement can provide useful. It combines the advantages of structured and unstructured meshes.[60]

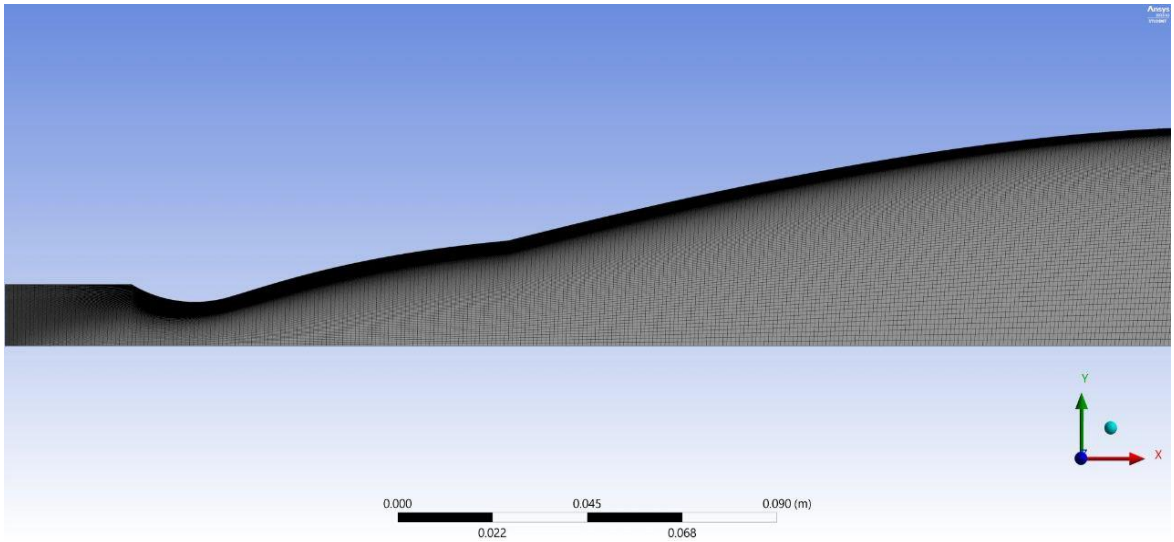

Figure*(IV.4):the mesh of the combustion chamber and the DBN using ANSYS software.*

IV-2 -1-2-2.Mesh Quality Metrics

- Mesh Metrics are available underMesh Options to set and review mesh metric information and to evaluate mesh quality

- Different physics and different solvers have different requirementsfor mesh quality

- There are several Mesh metrics available in ANSYS Meshing , we will present the most common :

— Element Quality

— Skewness

— Aspect Ratio

— Orthogonal Quality

— The Y+ Value

IV-2 -1-2-2.Mesh Quality Metrics

1.Element Quality

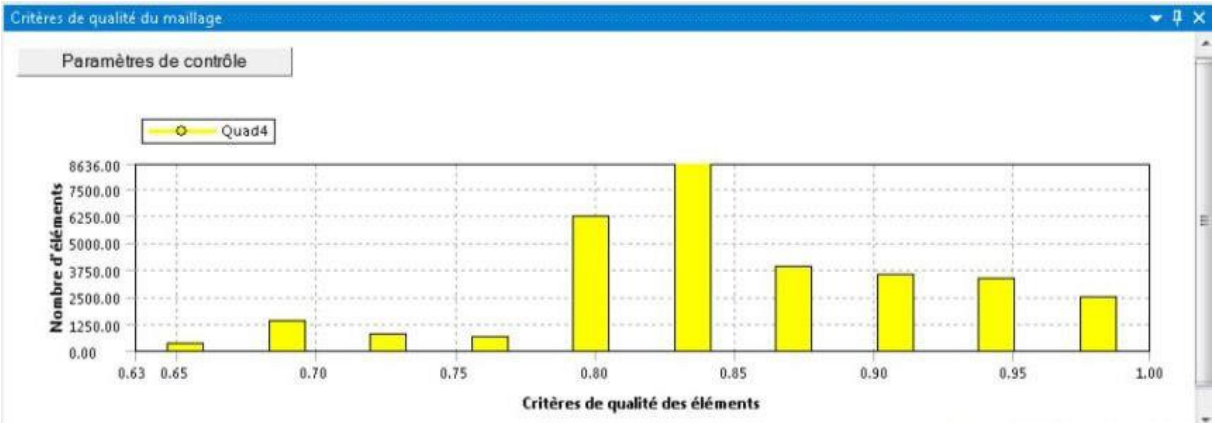

Figure (IV.5): *The mesh and the criteria (element number)*

Details of "Maillage"

Element Order	Linear
Element Size	1.e-003 m
Export Format	Standard
Export Preview Surface Mesh	No
Sizing	
Quality	
Check Mesh Quality	Yes, Errors
Target Skewness	Default (0.9)
Smoothing	Medium
Mesh Metric	Element Quality
Min	2.9932e-002
Max	0.98471
Average	0.3672
Standard Deviation	0.27594
Inflation	
Batch Connections	
Advanced	
Statistics	

Figure (IV.6): *Element quality*

IV-2 -1-2-2.Mesh Quality Metrics

2. Skewness

Determining skewness:Based on the Equilateral Volume deviation:

- $\text{Skewness} = \dfrac{\text{optimal cell size} - \text{cell size}}{\text{optimal cell size}}$
- Applies only to triangles and tetrahedra.
- Default method for triangles and tetrahedras.

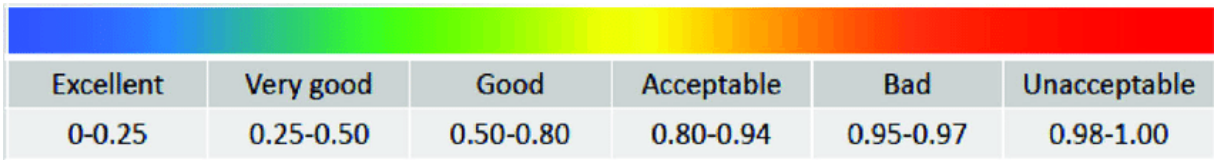

Excellent	Very good	Good	Acceptable	Bad	Unacceptable
0-0.25	0.25-0.50	0.50-0.80	0.80-0.94	0.95-0.97	0.98-1.00

Figure(IV.7): Skewness mesh metrics spectrum

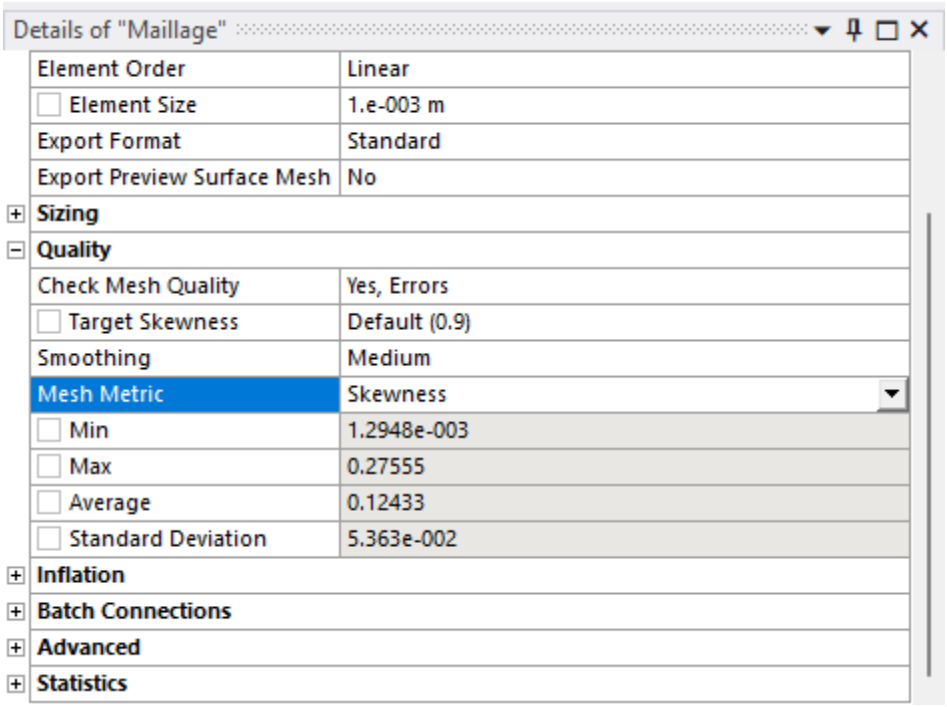

Figure *Skewness* ***(IV.8):***

IV-2 -1-2-2.Mesh Quality Metrics

3. Aspect Ratio

-Aspect for generic triangles and quads is a function of the ratio of longest side to the shortest side of the reconstructed quadrangles.

-Equal to 1 (ideal) for an equilateral triangle or a square.

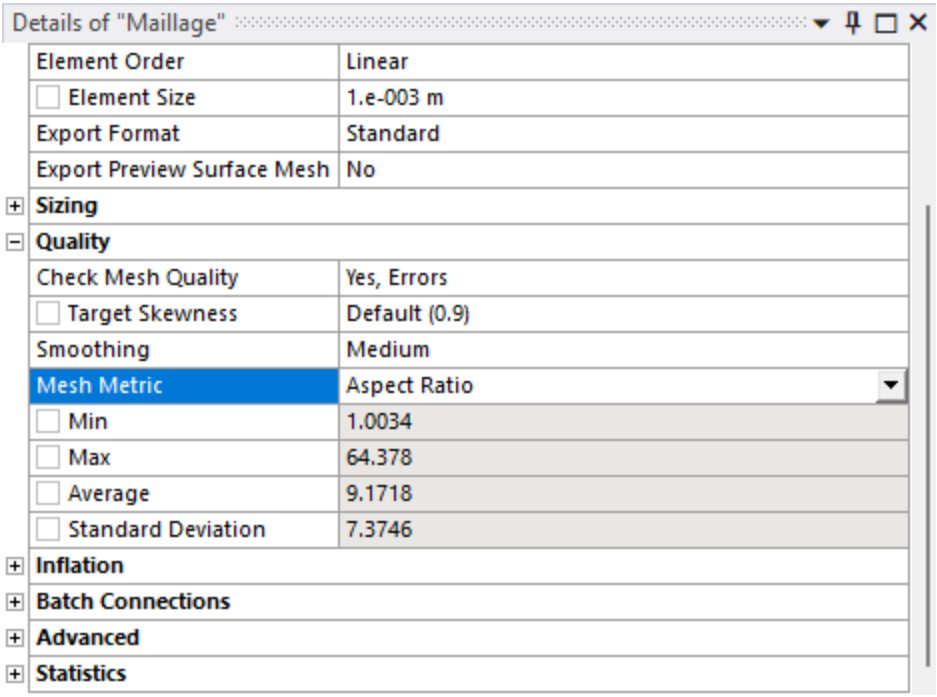

Figure(IV.9): Aspect Ratio

IV-2 -1-2-2.Mesh Quality Metrics

4.Orthogonal Quality

• It adds numerical diffusion to the solution.

• It mainly affects the diffusive terms.

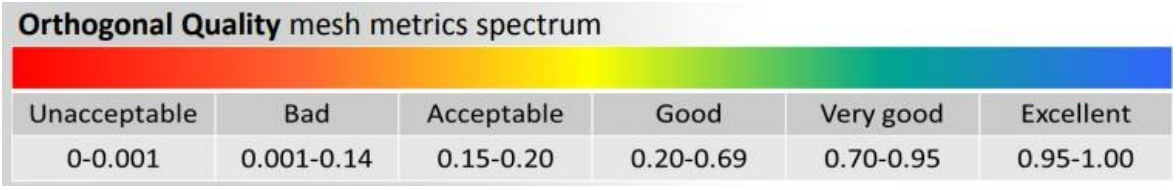

Figure(IV.10): Orthogonal quality mesh metrics spectrum

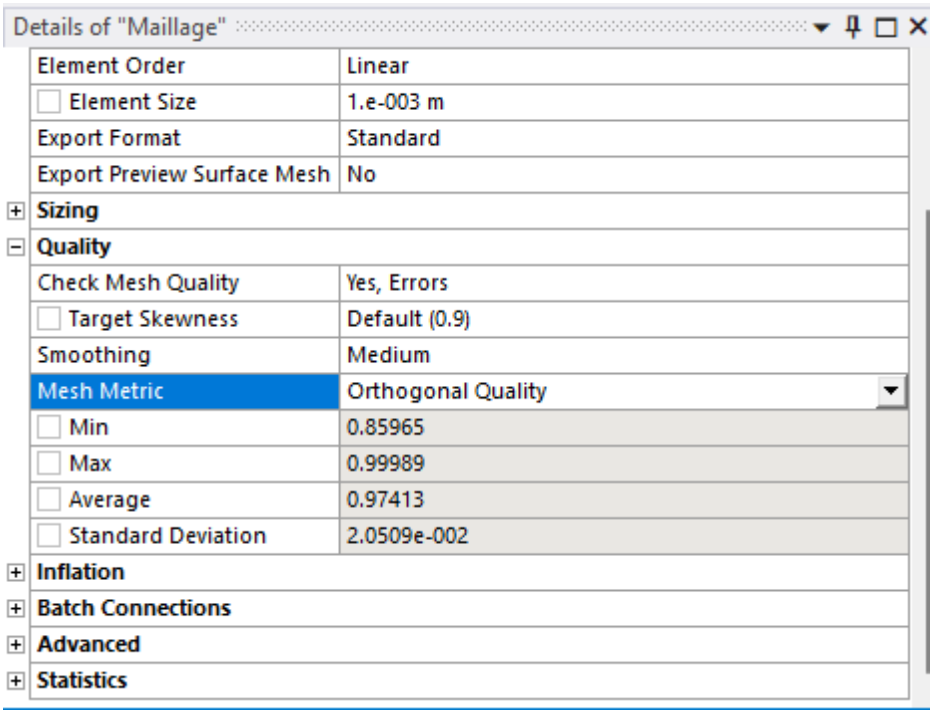

Figure(IV.11): Orthogonal Quality

- The min, max, averaged and standard deviation for the selected mesh metric are shown for the surface mesh (after Preview Surface Mesh generation) and for the volume mesh (after Preview Inflation layer or Generate Mesh generation)

- FLUENT requires high quality mesh to avoid numerical diffusion.

- Several Mesh Quality Metrics are involved in order to quantify the quality, however the skewness is the primary metric.

- The aspect ratio and cell size change mesh metrics are also veryimportant

- In worst scenarios and depending on the solver used (density based or pressure based) FLUENT can tolerate poor mesh quality. However some applications may require higher mesh quality, resolution and good mesh distribution.

- The location of poor quality elements helps determine their effect.

- Some overall mesh quality metrics may be obtained in Ansys Meshing under the Statistics object.

IV-2 -2. Processing:

IV-2 -2.1 Finite volume based solver:

Fluent is one of the two computational fluid dynamics (CFD) packages included with the ANSYS computational mechanical software suite. Fluent is a Green-Gauss Finite Volume Method with a Cell-Centered formulation (and we'll cover what that means in a few minutes). The major point is the finite volume method (FVM).

Computational engineers solve partial differential equations. There are three numerical methods for the solution of partial differential equations we'll compare in this class. Essentially, - the finite difference method (FDM) discretizes the classical form of the PDE; - the finite element method (FEM) discretizes the weak form of the PDE; and - the finite volume method (FVM) discretizes the conservation form of the PDE.

FVM has the relative advantage of being mathematically straightforward (particularly over some of the more abstruse versions of FEM) and in particular is excellent for problems in which quantity conservation is vital.

IV-2 -2.1.1 The Semi-Discretized Equation:

The conservation equation for a general scalar φ may be written,

$$\frac{\partial(\rho\varphi)}{\partial t} + \nabla \cdot (\rho\vec{v}\varphi) = \nabla \cdot \left(\Gamma^{\varphi}\nabla_{\varphi}\right) + Q^{\varphi} \qquad \textbf{(IV.1)}$$

Respectively, a transient term, convective term, diffusive term, and source term. Γ represents the diffusive coefficient. Recollect the physical definitions of the convective and diffusive terms: "Convection is a physical process that occurs in a flow of gas in which some property is transported by the ordered motion of the flow. Diffusion is a physical process that occurs in a flow of gas in which some property is transported by the random motion of themolecules of the gas. [62]

Assuming that the foregoing equation (1) is steady-state (the transient term goes to zero) and (2) applies to a single control volume C, this becomes :

$$\int_{V_c} dV\nabla \cdot (\rho\vec{v}\varphi) = \int_{V_c} dV\nabla \cdot \left(\Gamma^{\varphi}\nabla_{\varphi}\right) + \int_{V_c} dV\, Q^{\varphi} \qquad \textbf{(IV.2)}$$

Finally, we apply the Gaussian divergence theorem to replace the volume integrals over the control volume by surface integrals over the control surface:

$$\oint_{\partial V_c} d\vec{s} \cdot \nabla \cdot (\rho\vec{v}\varphi) = \oint_{\partial V_c} d\vec{s} \cdot \left(\Gamma^{\varphi}\nabla_{\varphi}\right) + \int_{V_c} dV\, Q^{\varphi} \qquad \textbf{(IV.3)}$$

This final form represents the conservative form of the PDE, and FVM focuses on efficiently solving this statement. (This is what we mean by cell-centered FVM; LongND summarizes alternative formulations.) There are two types of quantities represented: surface flux terms and a volume source term.

IV-2.2 Solver Setup:

IV -2.2.1 Dimension :

The 2-D Dimension is chosen as the problem that is being analysed is a 2D dimension problem.

IV -2.2.2 Solver Processes :

Parallel processing in ANSYS FLUENT involves an interaction between ANSYS FLUENT, a host process, and a set of compute-node processes. ANSYS FLUENT interacts with the host process and the collection of compute nodes using a utility called cortex that manages ANSYS FLUENT's user interface and basic graphical functions.

Parallel ANSYS FLUENT splits up the mesh and data into multiple partitions, then assigns each mesh partition to a different compute process (or node). The number of partitions is an integral multiple of the number of compute nodes available to you (e.g., 8 partitions for 1, 2, 4, or 8 compute nodes). The compute-node processes can be executed on a massively-parallel computer, a multiple-CPU workstation, or a network cluster of computers. [63]

The number of processes depend on the capabilities of the machine. By default, 2 processes are being used.

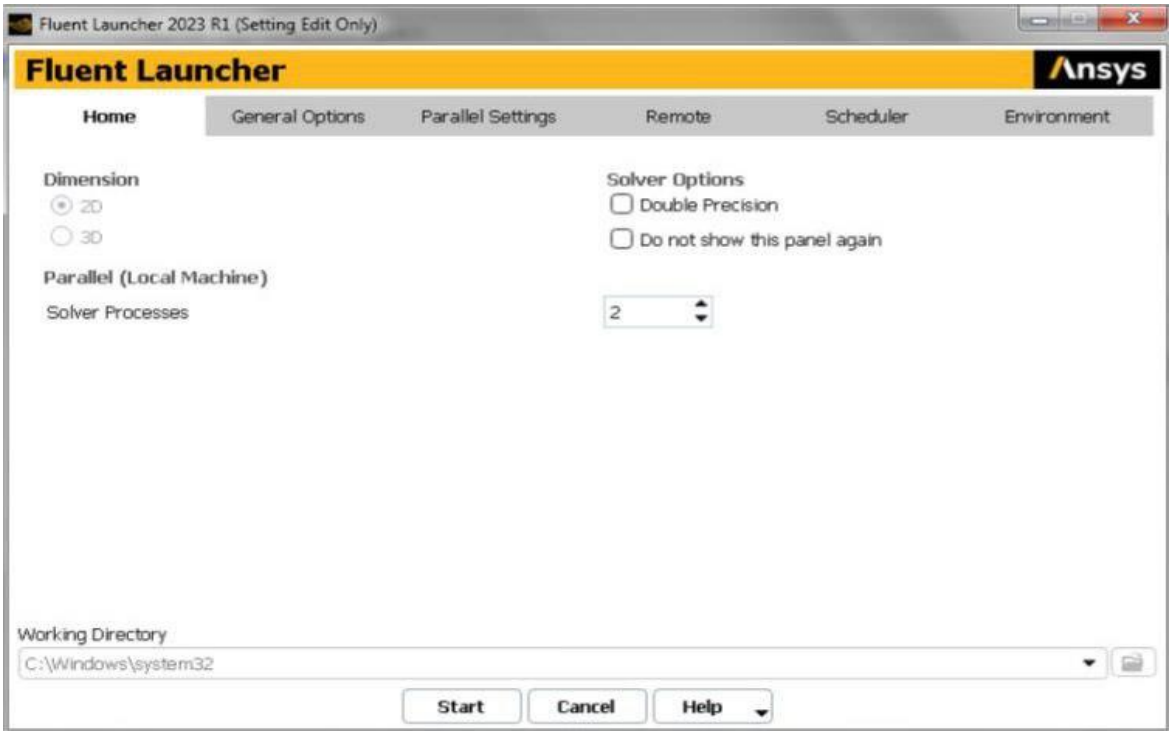

Figure(IV.12): Solver setup

IV -2.2.3 Solver type:

$$U_{vel}, V_{vel}, W_{vel}$$

ANSYS FLUENT allows you to choose one of the two numerical methods:

- Pressure-based solver
- Density-based solver

The density-based solver solves the governing equations of continuity, momentum, and (where appropriate) energy and species transport simultaneously (i.e., coupled together). Governing equations for additional scalars will be solved afterward and sequentially.

The pressure-based solver type has been chosen because it can handle both the combustion process and the compressible flow simulations.

The pressure-based solver employs an algorithm which belongs to a general class of methods called the projection method [64]. In the projection method, wherein the constraint of mass conservation (continuity) of the velocity field is achieved by solving a pressure (or pressure correction) equation. The pressure equation is derived from the continuity and the momentum equations in such a way that the velocity field, corrected by the pressure, satisfies the continuity. Since the governing equations are nonlinear and coupled to one another , the solution process involves iterations wherein the entire set of governing equations is solved repeatedly until the solution converges.

IV -2.2.3.1 The Pressure-Based Segregated Algorithm and Coupled Algorithm

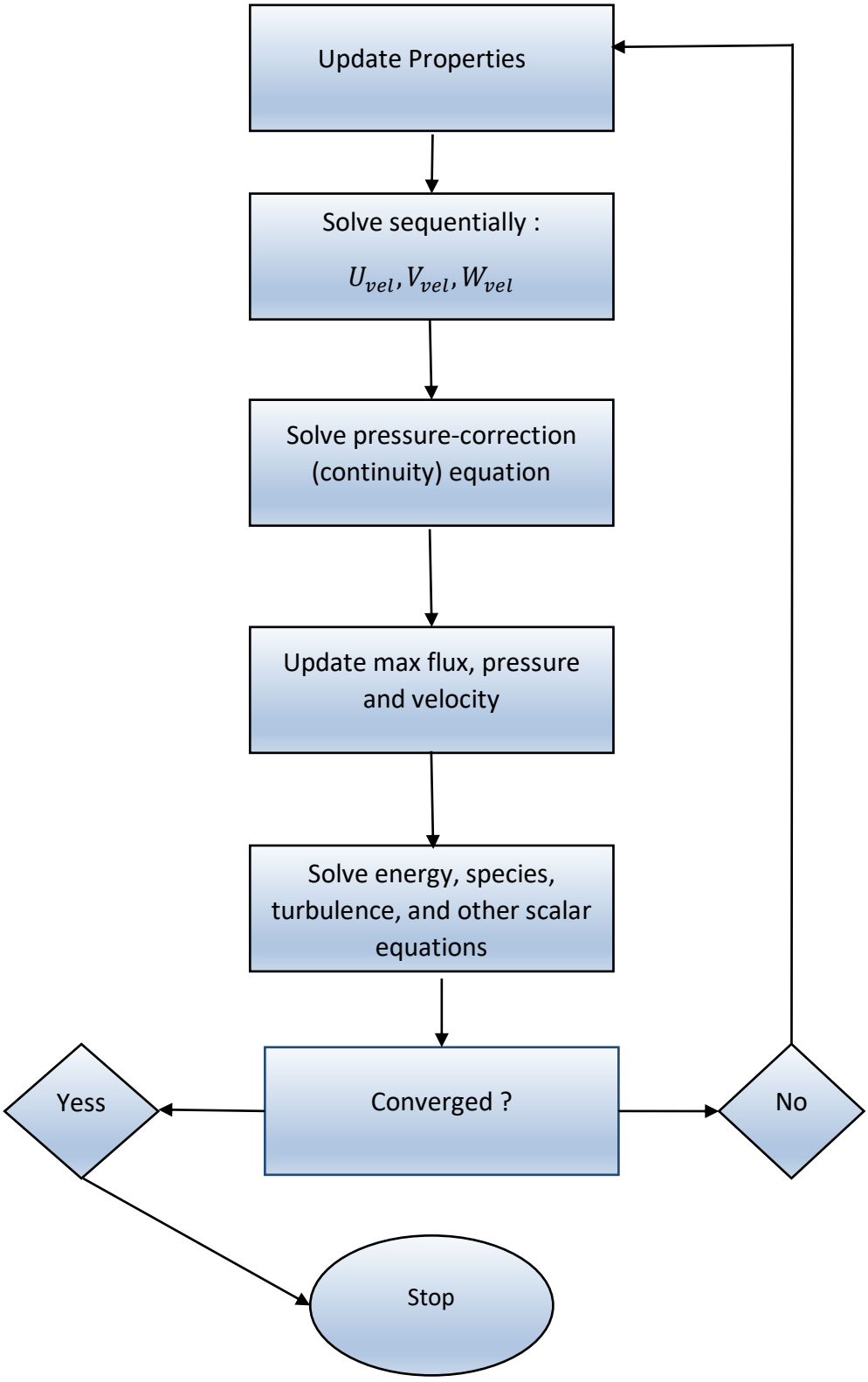

Fig (IV.13): The Pressure-Based Segregated Algorithm

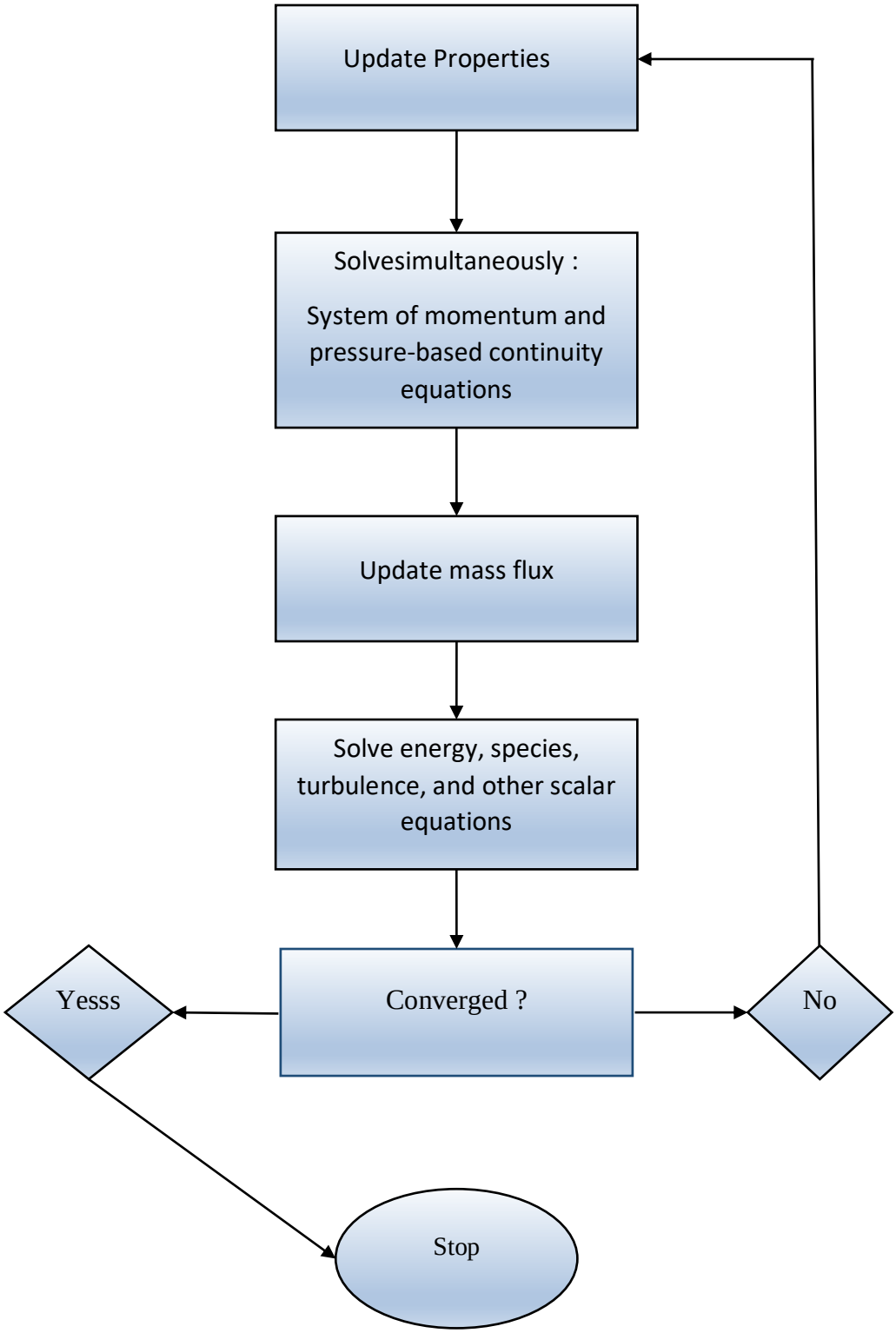

Fig (IV.14): The Pressure-Based Coupled Algorithm

IV -2.2.4 Axisymmetric model :

Since the problem that is being handled is related to a 2D Axisymmetric geometry that includes the combustion chamber and the nozzle, the Axisymmetric model will be used in this case.

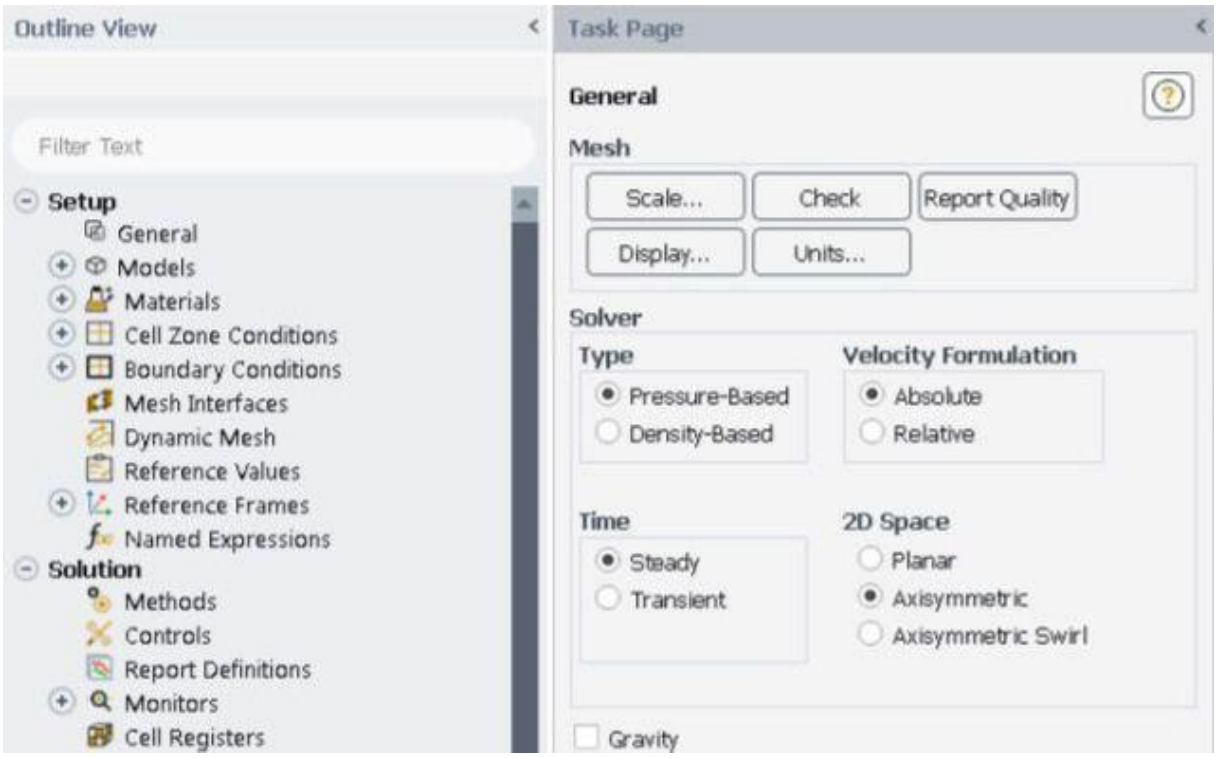

Figure(IV.15): The Axisymmetric model

IV -2.2.5 Steady vs Transient time :

Steady-state simulation involves computing a solution that remains constant over time. This is achieved by using mean values. Compared to transient simulation, steady-state simulation is significantly faster. In contrast, transient simulation involves computing instantaneous values for each quantity at each time step, which requires significantly more resources such as CPU time, disk storage, and result evaluation.

IV -2.2.6 Energy:

Energy equations under Model tab will be enabled, the reason is that our the flow in the dual-bell nozzle is compressible.

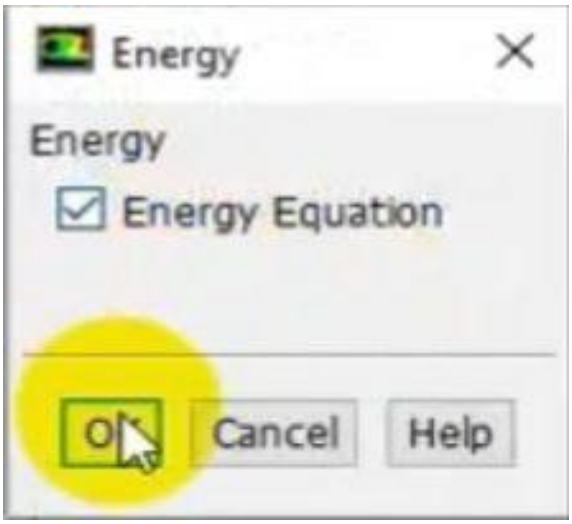

Figure(IV.16): Energy Equation

IV -2.3 Turbulence models:

Spalart Allmaras, k-epsilon and k-omega sst, in order to investigate the influence of these models on the wall nozzle thermodynamics parameters (static pressure, static temperature, Mach number). The Mach number predicted by the three models will be different due to the wall treatment and y+ values differences of the turbulence models.

IV -2.3.1 Spalart Allmaras model :

In addition to the averaged Navier-Stokes equations, it solves a transport equation for a turbulent quantity in order to compute μt. This scalar is a modified turbulent kinematic viscosity ()v, to take into account wall effects [65]. In this model, the turbulent dynamic viscosity is calculated from the following formula:

$$\mu_t = \rho \bar{\nu} f_v \qquad \textbf{(IV.4)}$$

Where f_v is the damping function.

The Spalart-Allmaras turbulence model offers several advantages, including a reduction in dimensionality, which simplifies the problem and reduces simulation time. Unlike other turbulence models, it does not require the use of local thickness of the shear layer to calculate a length scale. It is also useful for boundary layer flows with arbitrary pressure gradients. Despite these benefits, there are limitations to its use, as it is unreliable for describing the decay of turbulent flows, and its applicability beyond wall-bounded systems is still uncertain. Nonetheless, research into variations of the Spalart-Allmaras turbulence model is an ongoing area of study, and its applicability to broader systems with turbulent flow is still being explored.

IV -2.3.2 k-epsilon Model :

This model emphasizes the mechanisms affecting turbulent kinetic energy based on the modeling of two transport equations. The first equation is that of turbulent kinetic energy k and the second is its rate of viscous dissipation ε and the dynamic viscosity μ_t. The model is as

follows, Kinematic Eddy Viscosity [66] :

$$\mu_t = \rho C_\mu \frac{k^2}{\varepsilon} \quad \textbf{(IV.5)}$$

The K-epsilon model is one of the most common turbulence models, although it just doesn't perform well in cases of large adverse pressure gradients It is a two equation model, that means, it includes two extra transport equations to represent the turbulent properties of the flow. This allows a two equation model to account for history effects like convection and diffusion of turbulent energy [66].

The K-epsilon model has been proven to be effective in free-shear layer flows that have relatively minor pressure gradients. However, for wall-bounded and internal flows, the model provides reliable outcomes only if mean pressure gradients are low. Research studies have demonstrated that the model's accuracy decreases in flows that have large adverse pressure gradients. As a result, one could conclude that the K-epsilon model may not be suitable for certain problems, such as those involving inlets and compressors. [67]

IV -2.3.2 K- ω SST Model :

The SST k-ω turbulence model, developed by Menter in 1993, has gained significant popularity due to its effectiveness. This two-equation eddy-viscosity model utilizes the shear stress transport (SST) formulation, which combines the advantages of two different approaches. By implementing a k-ω formulation in the inner boundary layer, the model can be used directly down to the wall, making it a useful Low-Re turbulence model without any extra damping functions. The SST formulation also addresses the k-ω model's sensitivity to inlet free-stream turbulence properties by switching to a k-ε behavior in the free-stream. The SST k-ω model is commonly praised for its superior performance in adverse pressure gradients and separating flow. However, it does tend to produce slightly higher turbulence levels in regions with significant normal strain, such as stagnation regions and areas with strong acceleration, although this tendency is much less pronounced than with a typical k-ε model [68].

The K- ω SST Model has a similar form to the standard K- ω model:

IV-2.3.2.1 Turbulence Kinetic Energy:

$$\frac{\partial}{\partial t}(\rho k) + \frac{\partial}{\partial x_i}(\rho k u_i) = \frac{\partial}{\partial x_j}\left(\Gamma_k \frac{\partial k}{\partial x_j}\right) + \tilde{G}_k - Y_k + S_k \quad \textbf{(IV.6)}$$

IV-2.3.2.2 Specific Dissipation Rate:

$$\frac{\partial}{\partial t}(\rho \omega) + \frac{\partial}{\partial x_i}(\rho \omega u_i) = \frac{\partial}{\partial x_j}\left(\Gamma_\omega \frac{\partial \omega}{\partial x_j}\right) + G_\omega - Y_\omega + D_\omega + S_\omega \quad \textbf{(IV.7)}$$

Where In these equations, $\tilde{G}_k$ represents the generation of turbulence kinetic energy due to mean velocity gradients. G_ω represents the generation of ω. Γ_k and Γ_ω represent the effective diffusivity of k and ω respectively. Y_k and Y_ω represent the dissipation of k and ω due to turbulence. D_ω represents the cross-diffusion term. S_k and S_ω are user-defined source terms.

IV-2.3.2.3 Modeling the Effective Diffusivity:

The effective diffusivities for the The K- ω SST Model are given by :

$$\Gamma_k = \mu + \frac{\mu_t}{\sigma_k} \quad \textbf{(IV.8)}$$

$$\Gamma_\omega = \mu + \frac{\mu_t}{\sigma_\omega} \quad \textbf{(IV.9)}$$

Where σ_k and σ_ω are the turbulent Prandtl numbers for k and ω, respectively. The turbulent viscosity, μ_t, is computed as follows:

$$\mu_t = \frac{\rho k}{\omega} \frac{1}{max\left[\frac{1}{\alpha^{*\prime}}, \frac{SF_2}{a_1 \omega}\right]} \quad \textbf{(IV.10)}$$

where S is the strain rate magnitude and

$$\sigma_k = \frac{1}{F_1/\sigma_{k,1} + (1-F_1)/\sigma_{k,2}} \quad \textbf{(IV.11)}$$

The coefficient α^* damps the turbulent viscosity causing a low-Reynolds-number correction.

The blending functions F_1 and F_2 are given by:

$$F_1 = \tanh(\Phi_1^4) \quad (\textbf{IV.12})$$

$$\Phi_1 = min\left[max\left(\frac{\sqrt{k}}{0.09\omega y}, \frac{500\mu}{\rho y^2 \omega}\right), \frac{4\rho k}{\sigma_{\omega,2} D_\omega^+ y^2}\right] \quad (\textbf{IV.13})$$

$$D_\omega^+ = max\left[2\rho \frac{1}{\sigma_{\omega,2}} \frac{1}{\omega} \frac{\partial k}{\partial x_j} \frac{\partial \omega}{\partial x_j}, 10^{-10}\right] \quad (\textbf{IV.14})$$

$$F_2 = \tanh(\Phi_2^2) \quad (\textbf{IV.15})$$

$$\Phi_2 = max\left[2\frac{\sqrt{k}}{0.09\omega y}, \frac{500\mu}{\rho y^2 \omega}\right] \quad (\textbf{IV.16})$$

Where y is the distance to the next surface and D_ω^+ is the positive portion of the cross-diffusion term.

IV-2.4 Species transport [63] **:**

ANSYS FLUENT predicts the local mass fraction of each chemical species, Y_i by solving a convection-diffusion equation specific to the i -th species. This equation represents the conservation of mass and has a general form:

$$\frac{\partial}{\partial t}(\rho Y_i) + \nabla \cdot (\rho \vec{v} Y_i) = -\nabla \cdot \vec{J_i} + R_i + S_i \quad \textbf{(IV.17)}$$

where R_i is the net rate of production of species i by chemical reaction and s_i is the rate of creation by addition from the dispersed phase plus any user-defined sources. An equation of this form will be solved for $N-1$ species where N is the total number of fluid phase chemical species present in the system. Since the mass fraction of the species must sum to unity, the N th mass fraction is determined as one minus the sum of the $N-1$ solved mass fractions. To minimize numerical error, the N th species should be selected as that species with the overall largest mass fraction, such as $N-2$ when the oxidizer is air.

IV-2.4.1 Eddy Dissipation Model [69] **:**

This model has been used for reaction rate modeling. The Eddy Dissipation model, based on the work of Magnussen and Hjertager, considers chemistry to be very fast compared to turbulence. In this case, combustion, which is controlled only by turbulence, transports the mixture of fresh gases with hot products into the reaction zone where the chemical kinetics rapidly take place.

Therefore, the chemical kinetics can be neglected. The reaction rate $R_{i,r}$ of species i due to the reaction is given by the minimum of the following expressions:

$$R_{i,r} = v'_{i,r} M_{w,i} A \rho \frac{\varepsilon}{k} min\left(\frac{Y_R}{v'_R M_{w,R}}\right) \quad \textbf{(IV.18)}$$

$$R_{i,r} = v'_{i,r} M_{w,i} AB \rho \frac{\varepsilon}{k} \left(\frac{\sum p Y_p}{\sum_J^N v''_{j,r} M_{w,j}}\right) \quad \textbf{(IV.19)}$$

Where :

Y_p: is the mass fraction of species p in the products.

Y_R: is the mass fraction of species r in the reactants.

A and B: are empirical constants with respective values of 4 and 5;

$M_{w,i}$: is the molar mass of species i.

The mixtures that will be used in this simulation are :

- CH_4 (Fuel) / O_2 (Oxidizer)
- H_2 (Fuel) / O_2 (Oxidizer)
- $C_{12}H_{23}$ (Fuel) / O_2 (Oxidizer)

IV-2.5 Y Plus, Boundary Layer and Wall Function in Turbulent Flows:

In a flow bounded by a wall, different scales and physical processes are dominant in the inner portion near the wall, and the outer portion approaching the free stream. These layers are typically known as the inner and outer layers. Considering the flow over a smooth flat plate the boundary layer can be distinguished into two types namely laminar boundary layer and turbulent boundary layer. Since we are dealing with the turbulent boundary layer let us not get into the laminar boundary layer. Typical boundary layer structure over a flat plate is shown below. In between the laminar and turbulent boundary layer there lies a transition region. Typically for flow over a flat plate the transition usually occurs around $R_e = 5 \times 10^5$. [70]

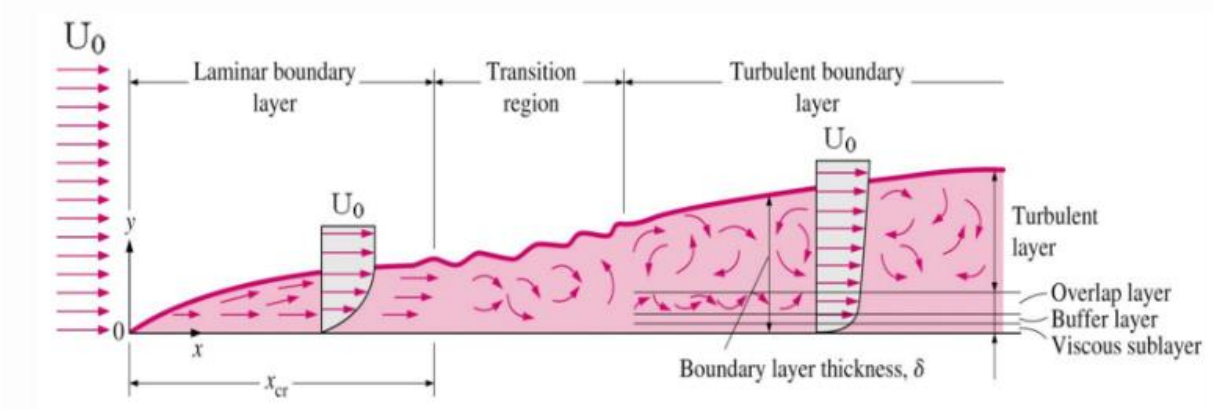

Fig (IV.17): Boundary layer theory [71]

In the near-wall region, kinematic quantities are generally related to the internal parameters of the boundary layer, namely the friction velocity u_τ and the kinematic viscosity ν of the fluid. We thus define dimensionless quantities such as the average velocity $\bar{U}^+$ and the distance y^+ by :

$$\bar{U}^+ = \bar{U}/u_\tau \text{ and } y^+ = y u_\tau / \nu \quad \textbf{(IV.20)}$$

IV-2.5.1 Linear sub-layer :

At the solid surface the fluid is stationary and the turbulent eddying motion must also

stop very close to the wall. The fluid very close to the wall is dominated by viscous shear in absence of the turbulent shear stress effects ($y^+ < 5$) and it can be assumed that the shear stress is almost equal to the wall shear stress τ_ω throughout the layer [70].

$$u^+ = y^+ \qquad \textbf{(IV.21)}$$

IV-2.5.2 Log-law layer :

Here is a region located at a certain distance from the wall, beyond the viscous sub-layer ($5 < y^+ < 30$, where both viscous and turbulent effects play significant roles. Within this inner region, the shear stress is considered to remain constant and equal to the wall shear stress, while gradually changing with distance from the wall. The relationship between two variables in this region is given as [70]:

$$u^+ = \frac{1}{k'} \ln y^+ + k'' = \frac{1}{k'} \ln k''' y^+ \qquad \textbf{(IV.22)}$$

Where k', k'' and k''' are constants whose values are found from measurements.

The relationship between two variables u^+ and y^+ in this context follows a logarithmic pattern. This expression is commonly referred to as the log-law, and the layer where y^+ takes on values ranging from 30 to 500 is known as the log-law layer.

IV-2.5.2 Outer Layer :

Tennekes and Lumley (1972) [72] proposed the following logarithmic law for identifying the matched overlap region.

$$\frac{U_{max} - U}{u_\tau} = \frac{1}{K'} \ln \frac{y}{\delta} + A' \qquad \textbf{(IV.23)}$$

IV-2.5.3 Buffer layer :

In the buffer layer, between 5 wall units and 30 wall units, neither law holds, such that:

For: $5 < y^+ < 30$ **(IV.23)**

With the largest variation from either law occurring approximately where the two equations intercept, at $y^+ = 11$. That is, before 11 wall units the linear approximation is more accurate and after 11 wall units the logarithmic approximation should be used, though neither are relatively accurate at 11 wall units [70].

IV-2 -3.Postprocessing (Results and discussions)

First of all, before using the simulation results, we need to check that the calculations are convergent. There are several ways of checking convergence in the fluent software, One of The criterion is the graph of residuals, which must decrease continuously.

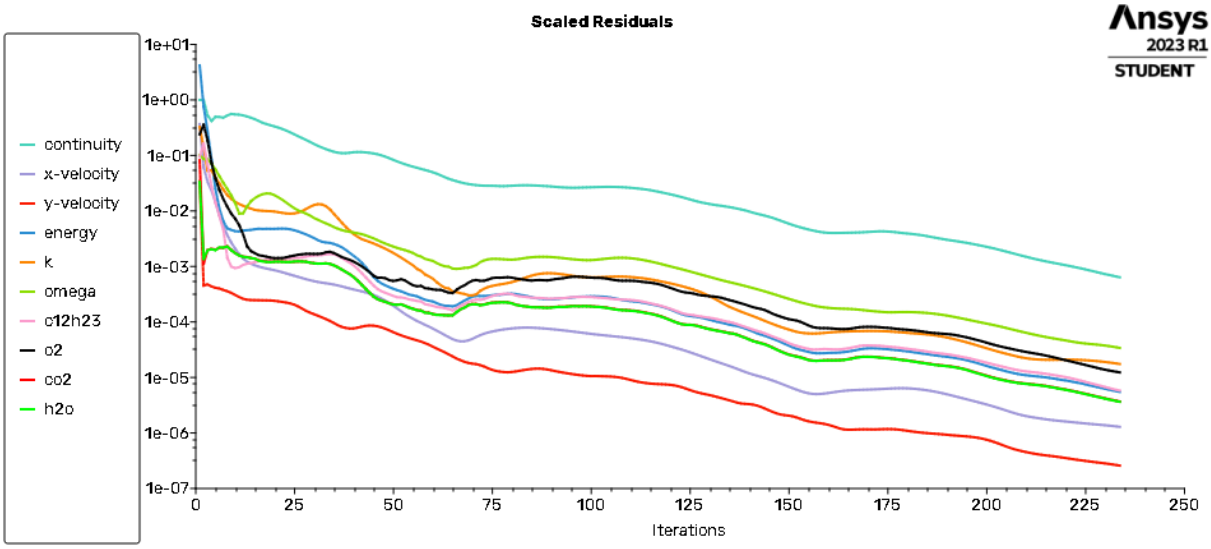

Figure(IV.18): The residuals plot of our simulation.

From the graphs of the residuals we can tell that the calculations are converging, since figure (IV.18) shows that the residuals are decreasing continuously.

IV-2-3-1. 1^{st} Application for Air (without combustion)

A dual bell nozzle can still be modelled in the event of an air application without combustion in order to assess and improve the flow characteristics. The air's movement through the nozzle is modelled as part of the simulation. Techniques for computational fluid dynamics (CFD) can be utilized to simulate the pressure distribution and flow patterns inside the nozzle.

Defining the geometry of the dual bell nozzle is the first step in the simulation. encompassing both the divergent and convergent portions. The distributions of velocity, pressure, and temperature along the nozzle are obtained by numerically solving the governing equations of fluid flow, such as the Navier-Stokes equations. The intended flow conditions are represented by boundary conditions, such as the beginning conditions and the inlet/outlet conditions.

To optimize the nozzle design for optimal efficiency, the simulation enables the investigation of a number of parameters, including the throat area ratio, nozzle length, and divergence angle. The objective is to maximize exhaust velocity and thrust while reducing losses and keeping the flow steady.

Engineers and researchers can learn a lot about the flow behavior and performance characteristics by simulating the dual bell nozzle for air applications. This knowledge may be put to use With the use of this knowledge, rocket nozzle designs can be improved, and air-based propulsion systems can operate more effectively, advancing aerospace technology.

› Parameters Evolution

•Mach number

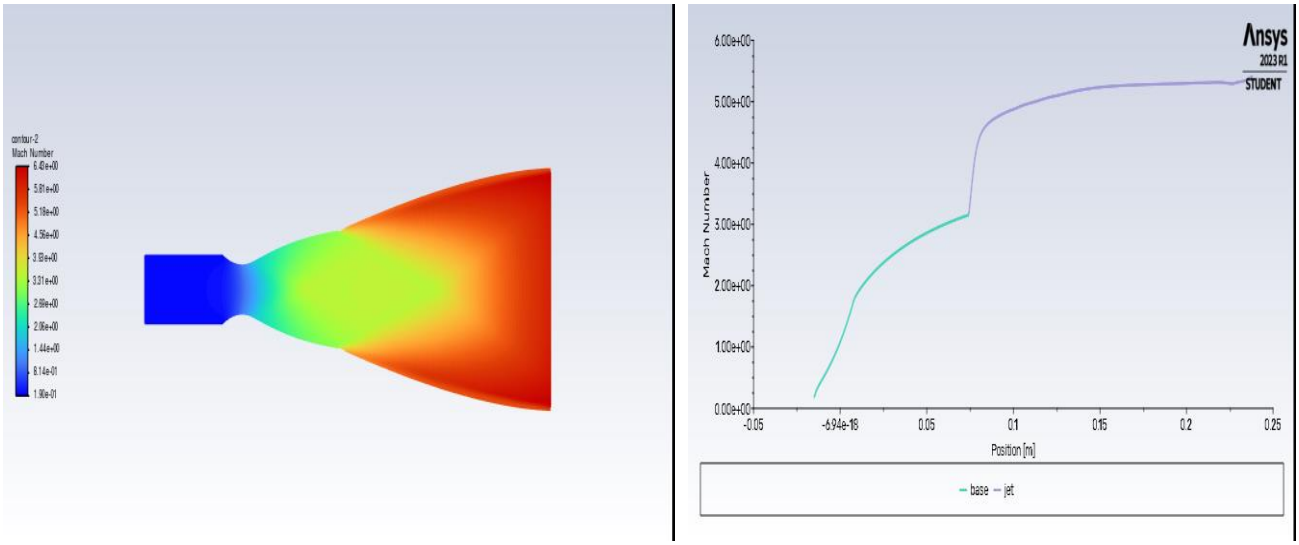

Figure(IV.19): Evolution of Mach number in DBN wall

In contrast to static pressure, the Mach number contour increases from blue, where M=1.33 (at the throat), to red (nozzle outlet), where M=5.90, and this without any loss of velocity on the wall, since we've assumed the condition of sliding on the wall (non-viscous flow).

•**Static Pressure**

The performance of a dual bell nozzle is heavily influenced by the pressure applied to its wall. This type of rocket nozzle consists of a short, constrictive throat region and a longer, divergent expansion zone. The gas velocity is very high at the throat region due to its converging shape, resulting in low pressure. As the gas expands into the divergent region, the pressure increases while the velocity decreases, enabling efficient expansion and energy conversion. The pressure on the nozzle wall depends on gas properties, chamber pressure, and nozzle design. Higher chamber pressure leads to increased pressure on the wall, necessitating strong materials. Excessive pressure can damage the nozzle, impacting performance. Proper design and material selection are crucial to withstand these pressures. In conclusion, pressure distribution along the dual bell nozzle wall is vital for efficient gas expansion and thrust generation, requiring careful consideration in nozzle design.

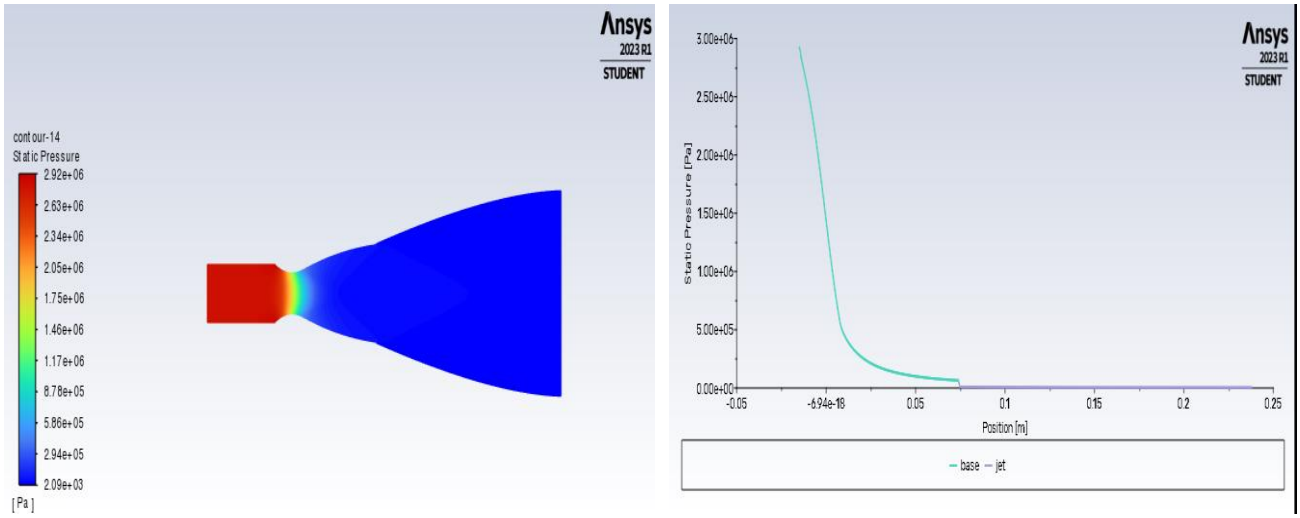

Figure(IV.20): The Evolution of static Pressure in DBN wall

We can see that the pressure decreases very rapidly at the throat and in the initial expansion zone, then slowly in the divergent part forming the 1st curve.

At junction point J, the expansion wave centered at this point is clearly visible, then the pressure remains constant throughout the second curve, equal to the imposed pressure.

•**Static temperature**

For the same number of mach, we were interested in the evolution of temperature along the nozzle, which is a very important parameter for calculating performance and choosing construction materials (see figure (IV.21)).

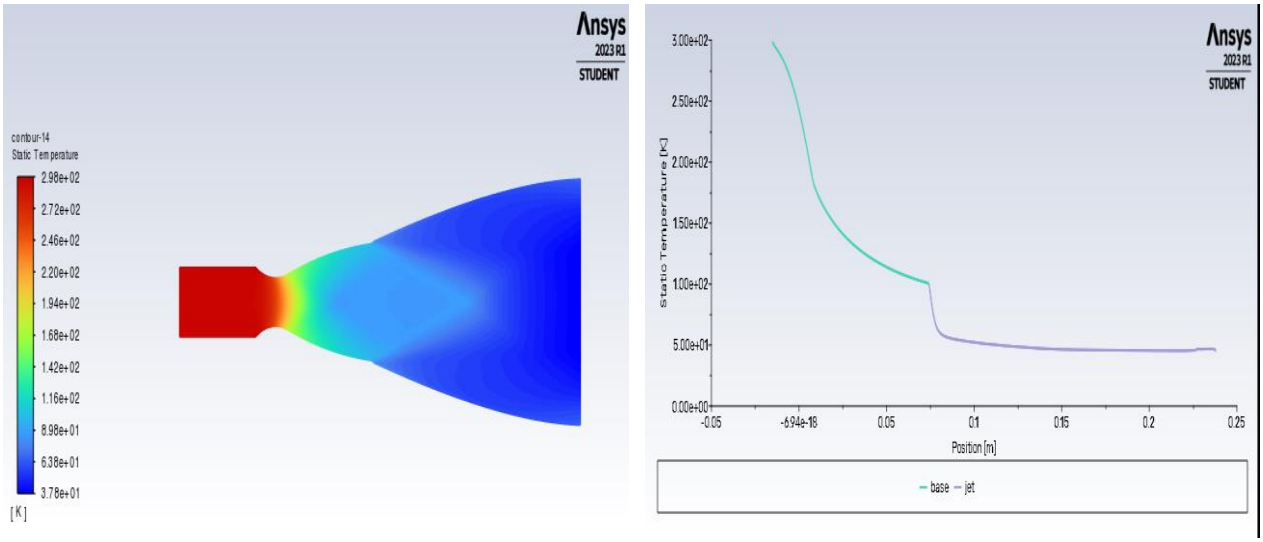

Figure(IV.21): The Evolution of static temperature in axis and DBN wall

It is well known that this static temperature decreases along the nozzle as the velocity increases, the flow is isentropic in the nozzle and, according to the law of perfect gases, this temperature is proportional to the pressure. This can be seen in figure (IV.21), since the wall temperature decreases continuously from the throat to the outlet.

•**Countour Density**

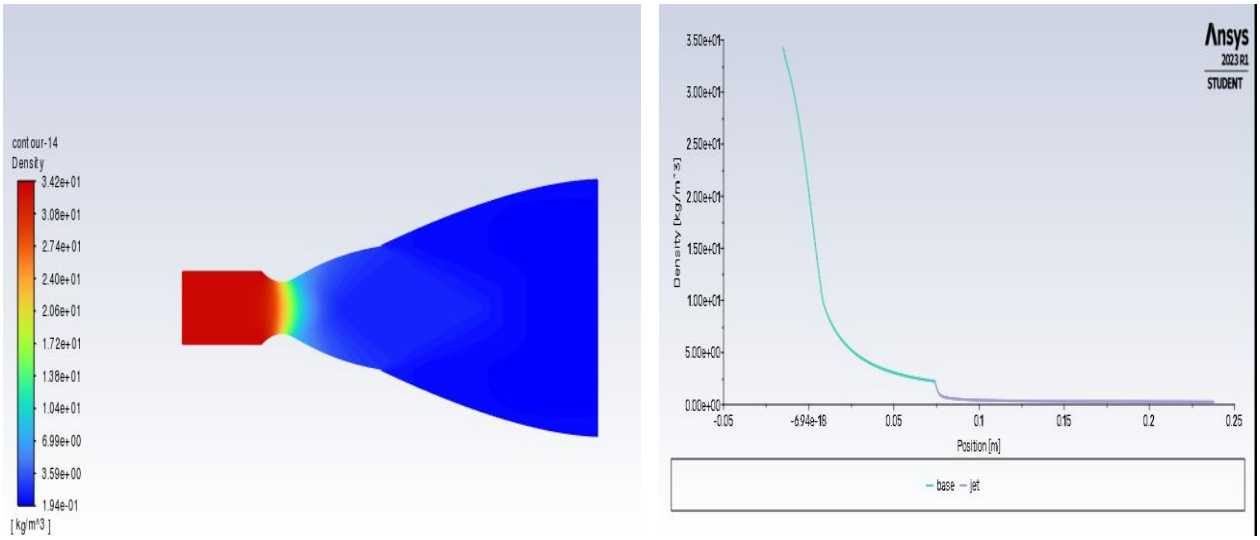

Figure(IV.22): Density contour

It is well known that this density must decrease with distance from the combustion chamber outlet,as shown in fig (IV.22).

IV-2-3-2. 2^{nd} Application for mixture Kerosene $C_{12}H_{23}$ (Fuel) / O_2 (Oxidizer)

The boundary conditions for the system include the following parameters: the fuel inlet with a pressure of 30 Bars, an angle of injection of 20, and a temperature of 400K. Similarly, the oxidizer inlet has a pressure of 30 Bars, an angle of injection of 20, and a temperature of 400K. The mass fraction for the fuel is 0.4, while the oxidizer has a mass fraction of 0.6. These specifications provide important inputs for analyzing and modeling the system's behavior.

› Parametres Evolution:

•Mach number

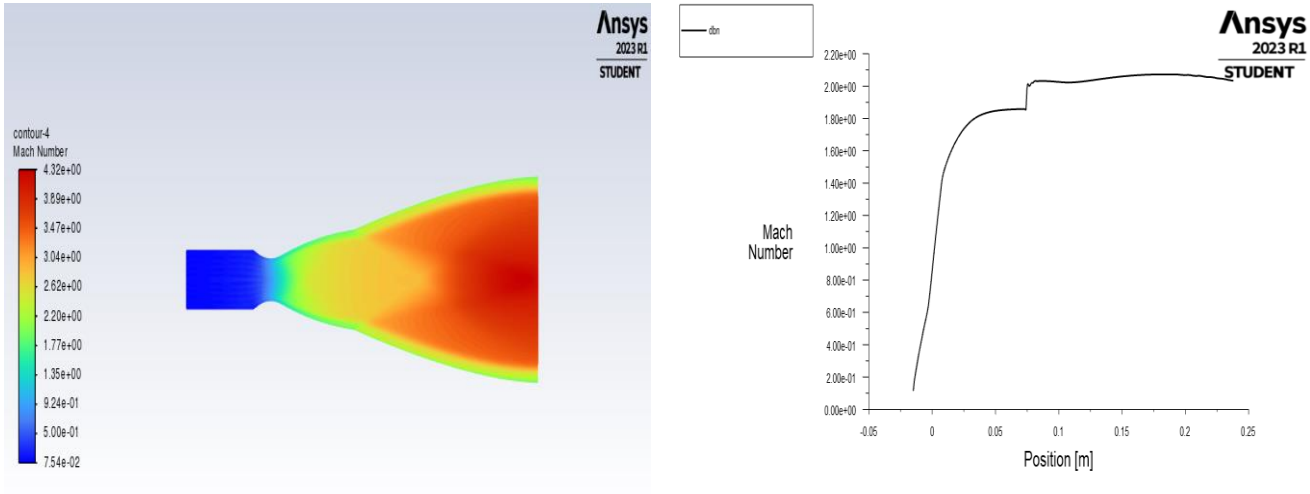

Figure(IV.23): Evolution of Mach number in the axis and in DBN wall

We can see that the Mach number evolves very rapidly at the throat and in the initial expansion zone up to a value of 1.77, then in the divergent part forming the 1st curve until it reaches a value of 2.8.

At junction point J, the Mach number takes on two values (2.8 and 3.6) due to the expansion wave centered at this point, then Mach remains constant throughout the second curve.

In contrast to static pressure, the Mach number contour increases from blue, where M=1.2 (at the throat), to red (nozzle outlet), where M=4.32, and this without any loss of velocity on the wall, since we've assumed the condition of sliding on the wall (non-viscous flow).

•**Static Pressure**

Static pressure is the pressure exerted by the fluid; specifically, it is the pressure measured when the fluid is still at rest.

Figure (IV.24) shows the evolution of static pressure along the nozzle, as the gas expands from the inlet where the pressure value is 2.99+06(Pa) towards the outlet, the pressure drops until it reaches a pressure of 3.66+03(Pa) at the outlet.

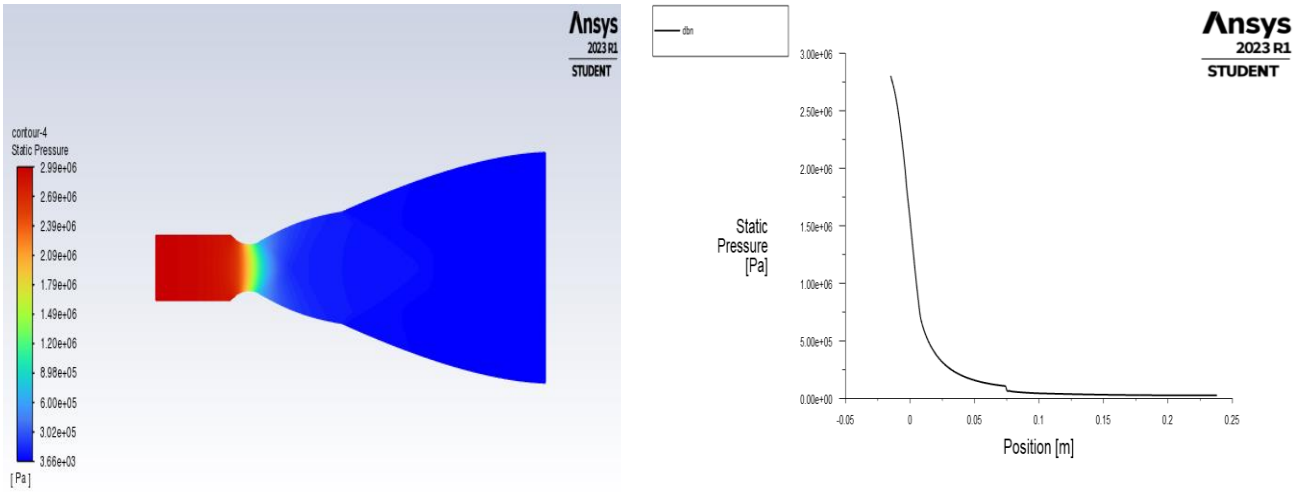

Figure(IV.24): The Evolution of static Pressure in axis and DBN wall

•**Static Temperature**

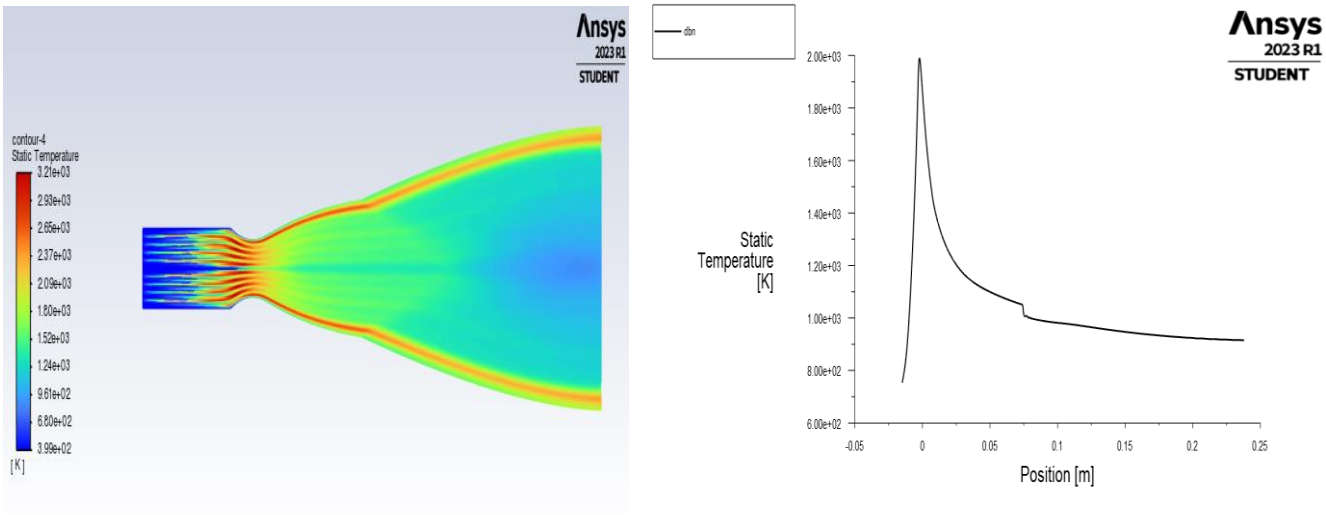

Figure(IV.25): The Evolution of static temperature in axis and DBN wall

Since the flow in the nozzle is completely isentropic, the evolution of temperature is proportional to pressure, according to the law of perfect gases. This can be seen in figure (IV.25), where the wall temperature decreases continuously from the throat to the outlet.

- **Contour of: Density**

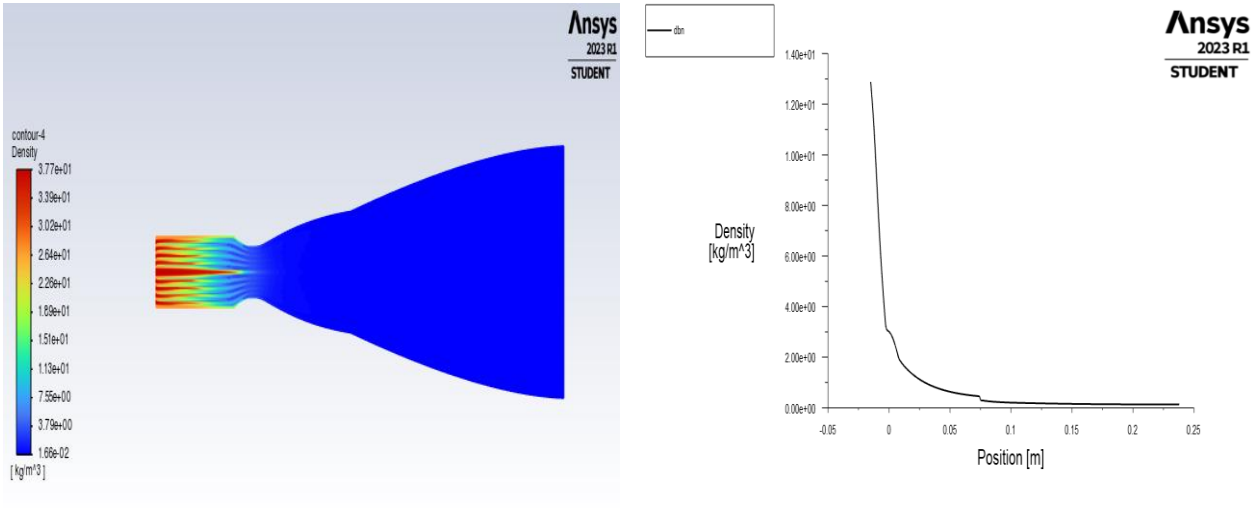

Figure(IV.26): Density Contour and plot

It is well known that this density must decrease with distance from the combustion chamber outlet, which is normal since pressure decreases, as shown in fig (IV.26).

- **Species Mass Fraction of: $C_{12}H_{23}$**

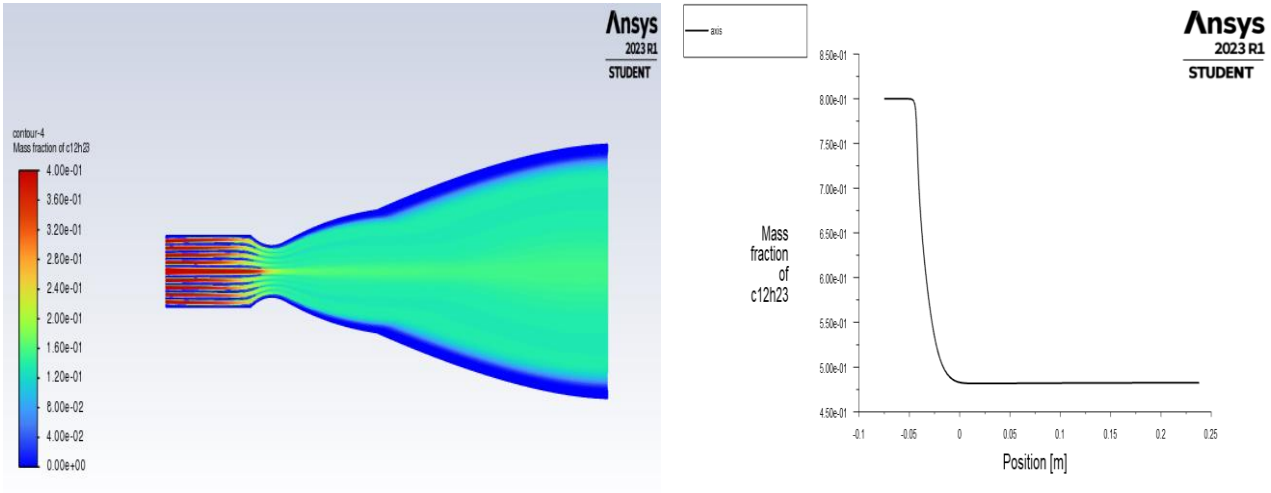

Figure(IV.27): The Evolution of Species mass fraction of $C_{12}H_{23}$

It is well known that the mass fraction must decrease with distance from the combustion chamber outlet, which is normal since the density of the mixture decreases, as shown in fig(IV.27).

- **Species Mass Fraction of: O_2**

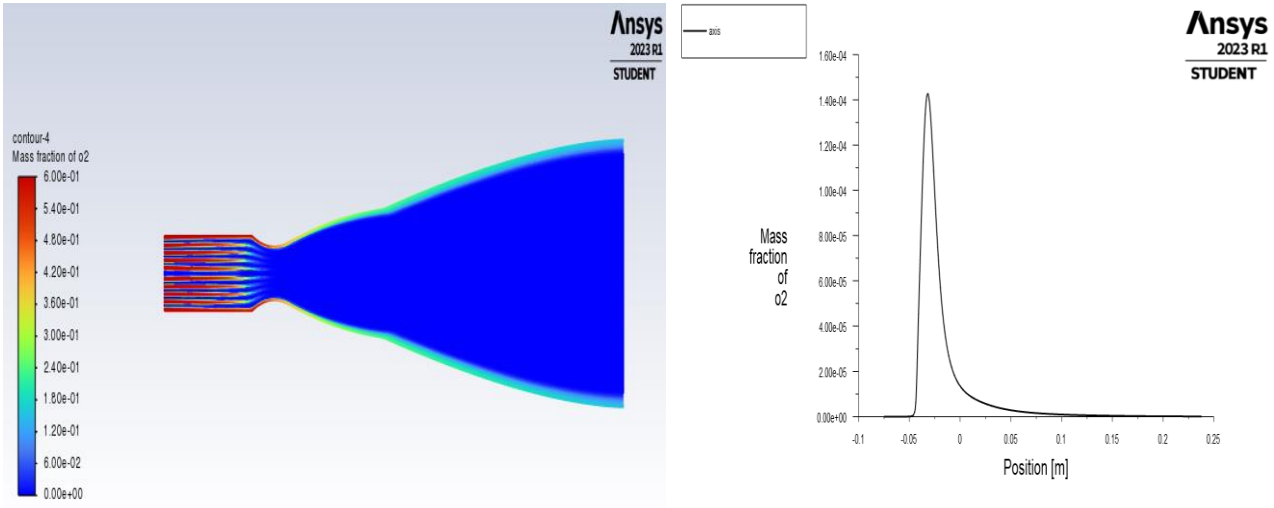

Figure(IV.28): The Evolution of Species mass fraction of O_2

It is well known that the mass fraction must decrease with distance from the combustion chamber outlet, which is normal since the density of the mixture decreases, as shown in fig(IV.28).

- **Contour of: Heat Of Reaction**

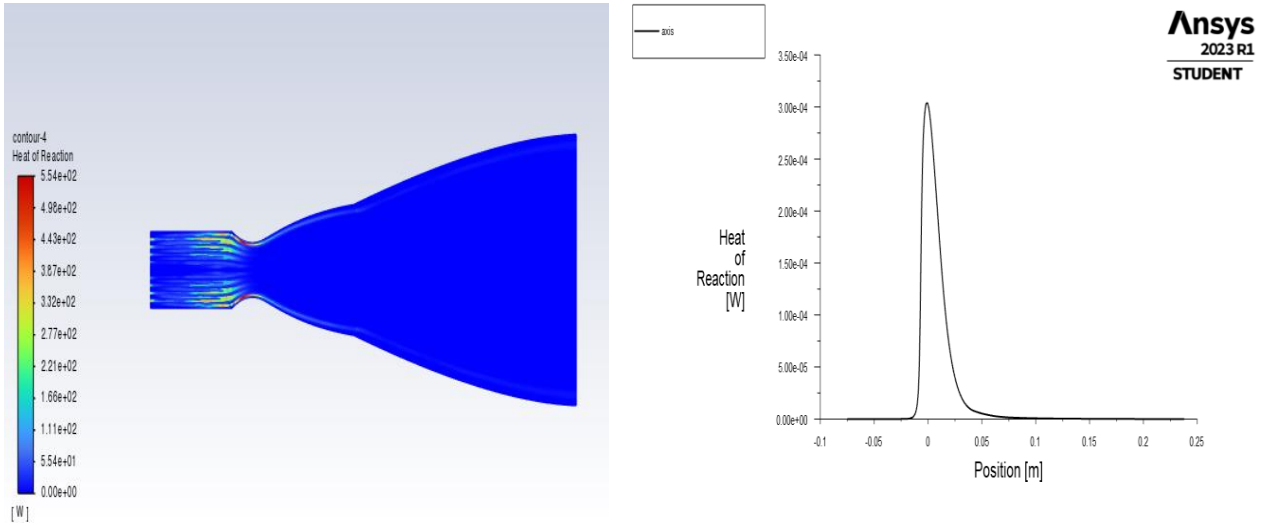

Figure(IV.29): Heat of Reaction contour and plot

The heat of reaction contour represents the variation in heat release or absorption rates across different regions of the combustion system. By displaying this information as a contour plot, ANSYS Fluent allows us to visualize the spatial distribution of heat generation or consumption, providing a comprehensive understanding of the combustion process. Analyzing

the heat of reaction contour helps identify regions with intense heat release, such as flame fronts or hot spots, as well as areas with heat absorption, such as cooling zones. This information is crucial for optimizing combustion efficiency, assessing the impact of heat transfer on system components, and identifying potential hotspots or cooling requirements.

IV-2-3-3. 3^{rd} Application for mixture H_2 (Fuel) / O_2 (Oxidizer)

For the third application involving the mixture of H2 (fuel) and O2 (oxidizer), the boundary conditions were set as follows. The fuel inlet had a pressure of 30 Bars, an angle of injection of 20 degrees, and a temperature of 700K. Similarly, the oxidizer inlet had a pressure of 30 Bars, an angle of injection of 20 degrees, and a temperature of 700K. The mass fraction of the fuel was determined to be 0.4, while the mass fraction of the oxidizer was 0.6. These specific boundary conditions were chosen to ensure the appropriate and controlled flow of the H2 and O2 mixture, facilitating a comprehensive analysis of their interaction and combustion properties. By carefully defining the boundary conditions, it becomes possible to study the behavior and performance of the mixture in a controlled environment, thereby contributing to a deeper understanding of its combustion characteristics and potential applications in various fields.

› Parametres Evolution:

- **Mach Number**

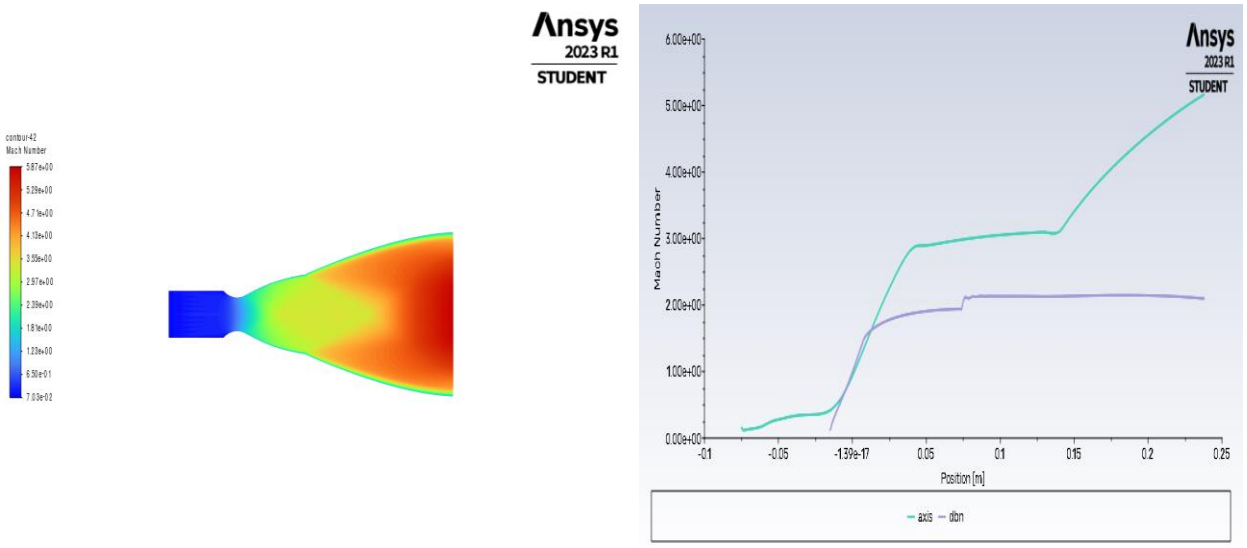

Figure(IV.30): Evolution of Mach number in the axis and in DBN wall

We can see that the Mach number evolves very rapidly at the throat and in the initial expansion zone up to a value of 1.60, then slowly in the divergent part forming the 1st curve until it reaches a value of 1.80.

At junction point J, the Mach number takes on two values (1.80 and 2.1) due to the expansion wave centered at this point, then Mach remains constant throughout the second curve.

In contrast to static pressure, the Mach number contour increases from blue, where M=1.1 (at the throat), to red (nozzle outlet), where M=5.17, and this without any loss of velocity on the wall, since we've assumed the condition of sliding on the wall (non-viscous flow).

- **Static Pressure**

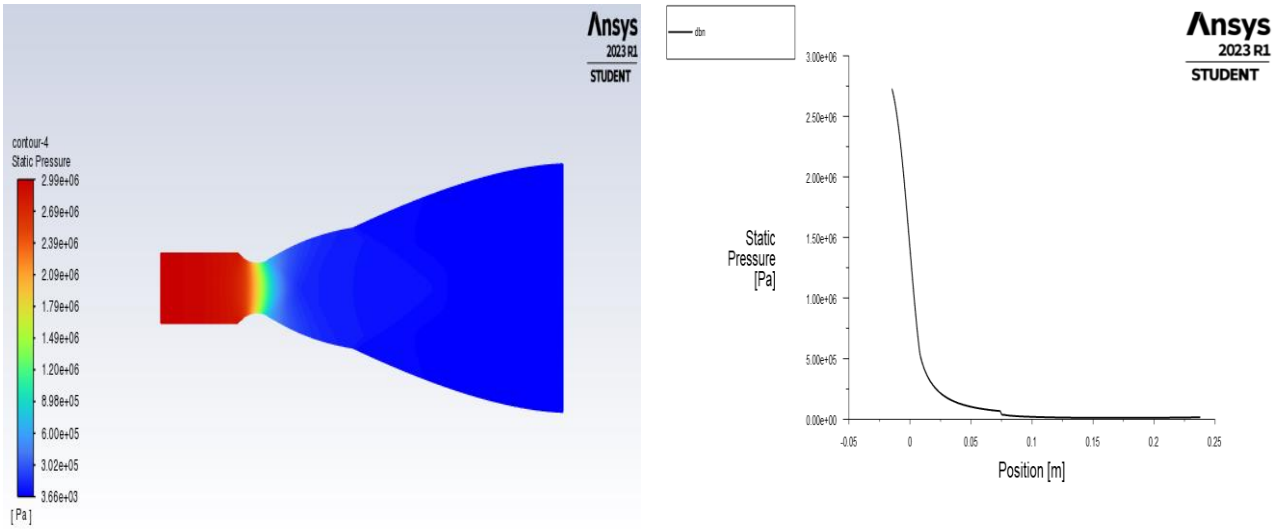

Figure(IV.31): The Evolution of static Pressure in axis and DBN wall

Static pressure is the pressure exerted by the fluid; specifically, it is the pressure measured when the fluid is still at rest.

Figure (IV.31) shows the evolution of static pressure along the nozzle, as the gas expands from the inlet where the pressure value is 2.99+06(Pa) towards the outlet, the pressure drops until it reaches a pressure of 3.66+03(Pa) at the outlet.

•**Static Temperature**

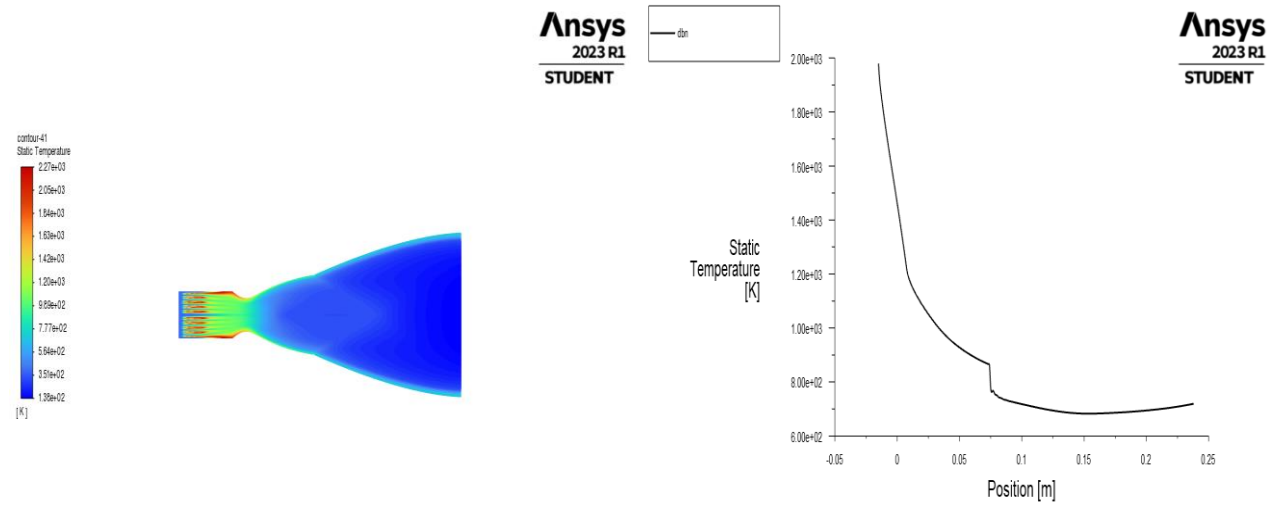

Figure(IV.32): The Evolution of static temperature in axis and DBN wall

Since the flow in the nozzle is completely isentropic, the evolution of temperature is proportional to pressure, according to the law of perfect gases. This can be seen in figure (IV.32), where the wall temperature decreases continuously from the throat to the outlet.

•**Contour of : Density**

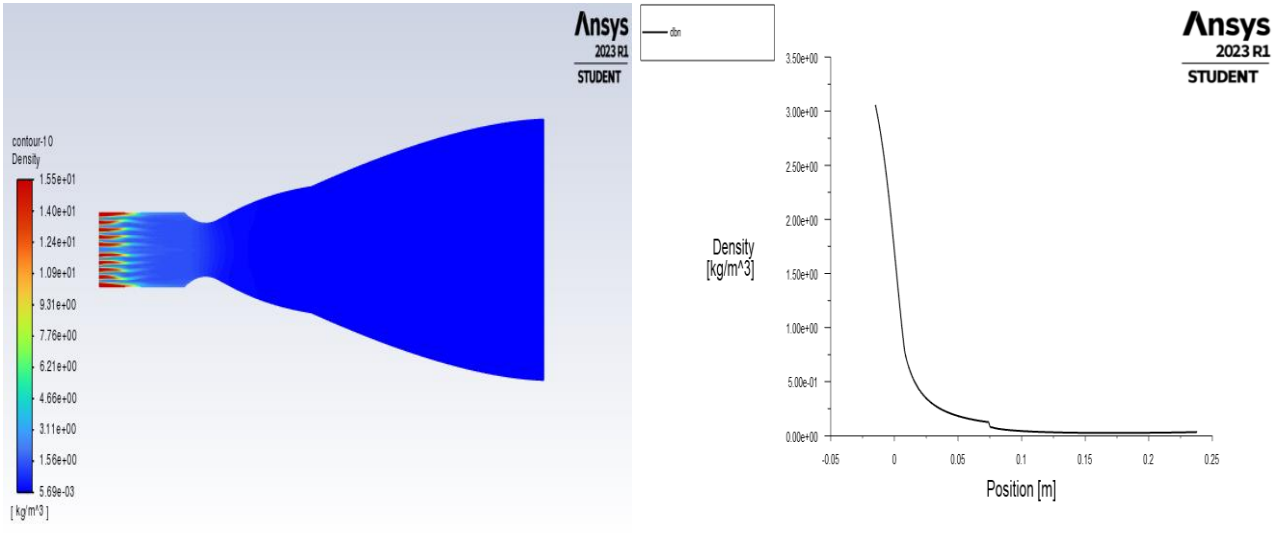

Figure(IV.33): Density Contour and plot

It is well known that this density must decrease with distance from the combustion chamber outlet, which is normal since pressure decreases, as shown in fig (IV.33).

•**Species Mass Fraction of: H_2**

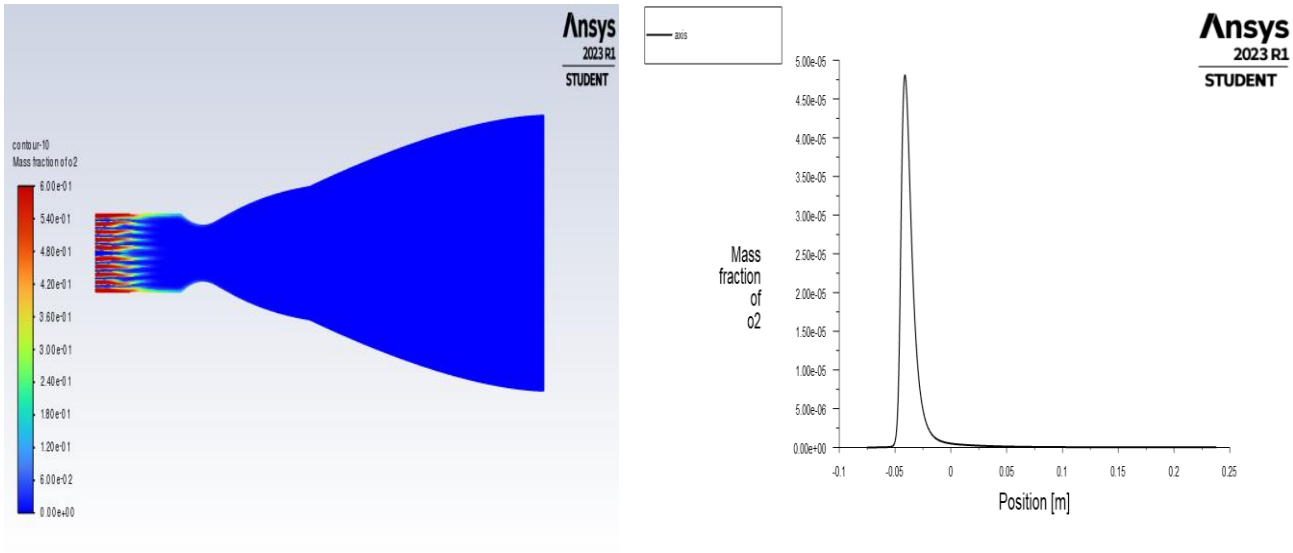

Figure(IV.34): The Evolution of Species mass fraction of H_2

It is well known that the mass fraction must decrease with distance from the combustion chamber outlet, which is normal since the density of the mixture decreases, as shown in fig(IV.34).

•**Species Mass Fraction of:O_2**

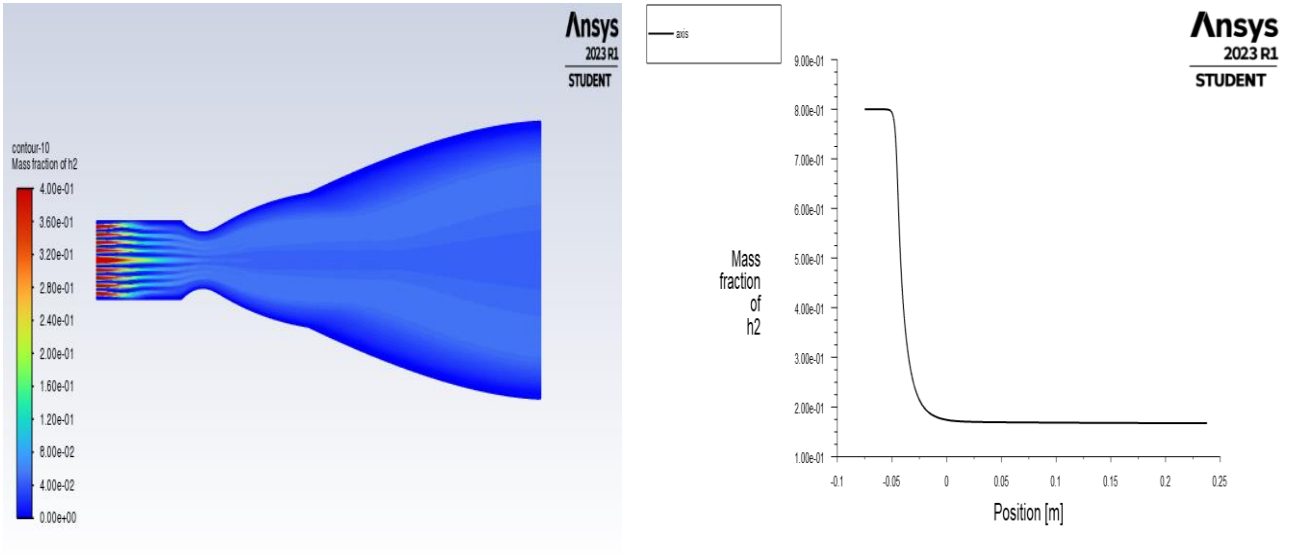

Figure(IV.35): The Evolution of Species mass fraction of O_2

It is well known that the mass fraction must decrease with distance from the combustion chamber outlet, which is normal since the density of the mixture decreases, as shown in fig(IV.35).

- **Contour of: Heat Of Reaction**

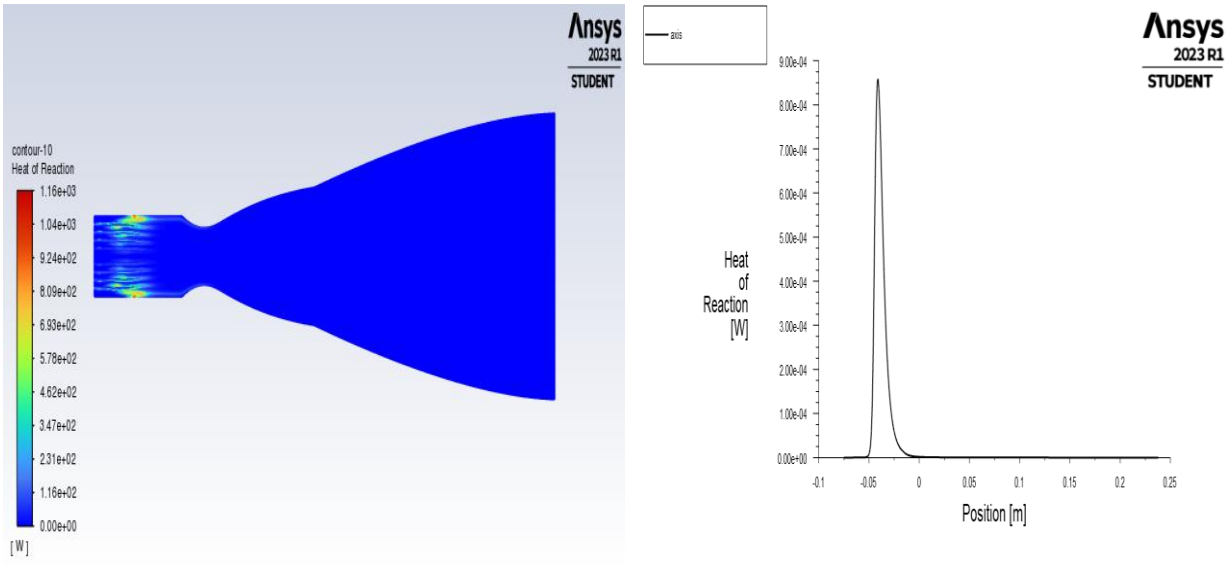

Figure(IV.36): Heat of Reaction contour and plot

The heat of reaction contour represents the variation in heat release or absorption rates across different regions of the combustion system. By displaying this information as a contour plot, ANSYS Fluent allows us to visualize the spatial distribution of heat generation or consumption, providing a comprehensive understanding of the combustion process. Analyzing the heat of reaction contour helps identify regions with intense heat release, such as flame fronts or hot spots, as well as areas with heat absorption, such as cooling zones. This information is crucial for optimizing combustion efficiency, assessing the impact of heat transfer on system components, and identifying potential hotspots or cooling requirements.

IV-2-3-4. 4^{th} Application for mixture CH_4 (Fuel) / O_2 (Oxidizer)

The fourth application involves the utilization of a mixture comprising CH4 (fuel) and O2 (oxidizer). To simulate this scenario, specific boundary conditions were established. The fuel inlet was set with a pressure of 30 Bars, an angle of injection of 20 degrees, and a temperature of 400K. Similarly, the oxidizer inlet was maintained at a pressure of 30 Bars, an angle of injection of 20 degrees, and a temperature of 400K. The mass fraction of the fuel was determined to be 0.4, while the oxidizer had a mass fraction of 0.6. These boundary conditions were carefully selected to ensure controlled and consistent flow of the CH4 and O2 mixture, thereby facilitating a comprehensive analysis of their combustion behavior. By accurately defining these boundary conditions, it becomes possible to study the interaction and performance of the CH4 and O2 mixture under specific parameters. This investigation contributes to a deeper understanding of the combustion characteristics of this particular mixture, offering valuable insights for potential applications in various industries and technological advancements.

› Parametres Evolution

- **Mach Number**

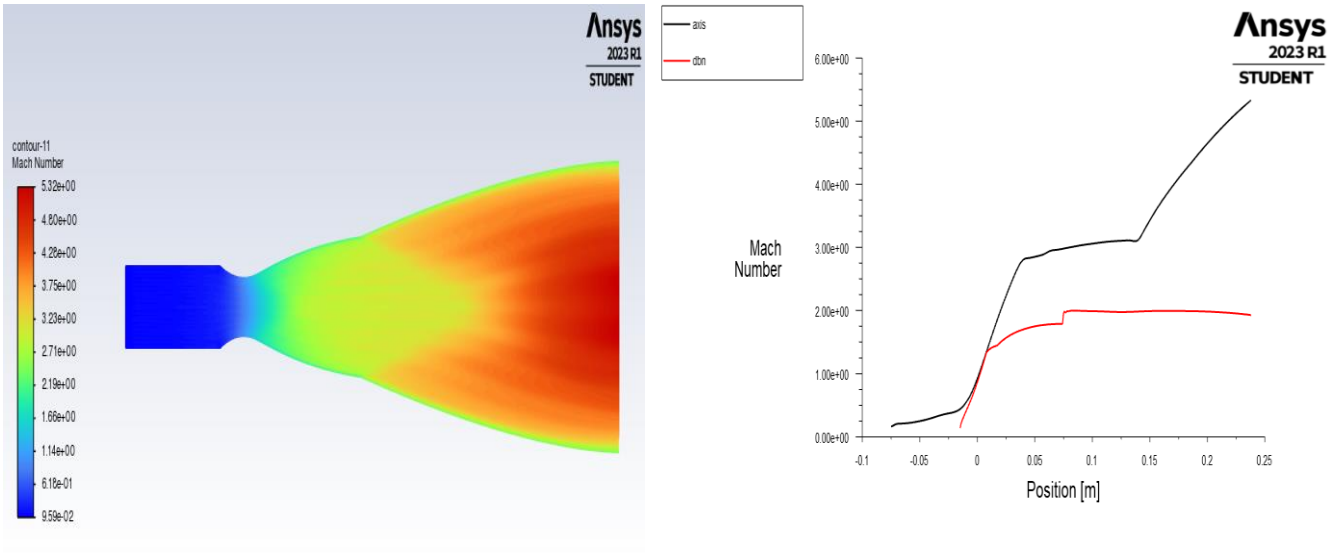

Figure(IV.37): Evolution of Mach number in the axis and in DBN wall

We can see that the Mach number evolves very rapidly at the throat and in the initial expansion zone up to a value of 1.60, then slowly in the divergent part forming the 1st curve until it reaches a value of 2.25.

At junction point J, the Mach number takes on two values (2.25 and 2.60) due to the expansion wave centered at this point, then Mach remains constant throughout the second curve.

In contrast to static pressure, the Mach number contour increases from blue, where M=1.1 (at the throat), to red (nozzle outlet), where M=5.32, and this without any loss of velocity on the wall, since we've assumed the condition of sliding on the wall (non-viscous flow).

•**Static Pressure**

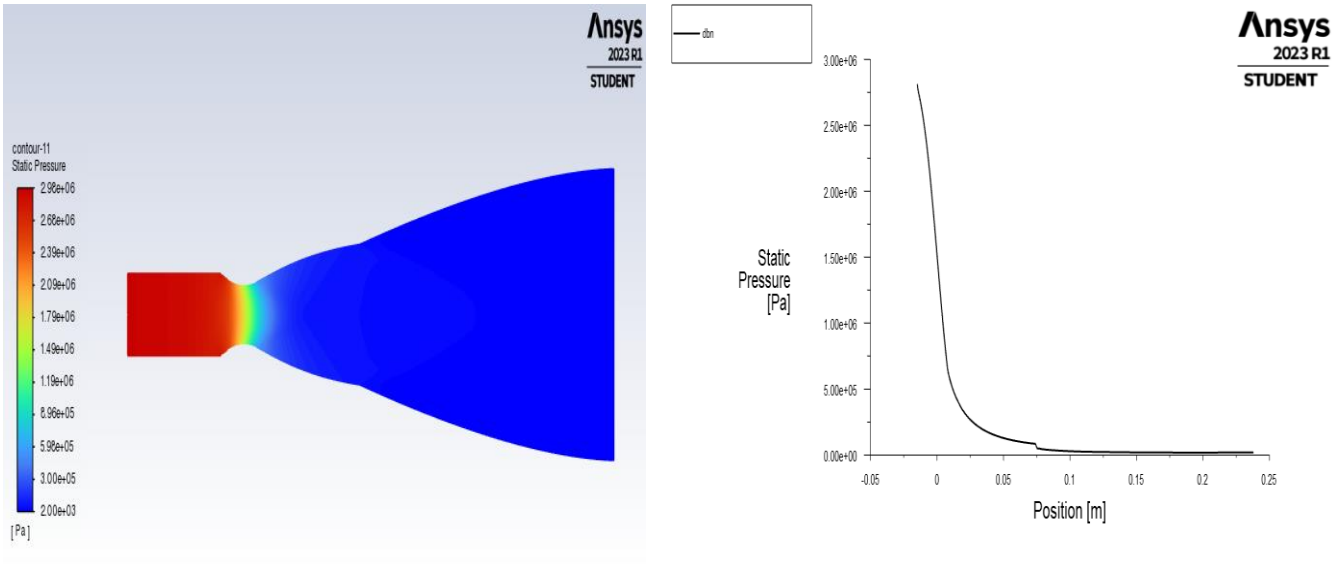

Figure(IV.38): The Evolution of static Pressure in axis and DBN wall

Static pressure is the pressure exerted by the fluid; specifically, it is the pressure measured when the fluid is still at rest.

Figure (IV.38) shows the evolution of static pressure along the nozzle, as the gas expands from the inlet where the pressure value is 2.98+06(Pa) towards the outlet, the pressure drops until it reaches a pressure of 2+03(Pa) at the outlet.

•**Static Temperature**

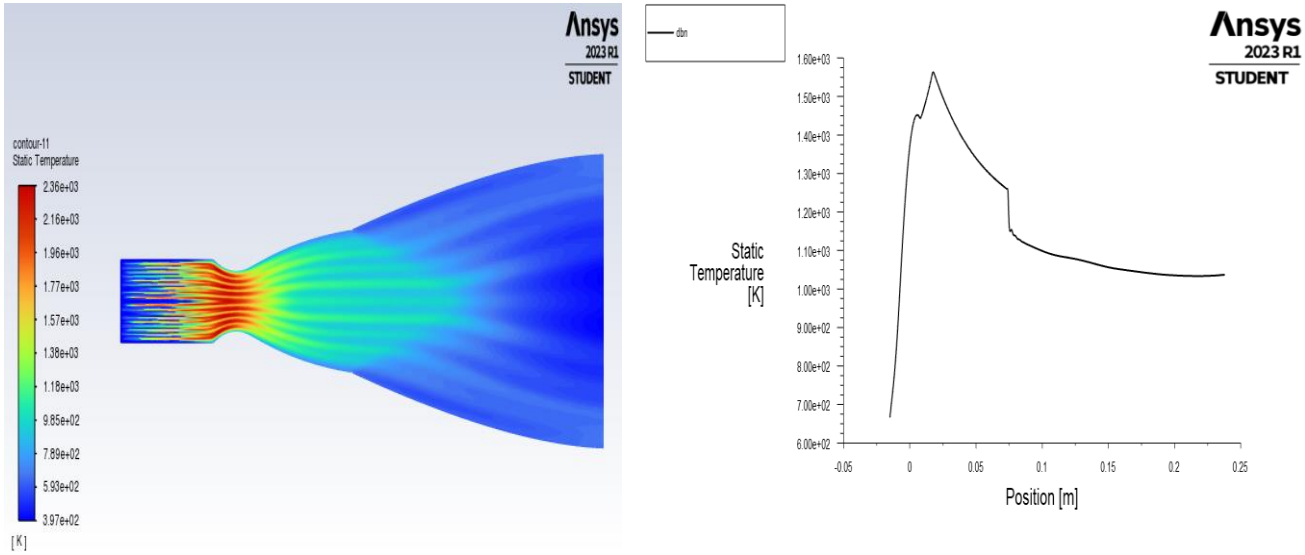

Figure(IV.39): The Evolution of static temperature in axis and DBN wall

Since the flow in the nozzle is completely isentropic, the evolution of temperature is proportional to pressure, according to the law of perfect gases. This can be seen in figure (IV.39), where the wall temperature decreases continuously from the throat to the outlet.

- **Contour of : Density**

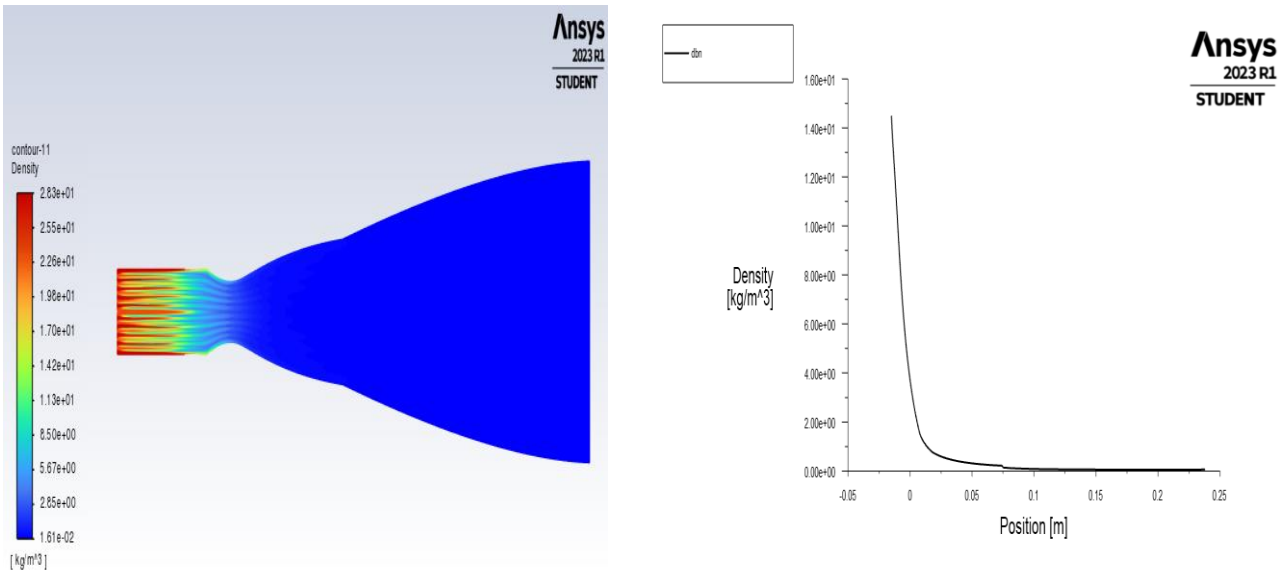

Figure(IV.40): Density Contour and plot

It is well known that this density must decrease with distance from the combustion chamber outlet, which is normal since pressure decreases, as shown in fig (IV.40).

- **Species Mass Fraction of: CH_4**

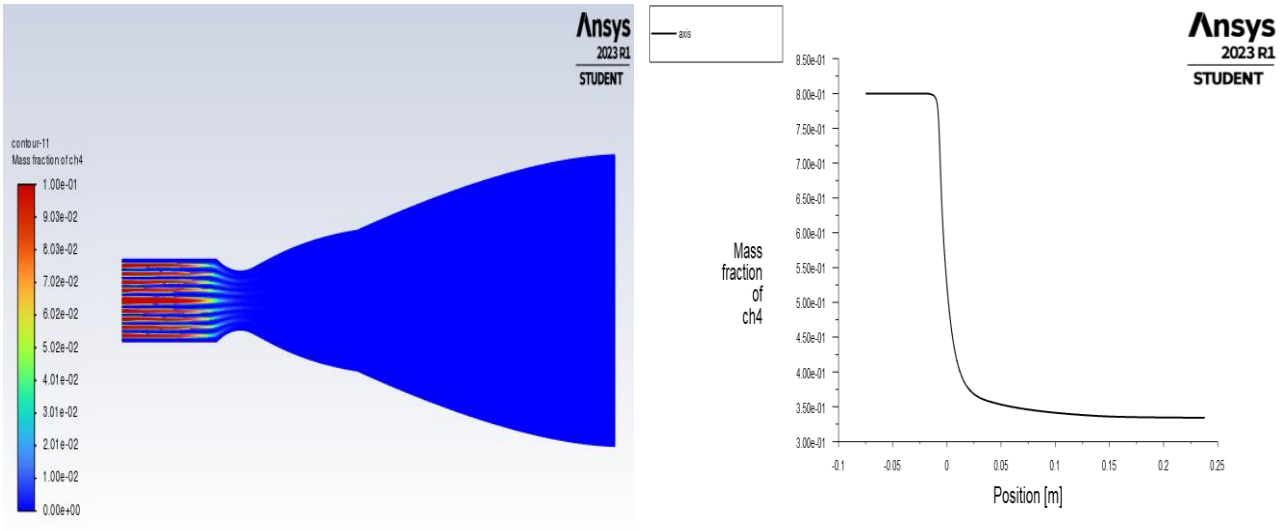

Figure(IV.41): The Evolution of Species mass fravtion of CH_4

It is well known that the mass fraction must decrease with distance from the combustion chamber outlet, which is normal since the density of the mixture decreases, as shown in fig(IV.41).

- **Species Mass Fraction of: O_2**

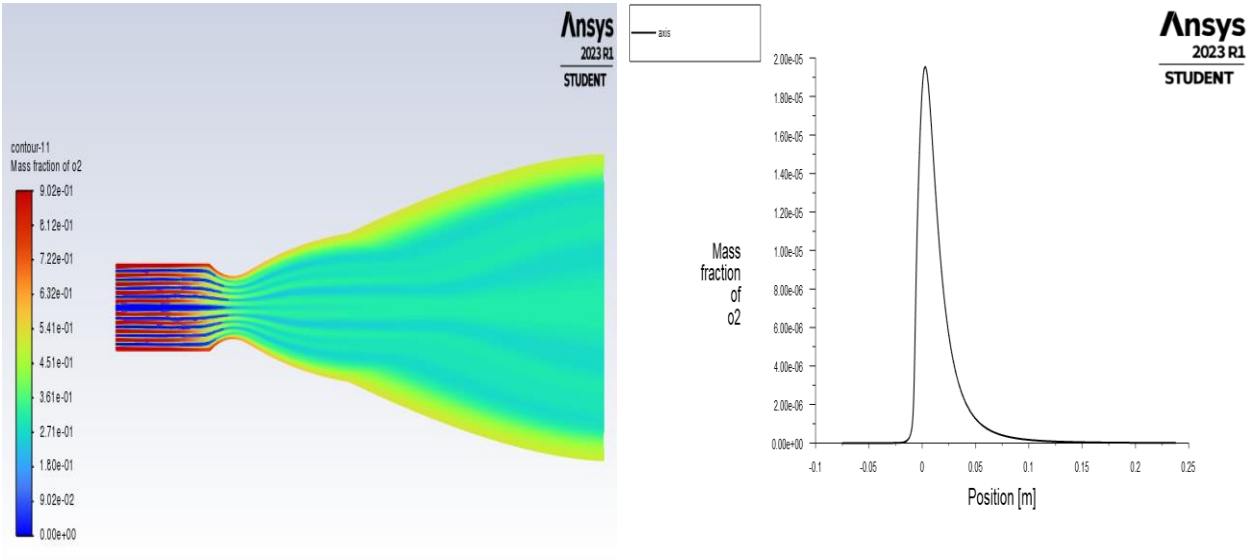

Figure(IV.42): The Evolution of Species mass fraction of O_2

It is well known that the mass fraction must decrease with distance from the combustion chamber outlet, which is normal since the density of the mixture decreases, as shown in fig(IV.42).

- **Contour of: Heat Of Reaction**

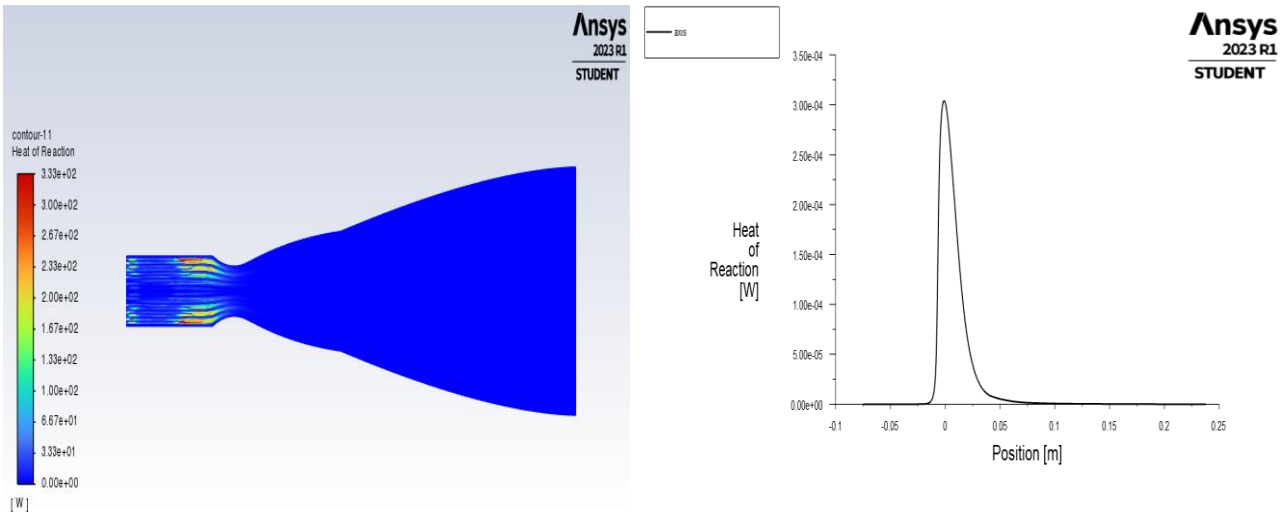

Figure(IV.43): Heat of Reaction contour and plot

The heat of reaction contour represents the variation in heat release or absorption rates across different regions of the combustion system. By displaying this information as a contour plot, ANSYS Fluent allows us to visualize the spatial distribution of heat generation or consumption, providing a comprehensive understanding of the combustion process. Analyzing the heat of reaction contour helps identify regions with intense heat release, such as flame fronts or hot spots, as well as areas with heat absorption, such as cooling zones. This information is crucial for optimizing combustion efficiency, assessing the impact of heat transfer on system components, and identifying potential hotspots or cooling requirements.

IV-2-3-5.Investigating the Effects of Different Parameters on Comparative Analysis of Turbulence Models

Viscous calculations were carried out with the same boundary conditions as the non-viscous calculation. The figures below show the iso-Mach and iso-pressure contours resulting from a viscous calculation without boundary layer correction.

- **Mach Number**

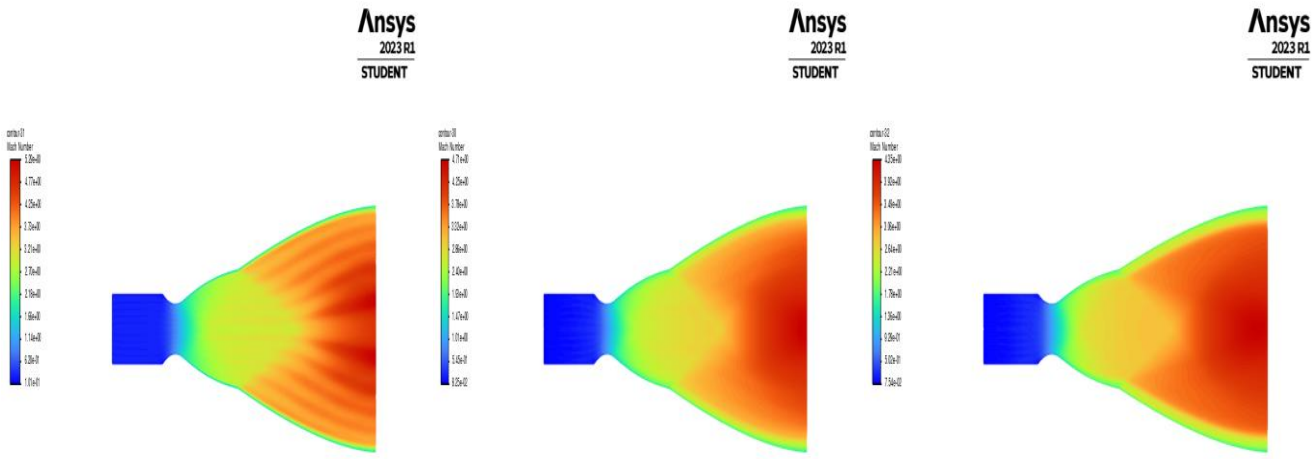

Figure(IV.44): Mach Number Contour Spalart-Allmaras,K-epsilon,K-Omega-SST

•**Static Pressure**

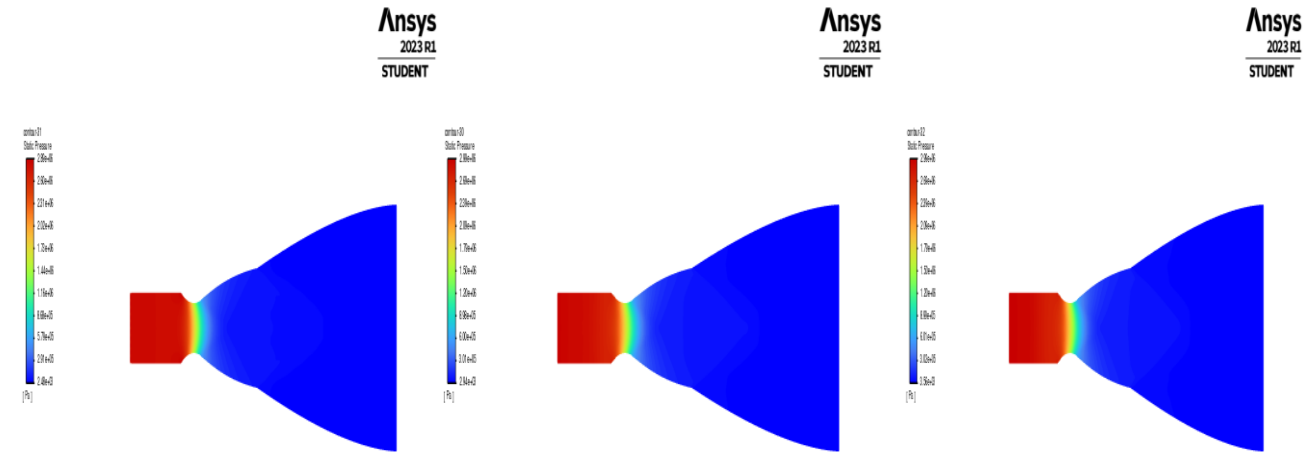

Figure(IV.45): Static Pressure Contour Spalart-Allmaras,K-epsilon,K-Omega-SST

•**Static Temperature**

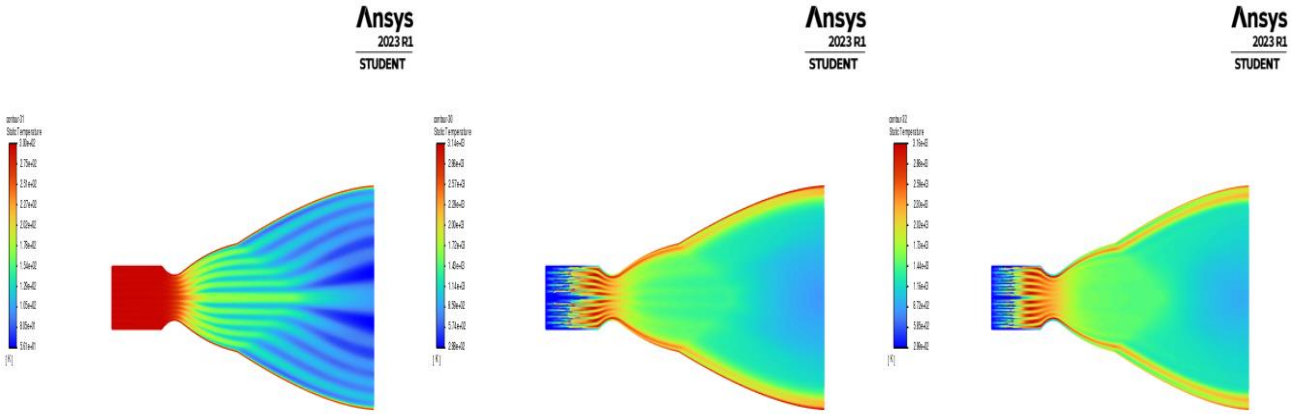

Figure(IV.46): Static Temperature Contour Spalart-Allmaras,K-epsilon,K-Omega-SST

It can be seen that the general flow structure is the same as in the non-viscous case. The presence of the boundary layer is observed in the viscous case. The thickness of the boundary layer increases from the nozzle inlet to the nozzle outlet. The flow is excluded from any disbonding.

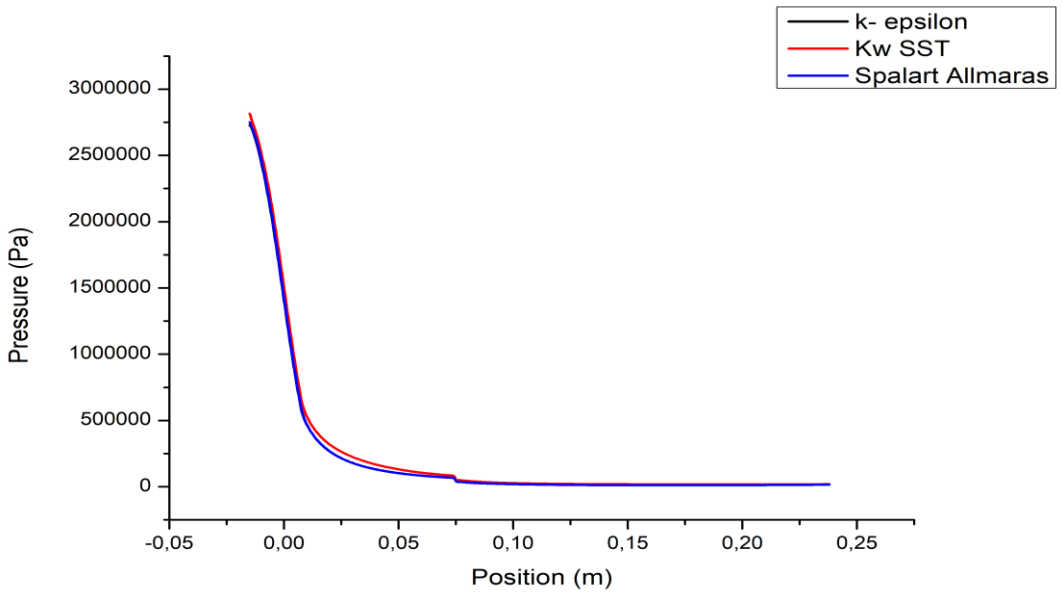

Figure(IV.47): Evolution of the Static Pressure Curve in the DBN wall for the three turbulence models

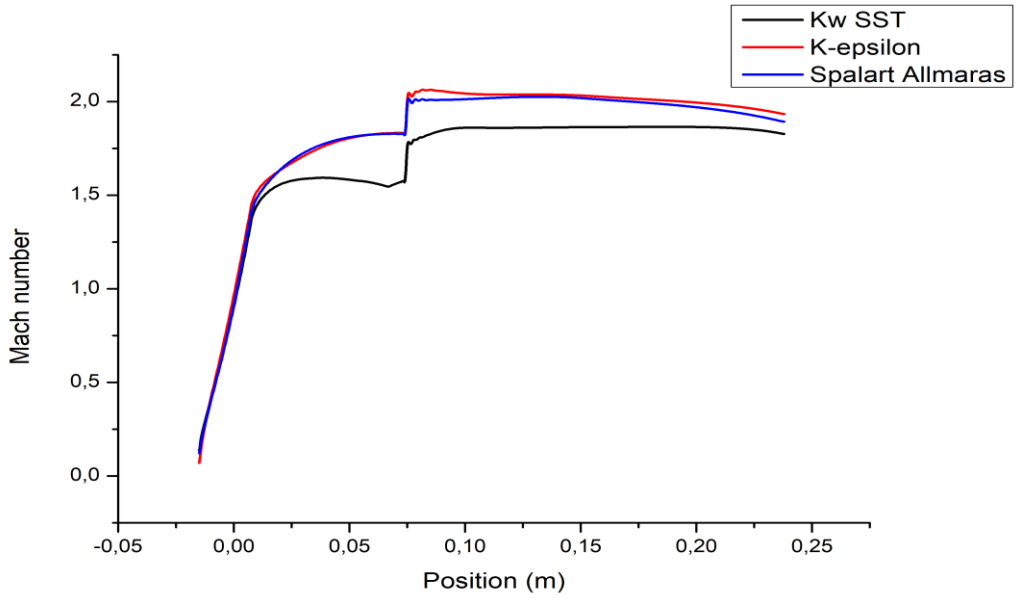

Figure(IV.48): Evolution of the Mach Number Curve in the DBN wall for the three turbulence models

Figures(IV.47)and (IV.48) represent the evolution of thermodynamic parameters in the nozzle using different turbulence models. The evolution is the same for K-epsilon and K-Omega-SST models, and the results obtained are very similar. On the other hand, The Spalart-Allmaras turbulence model simplifies turbulent flow by solving a single transport equation for turbulent viscosity. It offers computational efficiency and stability, making it suitable for various applications. However, its ability to accurately capture complex turbulent flows, especially in regions with strong vortices or high shear, is limited. Nevertheless, the simulations quickly converge with the k-Omega-SST turbulence model. It should also be noted that the Kω-SST model combines the advantages of both the K-e model in high Reynolds number regions (outer zone) and the Kω model, which behaves well in the vicinity of the wall (low Reynolds number region), This additional information helps in capturing complex flow features and resolving turbulence more accurately.

IV-2-3-6. Comparative Analysis of Parameters with Different Fuels

this analysis allows for a direct comparison of key combustion parameters, such as Mach Number ,temperature profiles, pressure distribution, and heat release rates, among different fuels. By examining these parameters across various fuel types, engineers gain insights into how fuel selection impacts combustion characteristics. This knowledge aids in identifying the most suitable fuel for achieving desired performance objectives, such as maximizing energy conversion efficiency, improving combustion stability, or reducing pollutant emissions.

- **Mach Number**

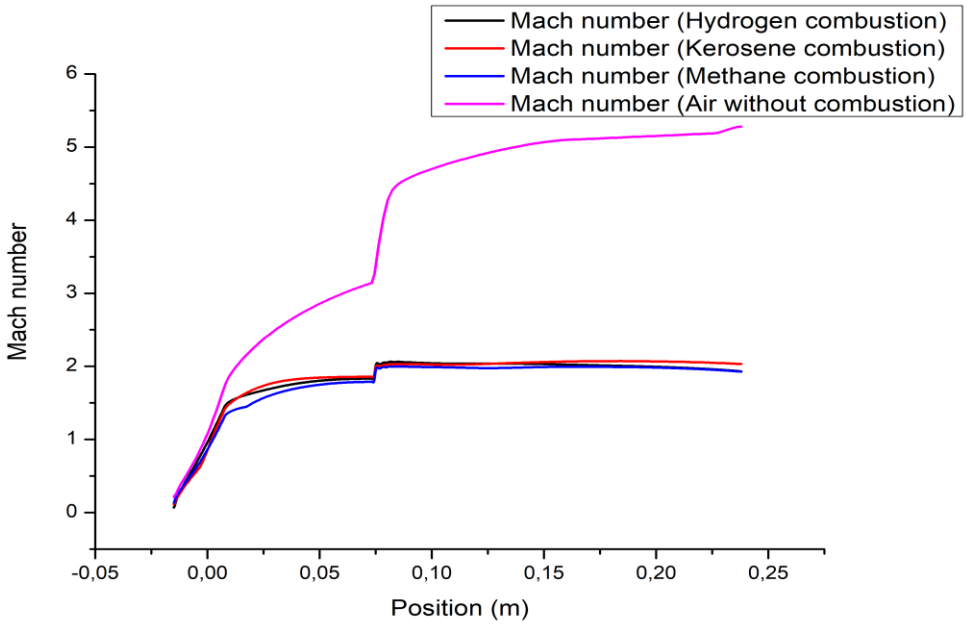

Figure(IV.49): Mach Number plot using different fuels

•**Static Pressure**

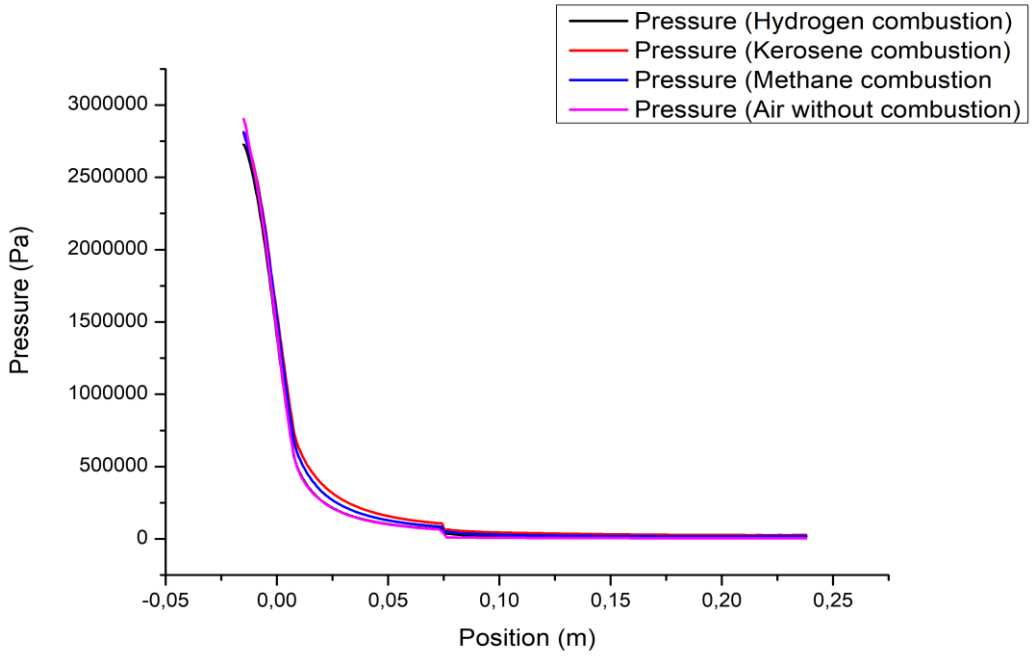

Figure(IV.50): Static Pressure plot using different fuels

•**Static Temperature**

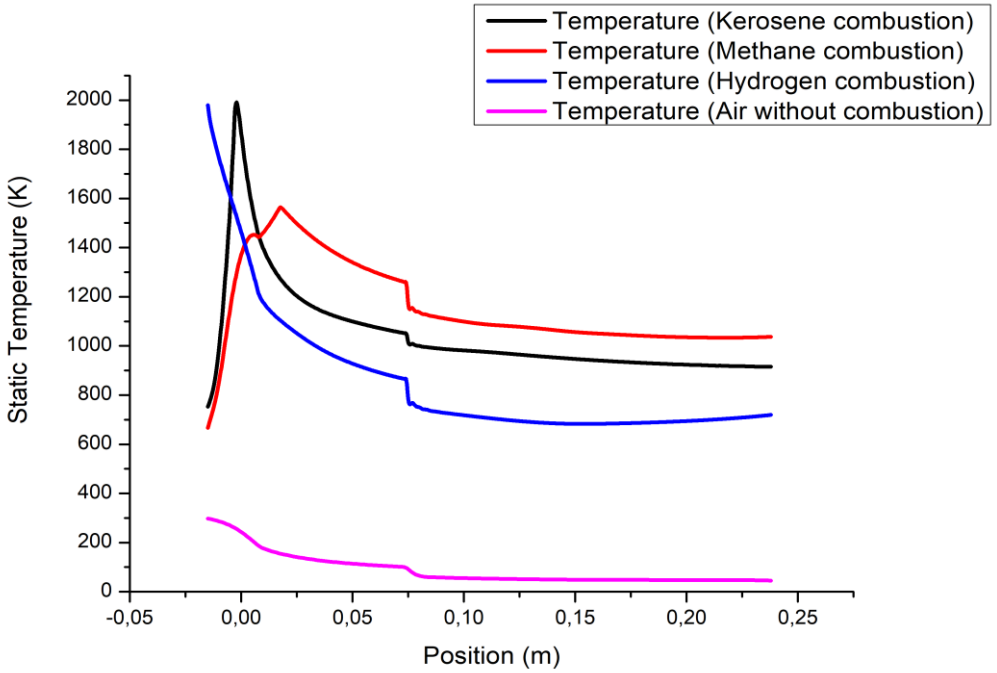

Figure(IV.51): Static Temperature plot using different fuels

Comparative Analysis of Mass Fraction of Combustion Products

the comparative analysis of mass fraction of combustion products in nozzle simulation offers the benefit of comprehensive performance evaluation, fuel optimization, emission control, and model validation. These insights enable engineers and researchers to make informed decisions, enhance nozzle system efficiency, and contribute to the development of cleaner and more efficient combustion technologies.

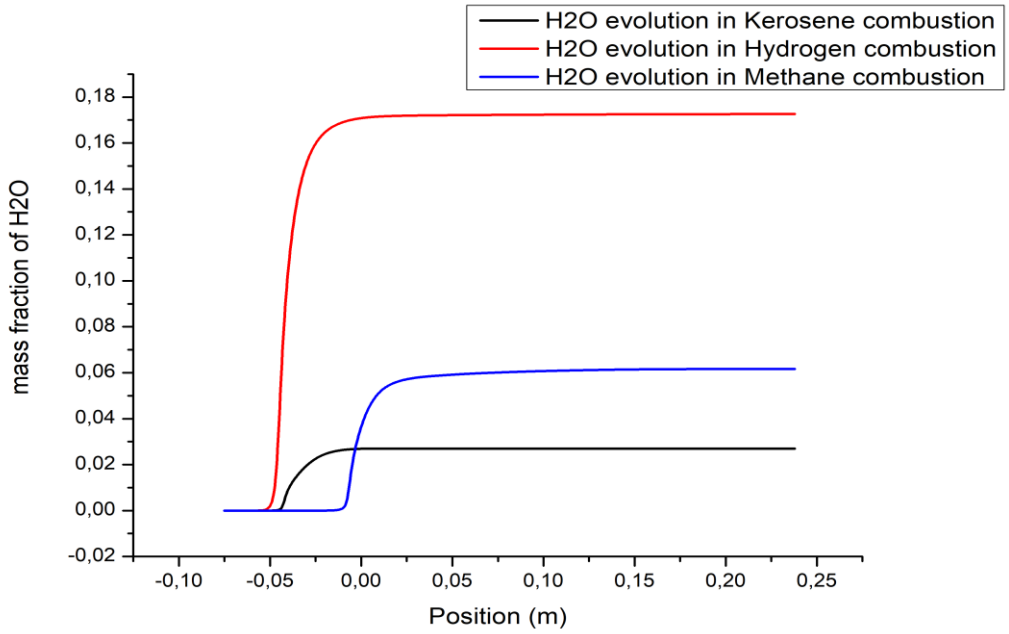

Figure(IV.52): The Evolution of H_2O Mass Fraction in Combustion of Various Fuels

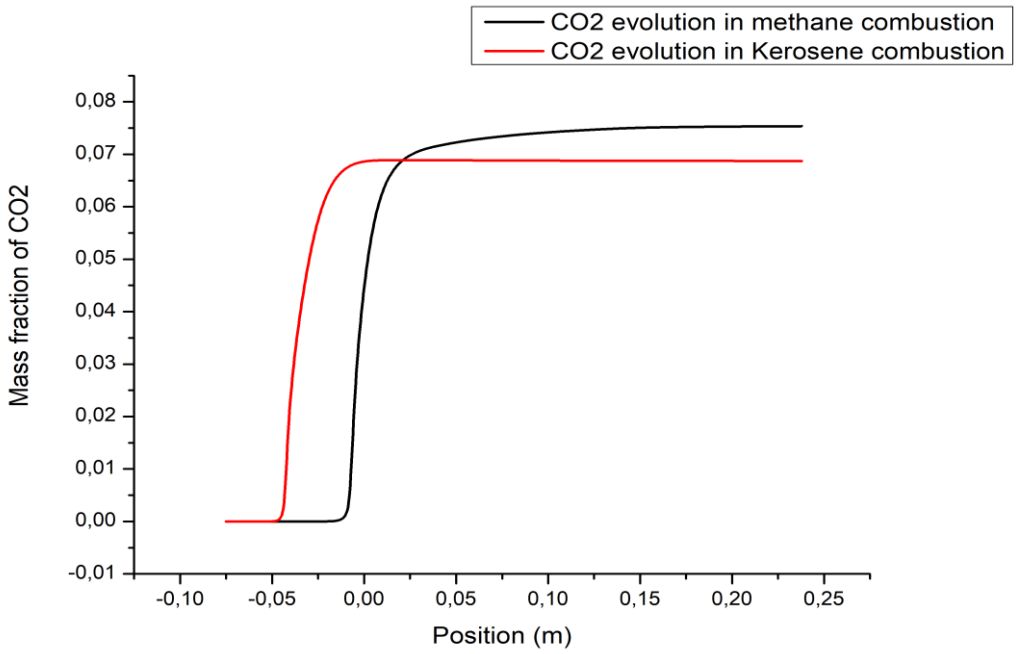

Figure(IV.53): The Evolution of CO_2 Mass Fraction in Combustion of Various Fuels

GENERAL CONCLUSION

The present study shows that the problems posed by the definition and realization of a nozzle for aerothermodynamic thrusters can be solved by numerical calculation, which is often highly accurate. Indeed, without even designing the nozzle, the builder can study the flow behavior and come up with a design with the best possible performance, and then move on to the design.

The work presented in this thesis is a Numerical Fluid Dynamics (CFD) study of flow in a DBN nozzle. As this type of nozzle is still in the study phase, the evolution of flow parameters (Mach number, pressure and density) in this nozzle has been studied and analyzed.

This study enabled us to familiarize ourselves with supersonic nozzle design methods in general, and Dual-Bell Nozzles in particular.

The design of Dual-Bell Nozzles is divided into two parts:

✦The first part is devoted to the design of the first curve. The first part is devoted to the design of the first curvature, starting with transonic flow calculations. This was simulated using the Sauer approach, which solves the small perturbation equation in terms of velocity components. Then, given the need to refine the calculation in the expansion zone (kernel zone), the inverse characteristic method was used to calculate the flow properties and subsequently plot the profile of this high-gradient zone. Finally, we simulated the profile of the supersonic zone at a second-degree polynomial and applied the direct characteristic method for calculations in this zone.

✦In the second part, we focused on the design of the second curvature. By applying the Prandtl-Meyer wave, we find the bending angle of the second curve relative to the first curve (at the bending point). Next, the expansion of the second divergent was carried out under the assumption of free jet flow.

Once the design has been obtained, the second part of the study consists in simulating and studying the flow behavior in the nozzle to fully understand the evolution of thermodynamic parameters in this type of nozzle.A simulation code called ANSYS Fluent was used. This stage was divided into four phases: creation of the surface geometry, meshing of the geometry, resolution and visualization.

The results obtained are represented in terms of curves showing the pressure and Mach number distributions along the walls of the Dual-Bell Nozzle studied, as well as the gas density. They show that combustion gases expand normally in all cases. This takes place rapidly along the circular arc downstream of the throat, up to the point of attachment (expansion zone). Beyond this point, it continues progressively to the exit of the first curve. This is in fact an intrinsic feature of profiled nozzles, mainly due to the large attachment angle chosen to impose that this expansion takes place almost entirely along the downstream circular arc of the throat, the remaining part essentially serving only to straighten the flow in order to make it axial and thus obtain a maximum thrust value. At the junction point, a Prandtl-Meyer wave is formed, bringing the second curvature down to an adaptation pressure.

all along the second curve. The results obtained using three different fuels are close and in good agreement with those obtained by other authors in the specialized literature. We also noted that the number of mach obtained at the exit is 5.87 for mixture H_2 (Fuel) / O_2 (Oxidizer),

representing a gain of 27% compared with(M=4.32) for mixture Kerosene $C_{12}H_{23}$ (Fuel) / O_2 (Oxidizer). In this case, thrust has increased, which is a major advantage for this type of nozzle. But the real advantage of this nozzle lies not only in the increase in performance, but also in its ability to operate at two different speeds without any flow disturbance or separation. Of course, knowledge of temperature evolution will also enable us to choose the right manufacturing material.

For viscous flow, it was found that the general structure of the flow is the same as in the non-viscous case. The presence of the boundary layer is remarkable in this case. The thickness of the boundary layer increases from the nozzle inlet to the nozzle outlet. We note that the flow is excluded from any detachment, but with a decrease in the mach number at the outlet due to friction.

And as an outlook, we propose :

- Evaluate the behavior of parameters in the Dual-Bell Nozzle at different altitudes (different NPR).

- Study the lateral loads exerted on the nozzle, particularly at the inflection point.

- Experimental tests to decisively validate such an approach.

- Compare simulation results with numerical results by developing a Fortran program.

References:

[1] Tim Edward, Liquid Fuels and Propellants for Aerospace Propulsion: 1903–2003 Journal of propulsion and power Vol. 19, No. 6, November–December 2003

[2] O.J. Haidn, M. Habiballah: Research on high pressure cryogenic combustion, Aerospace Science and Technology 7 (2003) 473–491

[3] Guillaume Ribert, Nan Zong, VigorYang, Laetitia Pons, Nasser Darabiha, Sébastien Candel: Counter flow diffusion flames of general fluids: Oxygen/hydrogen mixtures, Combustion and Flame 154 (2008) 319– 330

[4] Daniel T. Banuti and Klaus Hannemann, Effect of Injector Wall Heat Flux on Cryogenic Injection, 46th AIAA/ASME/SAE/ASEE Joint Propulsion Conference & Exhibit 25 - 28 July 2010, Nashville, TN

[5] Shabanian, Sayed Reza; Rahimi, Masoud; Khoshhal, Abbas, Ammar Abdul-Aziz Alsairafi, CFD Study on Hydrogen-Air Premixed Combustion in a Micro Scale Chamber, Iran J. Chem Chem Engg. Vol. 29, No. 4, 2010

[6] K. M. Pandey and S. K. Yadav, CFD analysis of a rocket nozzle with two inlets at mach 2.1, Journal of Environmental Research and Development Vol. 5 No. 2, October-December 2010

[7] D. Cecere a, *, A. Ingenito b, E. Giacomazzi a, L. Romagnosi a, C. Bruno b Hydrogen/air supersonic combustion for future hypersonic vehicles: International Journal of Hydrogen Energy Volume 36, Issue 18, September 2011, Pages 11969-11984

[8] V.B. Betelin a , V.F. Nikitin a,b , D.I. Altukhov a,b , V.R. Dushin a,b,n , Jaye Koo c : Supercomputer modeling of hydrogen combustion in rocket engines Acta Astronautica Volume 89, August–September 2013, Pages 46-59

[9] V.B. Betelin a, b, c, R.M. Shagaliev a, S.V. Aksenov a, I.M. Belyakov a, Yu.N. Deryuguin a , D.A. Korchazhkin a , A.S. Kozelkov a , V.F. Nikitin b,c,n , A.V. Sarazov a , D.K. Zelenskiy a Russian Federal Nuclear Center – Russian Scientific Resea: Mathematical simulation of hydrogen–oxygen combustion in rocket engines using LOGOS code Acta Astronautica Volume 96, March–April 2014, Pages 53-64

[10] N.N. Smirnov, V.N. Pushkin, V.R. Dushin, A.V. Kulchitskiy, Microgravity investigation of laminar flame propagation in monodisperse gas–droplet mixtures, Acta Astronaut. 61 (2007) 626–636.

[11] Liu B, He G-Q, Qin F, An J, Wang S, Shi L. Investigation of influence of detailed chemical kinetics mechanisms for hydrogen on supersonic combustion using large eddy simulation. Int J Hydrogen Energy 2019;44:5007–19

[12] C.R. Foster, F.B. Cowles, Experimental study of gas-flow separation in over expanded exhaust nozzles for rocket motors, http://ntrs.nasa.gov/search.jsp?R= 19630039654, 1949. (Accessed 9 December 2021).

[13] C. Génin, R. Stark, S. Karlt, D. Schneider, Numerical investigation of dual bell nozzle flow field, in: 48th AIAA/ASME/SAE/ASEE Joint Propulsion Conference and Exhibit 2012, American Institute of Aeronautics and Astronautics Inc., 2012.

[14] D. Schneider, C. Génin, Numerical investigation of flow transition behavior in cold flow dual-bell rocket nozzles, J. Propuls. Power 32 (5) (2016) 1212–1219, https://doi.org/10.2514/1.B36010.

[15] M. Verma, N. Arya, A. De, Investigation of flow characteristics inside a dual bell nozzle with and without film cooling, Aerosp. Sci. Technol. 99 (2020), https:// doi.org/10.1016/j.ast.2020.105741.

[16] N.v. Taylor, C.M. Hempsell, J. Macfarlane, R. Osborne, R. Varvill, A. Bond, S. Feast, Experimental investigation of the evacuation effect in expansion deflection nozzles, Acta Astronaut. 66 (2010) 550–562, https://doi.org/10.1016/ j.actaastro.2009.07.016.

[17] N. Taylor, J. Steelant, R. Bond, Experimental comparison of dual bell and expansion deflection nozzles, in: 47th AIAA/ASME/SAE/ASEE Joint Propulsion Conference and Exhibit 2011, American Institute of Aeronautics and Astronautics Inc., 2011.

[18] Andrea Ferrero Andrea Ferrero, Antonietta Conte, Emanuele Martelli , Francesco Nasuti , Dario Pastrone: Dual-bell nozzle with fluidic control of transition for space launchers Acta Astronautica Volume 193, April 2022, Pages 130-137

[19] G. Hagemann, H. Immich, T. Van Nguyen, G.E. Dumnov, Advanced rocket nozzles, J. Propul. Power 14 (5) (1998) 620–634.

[20] G. Luke, D. Adams, Use of nozzle trip rings to reduce nozzle separation side force during staging, in: 28th Joint Propulsion Conference and Exhibit, 1992, p. 3617.

[21] N. Goncharov, V. Orlov, V. Rachuk, A. Shostak, R. Starke, Reusable launch vehicle propulsion based on the RD-0120 engine, in: 31st Joint Propulsion Conference And Exhibit, 1995, p. 3003.

[22] V.V. Semenov, A.A. Sergienko, Rocket engine laval nozzle with gas injection device, 2008, Google Patents, URL https://patents.google.com/patent/ WO2008129372A3.

[23] R.A. Wasko, Performance of annular plug and expansion-deflection nozzles including external flow effects at transonic mach numbers, 1968, NASA-TN-D-4462.

[24] M. Horn, S. Fisher, Dual-Bell Altitude Compensating Nozzles, Tech. Rep., Rockwell International Corp, Canoga Park, CA, United States, 1993

[25] T. Tomita, M. Takahashlt, M. Sasaki, H. Tamara, Investigation on characteristics of conventional-nozzle-based altitude compensating nozzles by cold-flow tests, in: Collection of Technical Papers - AIAA/ASME/SAE/ASEE 42nd Joint Propulsion Conference, American Institute of Aeronautics and Astronautics Inc., 2006, pp. 656–664.

[26] AIAA JOURNAL Vol. 50, No. 1. January 2012 (Wall Pressure Unsteadiness and Side Loads in Over expanded Rocket Nozzles) Woutijn J. Baars and Charles E. Tinney University of Texas at Austin, Austin, Texas 78712 Joseph H. Ruf, Andrew M. Brown, and David M. AIAA JOURNAL Vol. 50, No. 1. January 2012 McDaniels and NASA Marshall Space Flight Center, Huntsville, Alabama 35812 DOI: 10.2514/1 JOS 1075.

[27] Ruf, Joseph H. McDaniels, David M. Brown, Andrew M. Date Acquired August 25, 2013 Publication Date July 26, 2010 Subject Category Spacecraft Propulsion And Power Meeting Information AIAA Joint Propulsion Conference (Nashville, TN) Distribution Limits Public Copyright Work of the US Gov. Public Use Permitted.

[28] Transient Side Load Analysis of Out-of-Round Film-Cooled Nozzle Extensions Ten-See Wang*, Jeff Lin†, Joe Ruf‡, and Mike Guidos§ NASA Marshall Space Flight Center, Huntsville, Alabama, 35812.

[29] Numerical investigation of supersonic nozzle flow separation Authors Qing Xiao, Her-Mann Tsai, Dimitri Papamoschou Publication date 2007/3 Journal AIAA journal Volume 45 Pages 532-541.

[30] Experimental, theoretical, and computational investigation of separated nozzle flows Craig A. Hunter Aerospace engineeringNozzleDischarge coefficient 1998 34th AIAA/ASME/SAE/ASEE Joint Propulsion Conference and Exhibit

[31] Nozzle Boundary-Layer Separation Near the Nozzle Exit in Highly Over expanded Jets Junhui Liu and Yu Yu Khine AIAA 2020-2561 Session: Jet Aeroacoustics IV Published Online:8 Jun 2020https://doi.org/10.2514/6.2020-2561

[32] 6th International Symposium on Propulsion for Space Transportation of the XXIst century, Palais des Congres, Versailles, France, May 14 – 17, 2002Cold Gas Subscale Test Facility P6.2 at DLR LampoldshausenH. Kronmüller*, K. Schäfer§, H. Zimmermann&, R. Stark+DLR, Deutsches Zentrum für Luft- und RaumfahrtInstitute of Space Propulsion, D-74239 Lampoldshausen a. K., Germany.

[33] SUPERSONIC FLOW SEPARATION WITH APPLICATION TO ROCKET ENGINE NOZZLES by Jan Östlund June 2004 Technical reports from Royal Institute of Technology Department of Mechanics S-100 44 Stockholm, Sweden.

[34] JOURNAL OF PROPULSION AND POWER Vol. 21, No. 2, March-April 2005 (Role of Wall Shape on the Transitionin Axisymmetric Dual-Bell Nozzles) Francesco Nasuti, Marcello Onofri, and Emanuele Martelli* University of Rome "La Sapienza" Rome 00184, Italy.

[35] JOSE A. MORINIGO (2004) , JOSE J. SALVA Three-dimensional simulation of the self-oscillating flow and side-loads in an over-expanded subscale rocket nozzle October 2006 Proceedings of the Institution of Mechanical Engineers Part G Journal of Aerospace Engineering 220(5):507-523

[36]Zhi-Wei Huang, Guo-Qiang He, Fei Qin, Rui Xue, Xiang-Geng Wei, and Lei Shi: Combustion oscillation study in a kerosene fueled rocket-based combined-cycle engine combustor Acta Astronautica Volume 129, December 2016, Pages 260-270

[37]A. Urbano , L. Selle , G. Staffelbach , B. Cuenot , T. Schmitt , S. Ducruix , S. Candel: Exploration of combustion instability triggering using Large Eddy Simulation of a multiple injector liquid rocket engine Combustion and Flame Volume 169, July 2016, Pages 129-140

[38]Simon Blanchard , Quentin Cazères, Bénédicte Cuenot : Chemical modeling for methane oxy-combustion in Liquid Rocket Engines Acta Astronautica Volume 190, January 2022, Pages 98-111

[39]Min Sona, Kanmaniraja Radhakrishnana, Youngbin Yoonb, Jaye Kooc: Numerical study on the combustion characteristics of a fuel-centered pintle injector for methane rocket engines: Acta Astronautica Volume 135, June 2017, Pages 139-149

[40]M. Masquelet, S. Menon, Y. Jin, R. Friedrich: Simulation of unsteady combustion in a LOX-GH_2 fueled rocket engine Aerospace Science and Technology Volume 13, Issue 8, December 2009, Pages 466-474

[41]Laurent Gomet, Vincent Robin, Arnaud Mura: Lagrangian modelling of turbulent spray combustion under liquid rocket engine conditions Acta Astronautica Volume 94, Issue 1, January–February 2014, Pages 184-197

[42]YATHIS GIOVANNI DELICAT « étude de la réactivité de l'iode transporte dans un mélange H2/H2O en conditions de combustion dans des flammes basse pression prémélangées ». -Thèse doctorat-2012.

[43] R. BORGHI & M. DESTERIAU La combustion et les flammes, TECHNIP (1975).

[44] « étude et simulation numérique de la combustion des flammes premelanges suspendus

de méthane-air pour des bruleurs a faible nombre de swirl » thèse de doctorat, université de

Boumardas-2013.

[45] MAGNUSSEN B, HJERTAGER BH 16th symposium (int.) on combustion, 719-729,

The Combustion Institute, Pittsburgh. (1976).

[46] mémoire présente en vue de l'obtention du diplôme de magistère « étudenumérique et expérimente de la flamme non-prémélangée ».

[47] JL Fernandez - Blagnac Saint Exupéry Cours Chambre de Combustion

[48] Memoire: Simulation de flamme de diffusion pour la combustion du mélange méthane/air
Encadré par : Dr R.RENANE (IAES) et Dr R.ALLOUCHE (IAES) Réalisé par : ABDELAZIZ Mourad.

[49] Pushing the Envelope: A NASA Guide to Engines a Guide for Educators and Students With
Chemistry, Physics, and Math Activities.

[50] http://www.grc.nasa.gov/WWW/K-12/airplane/otto. Html.

[51] Principia Cybernetica Web : Entropy and the Laws of Thermodynamics J. de Rosnay July 3, 1998

[52] Van Ness, H. C., & Abbott, M. M. (1987). Classical thermodynamics of non-electrolyte solutions. John Wiley & Sons.

[53] Callen, H. B. (1985). Thermodynamics and an introduction to thermostatistics. John Wiley & Sons.

[54] Atkins, P. W., & de Paula, J. (2006). Physical Chemistry (8th ed.). Oxford: Oxford University Press.

[55] Williams, F.A., "Combustion theory" Addison Wesley Publishing Company, Inc London, 1965.

[56] Thèse doctorat,'Contribution à la Modélisation des EcoulementsTurbulents Réactifs Partiellement Prémélangés 'Soutenu le 14.12.2007

[57] "Fundamentals of Fluid Mechanics" by Bruce R. Munson, Donald F. Young, and Theodore H. Okiishi.

[58]ANSYS FLUENT 12.0/12.1 Documentation, Overview of Physical Models in ANSYS FLUENT.

[59] « Simulation de flamme de diffusion pour lacombustion du mélange méthane/air », Realised by ABDELAZIZ Mourad. Framed by: Dr R.RENANE (IAES), Dr R.ALLOUCHE (IAES)

[60]Marek Wasilewski1,* , and Grzegorz Ligus, Effect of discretization method of a computational domain on particle separation in a cyclone separator.

[61]Appendix A Mesh Quality ANSYS Meshing Application Introduction, April 28, 2009 Inventory #002645.

[62] https://www.grc.nasa.gov/WWW/k-12/airplane/nseqs.html

[63] https://www.afs.enea.it/project/neptunius/docs/fluent/

[64] H. M. Glaz J. B. Bell, P. Colella.

Second-Order Projection Method for the Incompressible Navier-Stokes Equations.

Journal of Computational Physics, 85:257, 1989.

[65] A one-equation turbulence model for aerodynamic flows P. SPALART and S. ALLMARAS 1992, Published Online:17 Aug 2012

[66] Wilcox, David C (1998). "Turbulence Modeling for CFD". Second edition. Anaheim: DCW Industries, 1998. pp. 174.

[67] Bardina, J.E., Huang, P.G., Coakley, T.J. (1997), "Turbulence Modeling Validation, Testing, and Development", NASA Technical Memorandum 110446.

[68] Menter, F. R. (1993), "Zonal Two Equation k-ω Turbulence Models for Aerodynamic Flows", AIAA Paper 93-2906.

[69] MAGNUSSEN B, HJERTAGER BH , 719-729, The Combustion Institute, Pittsburgh. (1976).

[70]https://www.learncax.com/knowledge-base/blog/by-category/cfd/basics-of-y-plus-boundary-layer-and-wall-function-in-turbulent-flows

[71] Y. Cengel, Fluid Mechanics: Fundamentals and Applications.

[72] H Tennekes, JL Lumley – 1972 : A first course in turbulence.